A SOLID ELEMENT APPROACH TO ANALYZING CANDU FUEL ELEMENT BEHAVIOUR UNDER POST-DRYOUT HEAT TRANSFER CONDITIONS

UNE APPROCHE D'ÉLÉMENT SOLIDE POUR L'ANALYSE DU COMPORTEMENT DES GAINES DE COMBUSTIBLE CANDU SOUS CONDITIONS DE TRANSFERT DE CHALEUR POST-ASSÈCHEMENT

A Thesis Submitted

to the Division of Graduate Studies of the Royal Military College of Canada

by

Cody Josef Peter John Krasnaj, B.Sc. (Eng)

In Partial Fulfillment of the Requirements for the Degree of

Master of Applied Science in Nuclear Engineering

April 2015

ROYAL MILITARY COLLEGE OF CANADA
COLLÈGE MILITAIRE ROYAL DU CANADA

DIVISION OF GRADUATE STUDIES AND RESEARCH
DIVISION DES ÉTUDES SUPÉRIEURES ET DE LA RECHERCHE

This is to certify that the thesis prepared by / Ceci certifie que la thèse rédigée par

CODY JOSEF PETER JOHN KRASNAJ

entitled / intitulée

A SOLID ELEMENT APPROACH TO ANALYZING CANDU FUEL ELEMENT BEHAVIOUR UNDER POST-DRYOUT HEAT TRANSFER CONDITIONS

UNE APPROCHE D'ÉLÉMENT SOLIDE POUR L'ANALYSE DU COMPORTEMENT DES GAINES DE COMBUSTIBLE CANDU SOUS CONDITIONS DE TRANSFERT DE CHALEUR POST-ASSÈCHEMENT

complies with the Royal Military College of Canada regulations and that it meets the accepted standards of the Graduate School with respect to quality, and, in the case of a doctoral thesis, originality, / satisfait aux règlements du Collège militaire royal du Canada et qu'elle respecte les norms acceptées par la Faculté des études supérieures quant à la qualité et, dans le cas d'une thèse de doctorat, l'originalité,

for the degree of / pour le diplôme de

MASTER OF APPLIED SCIENCE IN NUCLEAR ENGINEERING /
MAITRISE DU SCIENCE EN GÉNIE NUCLÉAIRE

Signed by the final examining committee: /
Signé par les membres du comité examinateur de la soutenance de thèse:

_____ (Dr. Abdelkérim Ousman), Chair / Président

_____ (Dr. Tony Williams), External Examiner / Examinateur externe

_____ (Dr. Thomas Krause), Internal Examiner / Examinateur interne

_____ (Dr. Brent Lewis), Internal Examiner / Examinateur interne

_____ (Dr. Paul Chan), Main Supervisor / Directeur de thèse principal

_____ (Dr. Diane Wowk), Co-Supervisor / Co-Directeur de thèse principal

Approved by the Head of Department: /
Approuvé par le Directeur du Département : _____ Date : _____

To the Librarian: This thesis is not to be regarded as classified. /

Au Bibliothécaire : Cette thèse n'est pas considérée comme a publication restreinte.

_____
Main Supervisor / Directeur de thèse principal

ACKNOWLEDGEMENTS

First and foremost, I would like to thank my talented supervisors Dr. Paul Chan and Dr. Diane Wowk for providing me an opportunity to challenge myself and grow as an individual. Their guidance, encouragement and support offered throughout the past three years were instrumental in helping me complete this research. Their flexibility in accommodating my co-op work term with the Canadian Nuclear Safety Commission, for my benefit, was very much appreciated.

I would like to thank the Canadian Nuclear Safety Commission for supporting a RMC-CNSC co-op opportunity which has provided an invaluable learning experience for upgrading my skillset. In particular, I would like to thank my Director, Dr. Michel Couture, and my co-workers within the Physics and Fuel Division for their continued support throughout my two year term. I have acquired a tremendous amount of practical knowledge and experience which has expanded my career opportunities. I must extend a special thanks to my mentor, Dr. Ali El-Jaby, whose supervision kept me actively engaged and challenged while undertaking both my work term objectives and thesis research. His sincere generosity in helping me succeed with this work by always being available for technical discussions, and offering feedback to improve all aspects of my work, regardless of his busy schedule, was truly an asset which I am most grateful.

I would like thank Dr. Hugues Bonin for his time and effort spent while translating my abstract to French.

I would like to acknowledge the Natural Sciences and Engineering Research Council of Canada (NSERC) under CRDPJ 415247-11 and CAMECO for their financial support of this research.

I would like to thank my many friends both in Ottawa and beyond for joining me in making these years some of the best. A special thanks to the boys in Kingston, who remained after I departed to the CNSC, for their hospitality when I needed to return to work at RMC on weekends.

Most of all, I would like to thank my Mom, Dad and Sister, whose support, love and encouragement throughout this endeavor has been graciously appreciated.

ABSTRACT

With the age of many nuclear power plants either reaching or approaching the end of their design life, the effects of aging phenomena on both plant performance and safety analysis has become more of an interest to regulators and nuclear energy corporations. Although aging effects were considered individually in design and manufacturing, the rate and integrated impact on safety analysis is greater than expected.

One particular fuel channel interaction of interest under abnormal conditions is fuel element to pressure tube contact. Elements in a CANDU® fuel bundle can deform (i.e., deflect or bow) during their residence in the fuel channel by thermally-induced phenomena. Under nominal design conditions, these deflections are small and pose minimal risk to fuel channel integrity. However, as the pressure tube ages with operational life, the diameter of the pressure tube begins to creep. As a result, the fuel channel geometry experiences a change in shape, which allows more coolant flow over the fuel bundle rather than through the subchannels. This increased flow by-pass will alter the critical heat flux which directly impacts where and when dryout will occur on the bundle. Under post-dryout conditions, deteriorated heat transfer can agitate these thermal phenomena to produce larger deflections, which may pose an increased risk to fuel and fuel channel integrity.

To prevent dryout in CANDU reactors, conservative parameters are used for the trip parameter acceptance criteria as stated in CNSC regulatory guide G-144. Limited in-reactor experiments have indicated that operational margins exist when compared to those stated in G-144. A 3-D model utilizing the finite-element method to examine fuel deformation under post-dryout heat

transfer conditions could be used as a tool to help better understand the effects of thermally-induced phenomena. A one-way coupled thermal-mechanical model is developed to simulate the deformation behaviour of a fuel element in contact with the pressure tube at the onset of dryout. The methodology and approach used for the model development and studies performed as part of the verification are presented.

Results obtained from this thesis conclude that the outer fuel element (FE) bearing pads play a significant role in reducing the extent of thermally driven deformation when the fuel element is positioned in contact with the pressure tube (PT). For a drypatch with a maximum sheath temperature of roughly 800°C located in-between the center and end bearing pad free span length, contact was not observed between the fuel element and pressure tube. Artificially high temperature gradients were used to demonstrate the model's FE-PT contact capabilities when sufficient thermal driving forces are present. The realised model may be useful for analysing complex thermal conditions under a typical Anticipated Operational Occurrence.

RÉSUMÉ

Avec l'âge de plusieurs centrales nucléaires qui atteignent ou s'approchent de la fin de leur vie utile, les effets des phénomènes reliés au vieillissement sur la performance de la centrale et l'analyse de la sûreté représentent un intérêt grandissant pour les responsables de la règlementation et des corporations en énergie nucléaire. Bien que les effets aient été considérés séparément aux étapes de la conception et de la fabrication, leur taux et leur impact intégré sur l'analyse de sûreté sont plus importants que selon les attentes.

Une interaction d'un intérêt particulier au niveau du canal de combustible en conditions anormales est celle du contact entre un élément de combustible et la paroi du tube de force. Les éléments d'une grappe de combustible CANDU peuvent se déformer (i.e. subir une déflexion ou devenir cambré) durant leur temps de résidence dans le canal de combustible à la suite de phénomènes induits thermiquement. Dans des conditions de design nominales, ces déflexions sont petites et ne représentent que des risques minimes pour l'intégrité du canal de combustible. Cependant, à mesure que le tube de force vieillit au cours de sa vie utile, le diamètre du tube commence à montrer des signes de fluage. Il en résulte que la géométrie du canal de combustible subit un changement dans sa forme ce qui permet à plus de caloporteur de s'écouler au-dessus de la grappe de combustible plutôt qu'à l'intérieur des sous-canaux. Ce contournement accru du flux de caloporteur va causer un changement du flux calorifique critique qui a un impact direct sur où et quand l'assèchement va se produire dans la grappe. Dans de telles conditions de post-assèchement, le transfert de chaleur réduit peut exacerber ces phénomènes thermiques au point de produire des déflexions encore plus importantes qui peuvent causer des risques accrus pour l'intégrité du combustible et du canal de combustible.

Afin de prévenir l'assèchement dans les réacteurs CANDU, on utilise des valeurs conservatrices pour les paramètres d'acceptation du déclenchement de l'arrêt du réacteur comme il est énoncé dans le guide G-144 de règlementation de la Commission canadienne de sûreté nucléaire. Des expériences en-pile limitées ont indiqué que des marges opérationnelles existent lorsque comparées à celles énoncées dans le document G-144. Un modèle 3-D basé sur une méthode par éléments finis pour examiner la déformation du combustible dans des conditions de transfert de chaleur post-assèchement peut être utilisé comme un outil pour aider à une meilleure compréhension des effets de phénomènes induits thermiquement. On a développé un modèle couplé thermique-mécanique à sens unique pour simuler le comportement de déformation d'un élément de combustible en contact avec le tube de force au début de l'assèchement. On présente la méthodologie et l'approche utilisées pour le développement de ce modèle et les études effectuées pour une partie de la vérification.

Les résultats obtenus de cette thèse permettent de conclure que les tampons d'appui jouent un rôle significatif dans la réduction de l'ampleur de la déformation induite thermiquement lorsque l'élément de combustible est placé en contact avec le tube de force. Pour une région sèche avec une température maximum de 800˚C pour la gaine située dans l'espace libre de tampon d'appui entre les tampons situés au centre et près des extrémités de la grappe, on n'a pas observé de contact entre l'élément de combustible et le tube de force. On a utilisé des gradients de température artificiellement élevés pour démontrer les capacités du modèle de prédire le contact entre l'élément de combustible et le tube de force lorsque des forces motrices thermiques suffisantes sont en présence. Le modèle ainsi réalisé peut être utile pour l'analyse de conditions thermiques complexes lors d'une occurrence opérationnelle anticipée.

Table of Contents

Chapter **Page Number**

List of Figures

List of Tables

List of Acronyms

AECL	Atomic Energy of Canada Limited
AOO	Anticipated Operational Occurrence
CANDU	CANada Deuterium Uranium
CANLUB	CANdu LUBricant
CCP	Critical Channel Power
CHF	Critical Heat Flux
CNSC	Canadian Nuclear Safety Commission
CNL	Canadian Nuclear Laboratories
CTF	Curvature Transfer Factor
DOF	degree of freedom
ELESTRES	ELEment Simulation and sTRESses
ELOCA	Element Loss of Coolant Analysis
FEA	Finite Element Analysis
FEM	Finite Element Method
FGR	Fission Gas Release
FPG	Fission Product Gas
FE-FE	Fuel Element to Fuel Element
FE-PT	Fuel Element to Pressure Tube
G-144	CNSC's Regulatory Guide: Trip Parameter Acceptance Criteria for the Safety Analysis of CANDU Nuclear Power Plants
GMWR	Galerkin Method of Weighted Residuals
HORSE	HORizontal nuclear fuel Simulation Environment
IAEA	International Atomic Energy Agency
LOF	Loss of Flow
LWR	Light Water Reactor
MATPRO	MATerial PROperties library
MOOSE	Multiphysics Object-Oriented Simulation Environment
N-R	Newton-Raphson
NOC	Normal Operating Condition
PHTS	Primary Heat Transport System
RBM	Rigid Body Motion
REF	Rigidity Enhancement Factor
ROE	Reference Overpower Envelope
RMCC	Royal Military College of Canada
SCC	Stress-Corrosion Cracking
TCC	Thermal Contact Conductance
V&S	Veeder and Schankula

List of Symbols

A	Parameter in $\mathrm{k}_{\mathrm{UO}_2}$
a	Inner sheath radius
a_p	Pellet radius
B	Parameter in $\mathrm{k}_{\mathrm{UO}_2}$
b	Outer sheath radius
C_v	Quantity defined in text relating to phonon contribution to specific heat at constant volume
$[D]$	Elastic stiffness matrix
D_1	Fraction of theoretical density
D	Flux depression factor
EI	Flexural rigidity
E_X, E_Y, E_Z	Young's modulus
E_p	Young's modulus of pellet
E_s	Young's modulus of sheath
F^a	Incremental Load Vector
F^{nr}	Restoring Load Vector
$F_{contact}$	Contact force
G	Shear modulus
G_{ps}	Pellet-to-sheath gripping factor
H	Quantity defined in text relating to total thermal impedance between the fuel surface and coolant
h_{ps}	Pellet-to-sheath heat transfer coefficient
h_{sc}	Sheath-to-coolant heat transfer coefficient
I	Gauss Quadrature Integral
K	Stiffness matrix
K^t	Jacobian matrix (tangent stiffness matrix)
K_1	Quantity defined in text relating to thermal bowing
K_2	Quantity defined in text relating to thermal bowing
K_3	Quantity defined in text relating to thermal bowing
K_4	Quantity defined in text relating to thermal bowing
k	Boltzmann's constant
k_{normal}	Contact stiffness constant
$\mathrm{k}_{\mathrm{UO}_2}$	Thermal conductivity of UO_2
k_{Zr-4}	Thermal conductivity of Zr-4
k_p	Thermal conductivity of pellet
k_s	Thermal conductivity of sheath
L	Fuel element length
n	Sum index in Gauss Quadrature
m	Sum index in Gauss Quadrature
N	Shape function
P	Applied mechanical load
Q	Internal heat generation
$\mathrm{q}_{interface}$	Heat flux at contact interface
R	Residual vector

T	Temperature
T'	Quantity defined in text relating to porosity correction factor for temperature in k_{UO_2}
T''	Quantity defined in text relating to correction factor for temperature
$T_{contact}$	Temperature of Contact surface
T_{target}	Temperature of Target surface
$\mathrm{T_{ref}}$	Reference temperature
$\bar{T}_c$	Nominal bulk coolant temperature
$\tilde{T}$	Approximate temperature solution
u	Field quantity vector
W_i	Weight factor associated with Gauss Quadrature
W_j	Weight factor associated with Gauss Quadrature
$\bar{w}$	Average linear power rating
x	Deviation from stoichiometry
$x_{penetration}$	Interpenetration of contact surfaces
x, y, z	Distance along axes
Y_1	Parameter in C_v
UO_2	Uranium Dioxide
Zr-4	Zircaloy-4

List of Symbols (Greek)

α	Coefficient of thermal expansion
α_p	Coefficient of thermal expansion for pellet
α_s	Coefficient of thermal expansion for sheath
β	Quantity defined in text relating to variation of coolant temperatures
γ	Quantity defined in text relating to heat transfer between pellet, sheath and coolant
δ	Magnitude of deflection at mid-plane
ε^{el}	Total strain vector
ε_{th}	Thermal strain vector
η	Distance of neutral axis from centroid
θ	Parameter in C_v
λ	Augmented Lagrange constant
$\nu_{XY}, \nu_{YZ}, \nu_{XZ}$	Poisson's ratio
ξ	Sampling point associated with Gauss Quadrature
ρ	Theoretical density
σ	Stress vector
κ	Sampling point associated with Gauss Quadrature

1 Introduction

World electricity demands will continue to grow as global development continually progresses. Over the next few decades there will be a pronounced shift in the generation-fuel mix as part of an international effort to counter climate change by reducing greenhouse gas emissions. Coal, which is the most widely used fuel today worldwide, will be phased out in favour of low price natural gas and other renewable fuels. Nuclear is a safe, reliable and carbon-free option that will continue to be an integral part of the generation-fuel mix moving forward. The International Atomic Energy Agency (IAEA) projects the world's nuclear power generation capacity to grow by 17% in a low case scenario and by 94% in a high case scenario by 2030 [1]. There are currently 435 nuclear power reactors operating worldwide generating a total nuclear capacity of over 372 gigawatts-electric [2]. Additionally, 72 reactors are currently under construction with another 92 planned expansions.

In 2014, 19 operational CANDU nuclear power reactors (8 Bruce, 4 Darlington, 6 Pickering and 1 Point Lepreau) made up roughly 16% of Canada's total electricity production. In the same year, 62% of Ontario's electricity generation demand was delivered by nuclear power [3]. As stated in Ontario's Long-Term Energy Plan, the current government has demonstrated their commitment to reduce greenhouse gas emissions by being the first province/state in North America to eliminate coal power generation by 2014. In addition, the updated plan includes full support to maintain nuclear as a significant part of Ontario's base load energy capacity in order to meet future electricity demands. This is evident by the planned refurbishments of the Darlington nuclear fleet beginning in 2016 [4].

Electrical power generation is the process of transforming one form of energy into electricity. Nuclear power is similar to other thermal power production in that heat from a fuel source is transferred by fluid flow, which acts as an intermediate energy carrier, to rotate a turbine and produce useful work. This mechanical work can be harnessed by an electrical generator through electromagnetic induction. Turbines driven by fluid flow commonly use steam as the fluid medium which is produced by boiling water with the heat generated by the fuel source. Various examples of fuels include: fossil fuels like coal and natural gas, nuclear fission, biomass, geothermal energy and solar thermal energy. Other fluid flows like gravity-fed running water and natural air movements are used in hydroelectric and wind power turbines respectively.

Heat generated within nuclear fuel is produced by fission. Nuclear fission is the process of splitting the nucleus of a heavy atom into two smaller nuclei through the absorption of a neutron. Nuclides capable of undergoing fission are known as fissile nuclides. The CANDU reactor uses natural uranium dioxide fuel which contains 0.71 wt. % fissile isotopes of ^{235}U. Roughly 200MeV of energy is liberated for every ^{235}U fission event that takes place. The majority of this energy is released as kinetic energy contained within the lighter fission product nuclei. About 94% of the total energy released is captured as heat deposited by inelastic collisions with neighbouring nuclides. Additionally, a secondary heat source is provided by the radioactive decay of the fission products as they proceed towards stability. Each ^{235}U fission will release two or three neutrons at high velocities that will interact with the surrounding environment. By moderating and reflecting these neutrons back into the fuel, the same fission process can be initiated and a chain reaction established. If controlled with other neutron absorbing systems, this process provides a stable heat source for use in a steam supply system.

The CANDU series of reactors are heavy water moderated, heavy water cooled pressure tube reactors designed specifically for natural uranium fuel. Heavy water slows down neutrons effectively without wasting them by absorbing neutrons. The reactor's horizontally orientated core configuration is a characteristic feature of CANDU that facilitates online refuelling for continuous operation. In contrast, light water reactors utilize enriched uranium fuel in a vertical arrangement, which requires off-line batch refuelling. The CANDU core houses all the critical components necessary to sustain a fission chain reaction. It is mainly contained within a stainless steel cylinder called the calandria vessel. This vessel holds the heavy water moderator at relatively low temperature (<80°C) and pressure (0.1MPa) [5]. The ends of the cylinder are closed with two parallel end shields that are perforated with holes for the fuel channels. Depending on whether the reactor is a CANDU-6 or CANDU-9 series, 380 or 480 calandria tubes are fastened between the end shield holes to form the fuel channels and make a leak-tight tank. An illustration of the calandria vessel geometry as part of the reactor core is presented in Figure 1-1.

Furthermore, the primary heat transport system (PHTS) is the pressurized coolant loop running through the reactor that is responsible for moving heat from the fuel to the steam generators. The heavy water coolant is pumped through the PHTS at a pressure of 10 MPa and enters the core at a temperature of approximately 260°C before exiting at 310°C [5]. As the reactor ages, friction losses within the coolant can increase from greater flow disturbances across the fuel string. This results in pressure energy being converted to heat and a corresponding rise in the coolant temperature. Towards the end of the pressure tube design life, the exiting temperature could be 15°C higher. Inside the fuel channels, coolant flows though pressure tubes which are supported

and separated from the calandria tube by garter springs. Each pressure tube contains 12 to13 half-metre long fuel bundles that are loaded by fuelling machines at both ends of the reactor. A horizontal axis for the reactor, combined with opposing directions of flow through adjacent channels, permits the use of two identical fuelling machines, one to insert new fuel at one end and one to remove irradiated fuel at the other end. After removing heat from the core the heavy water coolant is transferred to the steam generators to exchange heat with a separate light water steam supply system. A schematic of the reactor core including the full steam supply system with the turbines is presented in Figure 1-1.

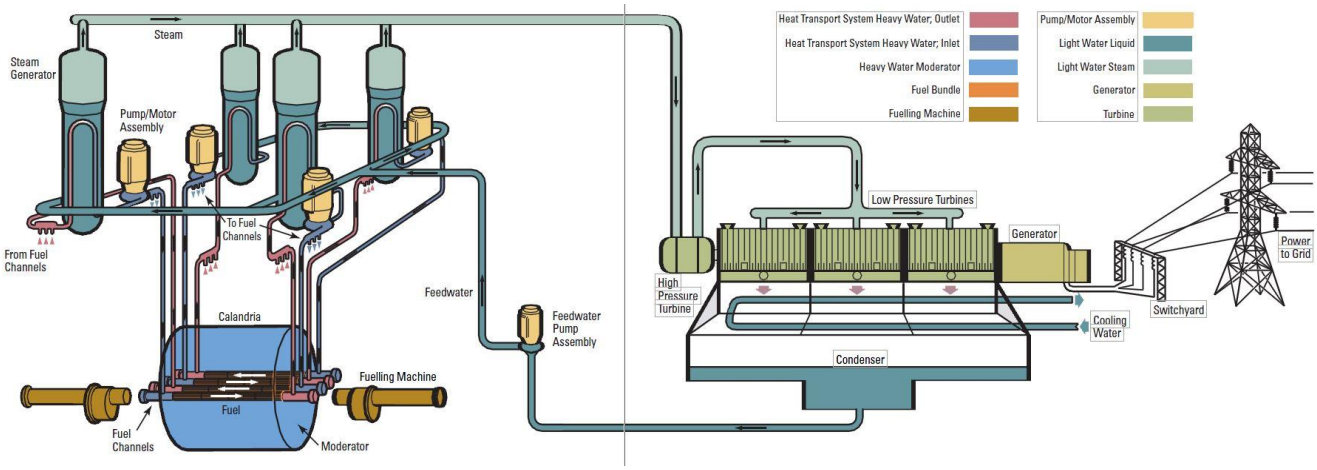

Figure 1-1: Schematic of a CANDU reactor core with the Nuclear Steam Supply System [6].

The CANDU fuel bundle is designed to maximize the amount of heat exchange between the uranium fuel and the heavy water coolant. At the same time, the design must be structurally robust to handle large in-reactor forces in order to prevent unwanted release and transport of radioactive fuel and fission-products within the PHTS. The UO_2 fuel is manufactured into small cylindrical ceramic pellets that measure roughly 12 mm in diameter by 16 mm in length. A Zircaloy tube cladding is used for its neutron transparency and resistance to aqueous corrosion to

isolate and contain the individual fuel pellets from the coolant. Approximately 30 fuel pellets are arranged end-to-end and placed inside a Zircaloy-4 sheath and sealed with end caps to produce what is known as a fuel element. The roughly initial 40 μm gap between the fuel pellets and sheath is filled with helium gas during end cap sealing to help provide efficient heat transfer from the fuel to sheath before the sheath collapses on the pellets. A graphite-based coating, called CANLUB for CANdu LUBricant, is applied to the inside sheath surface to protect against corrosive iodine fission products and mitigate stress-corrosion cracking (SCC) in the sheath. A fuel bundle is produced by assembling either 28 or 37 fuel elements, depending on the type of CANDU, in a concentric multi-ring shape and welding the endcaps to rigid endplates. Separation of fuel elements from each other is maintained by brazing spacer pads to the sheath's surface at the element mid-plane. Larger spacers called bearing pads are brazed to the outer ring fuel elements to provide adequate spacing between the pressure tube and bundle inside the fuel channel. The appendage spacing forms a coolant passage in the pressure tube for water to pass between adjacent elements, known as subchannels, as well as around the outside to extract the heat generated from fission. A schematic containing a cross section view of a fuel bundle in a pressure tube and an isometric view of a 37-element fuel bundle are shown in Figure 1-2.

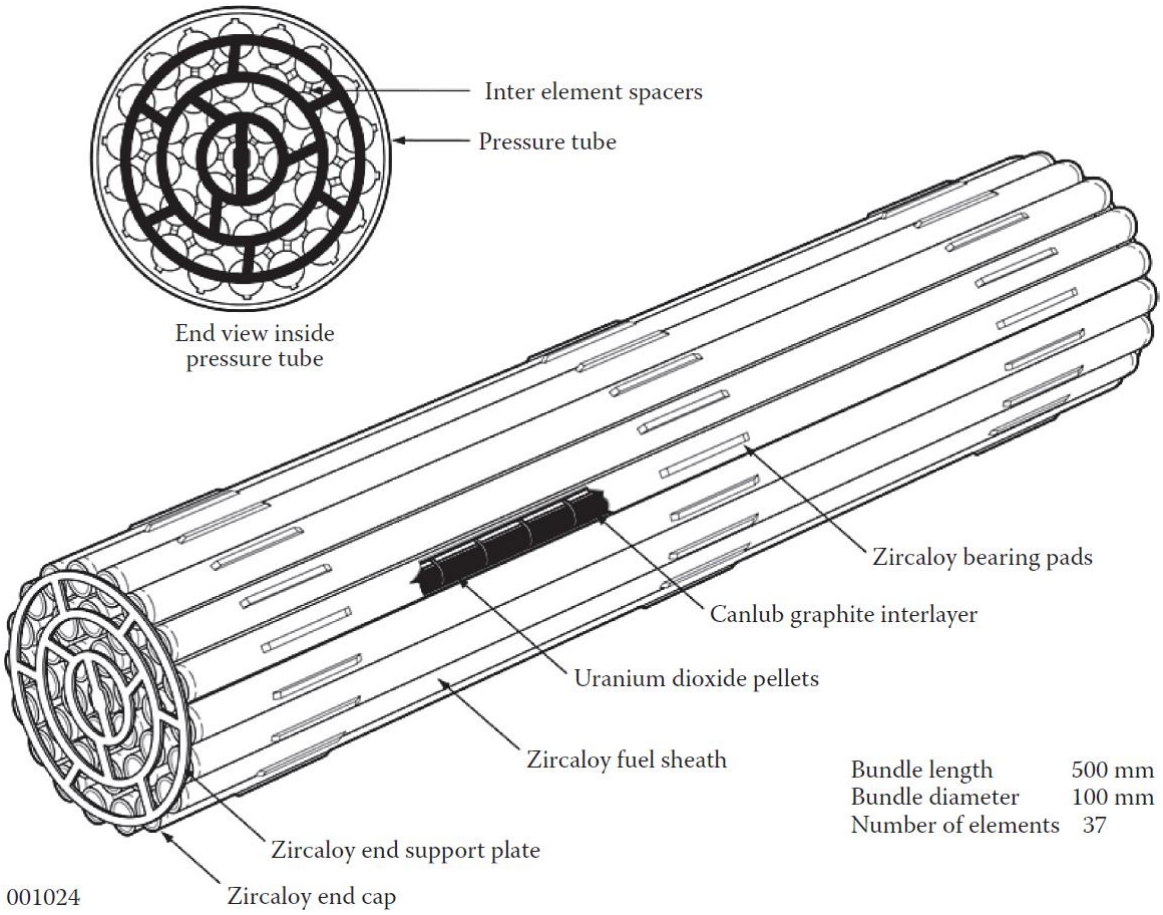

Figure 1-2: Schematic view of a CANDU 37-element fuel bundle with labelled components [5].

The 37-element CANDU fuel bundle is qualified to operate within a power verses burnup envelope that was derived from various fuel management simulations. It encompasses all bundle power histories based on operating experience along with added power to provide margin. The original envelope, called the Nominal Design Bundle Power Envelope, was based on the predicted performance of Bruce Nuclear Generating Station-A at 100 % full power [7]. A Nominal Design Peak Bundle Power was estimated as the maximum limiting bundle power to operate under the envelope, which corresponded to the plutonium peak at a burnup around 60 MWh/kgU. Values at other burnups were defined by normalising to the shape of the time-averaged fueling simulations. Since time-averaged powers were used, power ripples during

refueling results in a small number of bundles exceeding the nominal design power curve for a short time. Therefore, an overpower curve, slightly higher than the nominal design curve, was made to produce the Reference Overpower Envelope (ROE). The overpower curve is not a design or operational limit but rather a safety limit imposed on operation as bundle performance is not validated for powers that deviate higher from those given by the envelope. Fuel performance evaluation such as fission gas release or sheath strain are evaluated for fuel power histories defined by these envelopes and fuel integrity is verified by both out-reactor tests as well as in-reactor irradiation tests performed within experimental loops. When a reactor is operating under Normal Operating Condition (NOC), fuel bundle powers are within the envelope and damage is not expected to occur to the fuel or structures within the reactor core, provided the channel coolant conditions and pressure drop across the fuel string are normal. Under NOC, the fuel sheath surface should remain wet at all times to prevent the onset of local sheath dryout. Post-dryout heat transfer can lead to thermally induced phenomena such as fuel element bowing due to large thermal gradients. These deflections can put the integrity of the fuel and fuel channel at risk. There is adequate margin available during NOC and at the ROE before the Critical Channel Power (CCP) is reached for dryout to occur. However, during transients or accident sequences, abnormal thermalhydraulic conditions in the fuel channel can lower the CCP and reduce the available margins to dryout. To prevent fuel from operating outside of the qualified envelope, a set of reactor trip parameters must be defined to stop the reactor and prevent fuel damage. The Canadian Nuclear Safety Commission, as a regulator, published guidance document G-144 recommending the set of parameters that could be used for the trip parameter acceptance criteria in the licensee's safety analysis [8]. Adopting these parameters allows the licensee to demonstrate that direct or consequential failures of reactor fuel or pressure tube

failures due to any fuel failures are precluded. Fuel channel thermalhydraulics during post-dryout heat transfer are very complex and the effects on fuel behaviour during a transient are very difficult to analyze. The prevention of intermittent fuel sheath dryout in G-144 is a conservative trip parameter that greatly simplifies safety evaluations. Moreover, limited in-reactor experiments have indicated that operational margins exist when compared to those stated in G-144. The potential to relax the trip criteria in G-144 has been an ongoing discussion between industry and the CNSC. Expanding the fuel bundle experimental database for high temperature contact experiments is a necessary step as part of verification and validation of any proposed amendments to the trip parameters in the future. The purpose of this thesis is to provide a numerical modelling tool to assist in narrowing the knowledge gap for fuel element deformation behaviour at high transient temperatures. The use of numerical simulations to evaluate transient thermal behaviour of fuel elements can be used to guide new experiments as well as provide insights into physical phenomena observed in previously conducted experiments [9]. The development of a 3-D model utilizing the finite-element method to examine fuel deformation under post-dryout heat transfer conditions could be used as a tool to help better understand the effects of thermally-induced phenomena. The development of a one-way coupled thermal-mechanical model is presented in this thesis to simulate the deformation behaviour of a full-length fuel element in contact with the pressure tube at the onset of dryout.

2 Background

2.1 Boiling Heat Transfer and Dryout

Inside a fuel channel, energy is transferred from the fuel to the coolant by forced convective heat transfer. At low sheath temperatures, the heat transfer is dominated by single-phase convection to the liquid coolant. If the surface temperature begins to rise as a result of a transient, local subcooled boiling along the sheath will initiate small vapour bubbles to nucleate on the surface. These vapour bubbles grow into the cooler surrounding fluid where they collapse and generate turbulence within the liquid. This turbulent mixing causes a rise in the rate of heat transfer which acts as an effective mechanism for cooling the heated sheath surface [10]. It is therefore advantageous to operate within the nucleate boiling regime to obtain the largest surface heat flux at the cost of a marginal increase in wall temperature. However, if the wall temperature continues to rise then at some point the bubble formation will saturate and rather than collapse they will collect together to produce voids in the liquid. This is known as transition boiling because the increase in vapour quality causes a change in the heat transfer regime to two-phase forced convection. The subsequent effects of this changeover are a sharp decrease in surface heat flux with a corresponding rise in wall temperature. As the flow continues downstream the liquid film on the heated surface becomes very thin and interacts with the vapour formation. If the liquid film becomes sufficiently thin, the shear force of the void or vapour blanketing of the surface can strip the liquid film from the wall. The heated surface which is normally cooled by a liquid film, overheats, and leads to film dryout [10]. In the post-dryout regime, heat is transferred to saturated vapour causing a substantial deterioration in surface heat flux and a drastic rise in wall temperature within the liquid deficient region. The evolution of the flow and heat transfer regime as one progresses up to dryout and beyond is illustrated in Figure 2-1. Reversible

transitions between regimes are possible if local flow conditions change and rewetting of the fuel surface occurs. The maximum heat flux that can be maintained before dryout is known as the Critical Heat Flux (CHF) and occurs prior to the transition into the two-phase flow regime.

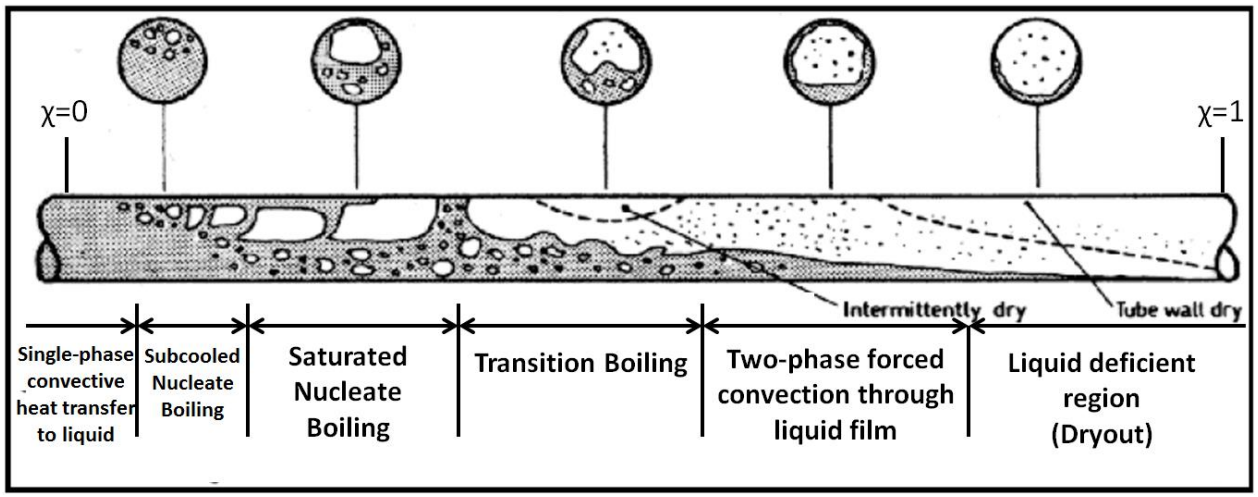

Figure 2-1: Vapour flow patterns during transition from single-phase to two-phase flow in a horizontal subchannel [11].

2.2 Subchannel and Bowing Analysis

It was mentioned that coolant flow passes in-between adjacent fuel elements, known as subchannels, to remove the heat generated by fission. The subchannel geometries are defined by control volumes that bound the flow area between neighbouring elements by connecting imaginary lines between the centers of adjacent elements. Applying this definition to a 37-element bundle creates 60 individual subchannels as shown in Figure 2-2.

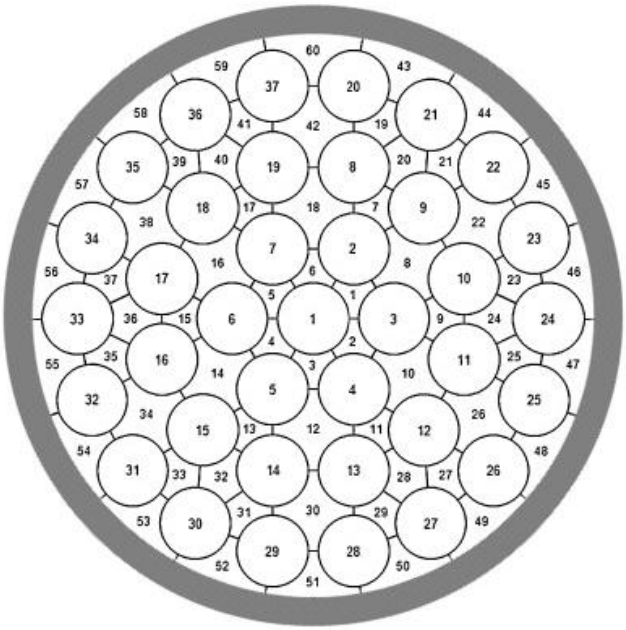

Figure 2-2: Subchannel control volume definition for a reference 37-element CANDU fuel bundle. A total of 60 subchannels are defined with 5 unique shapes [12].

The circular geometry of the fuel bundle and radial pattern of the fuel elements creates a set of varying sized control volumes. Consequently, the volume of coolant passing through each subchannel is not evenly distributed throughout the fuel channel. This can cause diverse flow distributions and multiple heat transfer regimes to arise around the circumference of each fuel element. As a result, temperature differences around the fuel and sheath can develop and produce differential axial strain in the fuel element. Bending moments, produced from uneven axial deformation, force the fuel element to deflect (bow) in the direction of the hotter side.

The present understanding of the bowing phenomenon suggests that fuel element deformations are primarily due to bending moments produced by thermal and mechanical mechanisms. The theory of Veeder and Schankula suggest that the thermal mechanisms are derived from asymmetric temperature distributions in the fuel pellets and sheath due to: (i) non-uniform temperature in the coolant surrounding an element due to imperfect mixing, (ii) non-uniform heat

transfer between the sheath and coolant due to variations in subchannel geometry and local flow conditions, (iii) asymmetric heat generation in the pellets due to neutron flux gradients across an element and (iv) differential thermal expansion between the sheath and pellet stack [13]. The complex interaction between these contributors make element bowing predictions difficult. Under NOC, both analysis and experimental results indicate the predominate factor in element bowing results from condition (iii). During a transient however, changes in subchannel conditions may cause local dryout to develop on one side of an element and leave the other side with sufficient cooling. In this flow scenario, the contributor expected to dominate the bowing process would be condition (ii). Other bending moments can arise from external loads such as gravity or hydraulic drag. It is crucial to understand and predict bow mechanisms as the potential for large thermal gradients, in transient situations, could cause large element deformations that challenge bundle integrity within the fuel channel. It is therefore desirable to operate as close to the CHF as possible to maximize heat transfer efficiency, while preventing excessive bow that could jeopardize fuel integrity.

2.3 Regulations that Address the Prevention of Fuel Sheath Dryout

The Canadian Nuclear Safety Commission (CNSC) is responsible for licensing Canadian nuclear energy corporations who wish to operate power reactors. To ensure safe operation, the CNSC requires licensees to demonstrate that sufficient safeguards are in place to meet requirements stated in regulatory documents. In Canadian Standard Association (CSA) standard N290.1, Requirements for Shutdown Systems for Nuclear Power Plants, it is specified that the integrity of fuel in the reactor, with no prior defects before an event, as well as the pressure tube as part of the Primary Heat Transport System, should not directly or consequentially fail due to fuel failure [14]. The CNSC's perspective is that the prevention of fuel sheath dryout is a reasonably

conservative criterion which should determine the setpoints for the reactor trip parameter. If no dryout occurs, there will always be sufficient heat transfer from the fuel to the coolant to prevent internal heat buildup and melting of the fuel. On the other hand, the licensees strive to operate with as much boiling as possible to maximize the effective power generation. One argument is that if dryout occurs, the low conductivity of the uranium dioxide fuel would limit the rate of rise in the fuel sheath temperature. Thus, there would be enough time to shut down the reactor before the integrity of the fuel sheath was at risk.

To assist licensees, the CNSC developed Regulatory Guide G-144 to encourage licensees to adopt a certain trip parameter acceptance criteria in their safety analysis to ensure the requirement stated above is met. In theory, imposed design limits to ensure the integrity of the sheath material should be expressed in terms of structural design parameters, e.g., stress and strain limits. However, this is not the case because it is not practical to measure the complex behavior of materials in irradiated and thermal environments characteristic of power reactors. For this reason, safety limits in power reactors have been imposed directly on certain temperature and heat fluxes. The trip parameter acceptance criteria for G-144 include the following [8]:

1. The primary trip parameter predefined limit on each shutdown system should be selected so as to prevent the onset of intermittent fuel sheath dryout; and
2. The backup trip parameters predefined limit on each shutdown system should be selected so as to prevent:
    a) fuel sheath temperature from exceeding 600°C, and
    b) the duration of post-dryout operation from exceeding 60 seconds

2.4 Post-Dryout Concerns - Challenges to the Fuel Element and Fuel Channel Integrity

Fuel sheath integrity is a very important parameter which characterises the integrity of the fuel bundle as a whole. The fuel sheath acts as a containment barrier and once it has been breached, radioactive and toxic fission products can migrate through the primary heat transport system. The rise in sheath surface temperature following dryout can induce a number of physical phenomena that can challenge the sheath integrity. The first mechanism is known as sheath ballooning. The reduced heat removal during dryout will cause a local increase in fuel pellet temperature and therefore an increase in thermal expansion and fission product gas (FPG) release to the pellet-sheath gap. The transport of the FPG from the grain boundaries to the pellet surface causes an increase in internal element gas pressure and subsequently reduces the gaseous component of the thermal gap conductance by diluting the helium filler. This can lead to a further increase in pellet temperature and initiate a positive feedback process. Once the internal gas pressure exceeds the subchannel coolant pressure, the fuel sheath will lift off from close pellet contact and expand outwards both radially and axially inducing large strains, hence the term ballooning. The second mechanism of concern is embrittlement due to sheath oxidation. Faster oxide layer growth during dryout will affect the sheath's ductility, which may affect its integrity when subjected to the thermal loads experienced during rewetting. Also, this oxidation process exposes the sheath to rapid hydriding. Hydrogen ingress in the Zircaloy sheath will influence the material strength and ductility which could make it susceptible to overstrain during cool-down. Although each mechanism is a potential concern, they require prolonged exposure to dryout conditions and would generally become damaging only after fuel element deformation has already occurred. Therefore, during the transition to dryout, the most challenging aspect of the fuel bundle to the PHTS integrity is fuel element bowing.

Fuel element deflections can put both the fuel sheath and pressure tube integrity at risk. The pressure tube is a pressure boundary of the PHTS and any possible interaction which may affect its integrity must be well understood. The prevention of fuel sheath dryout in G-144 was adopted in part due to our limited understanding of the interaction behaviour between the fuel bundle and pressure tube. Two specific fuel channel interactions of concern are fuel element to fuel element (FE-FE) contact and fuel element to pressure tube (FE-PT) contact. Inter-element spacer pads and outer-element bearing pads maintain a close spacing of roughly 1 mm between these components. However, out of plane deflections between appendages may reduce these separations and allow possible interaction. Fuel element deflections can be driven by a combination of bow and sag. Sagging is deformation caused by the continuous load of gravity acting on the pellets and sheath. At high temperatures, the sagging rate can accelerate as the sheath undergoes plastic deformation, including enhanced creep during alpha-beta phase transformation. Bowing of a fuel element will deflect in the direction of higher temperature due to larger thermal expansion. Once bowing initiates, a sufficiently strong feedback mechanism may occur, where higher fuel temperatures and element bowing would amplify each other. Further bowing can lead to higher temperatures and an unstable process may occur. As a result, fuel element deformation would continue until stopped by a physical constraint. In FE-FE contact, failure of the sheath could occur from localized coolant depletion, overheating or sheath oxidation. In FE-PT contact, failure of the sheath or pressure tube could occur from similar local flow starvation if the moderator does not have enough sub-cooling margin. The uncertainties associated with predicting bowing behaviours, combined with the limited number of experiments investigating the transient nature, have contributed to the selection of dryout prevention as part of the current trip parameters.

Calculations performed in safety analyses assume as-fabricated geometries for component specifications. Dimensional changes occurring from chemical and physical wear throughout reactor operation are not sufficiently accounted for in the original safety analyses. The high temperature and pressure environment of a nuclear reactor will certainly alter original geometry configurations over an operating life cycle. Aging phenomena are physical effects that are induced on system components that progressively effect operating conditions negatively. For example, increased diametral creep of the pressure tube is a known aging phenomenon affecting subchannel thermalhydraulics. During operation, the pressure tube is subjected to the high temperatures of the coolant, the weight of fuel bundles and high radiation. The constant force of gravity will cause the pressure tube to sag and the length and diameter will increase due to creep. This new geometry has a larger cross-sectional area for coolant to pass over the fuel bundles rather than through them (see Figure 2-3). The increased flow-bypass reduces flow through the subchannels, which will have a direct impact on the CHF value. As a result, dryout could occur sooner at a lower sheath temperature than those assumed in safety analyses. This implies that the risk of bundle deformation with aged components can be worse than with unaltered original geometries. One solution the industry has developed to counter aging and reclaim margin to dryout is to modify the design of the fuel bundle. The outcome was the 37-element modified bundle (37M) which differs from the regular bundle (37R) by a reduced center element diameter of roughly 1.5 mm to increase subchannel flows. Despite this improvement, the inability to precisely measure fuel element positions inside a channel, and any corresponding impact on CHF, emphasizes the importance of avoiding dryout scenarios in aged component systems, in order to maintain adequate safety margin through prolonged operational life.

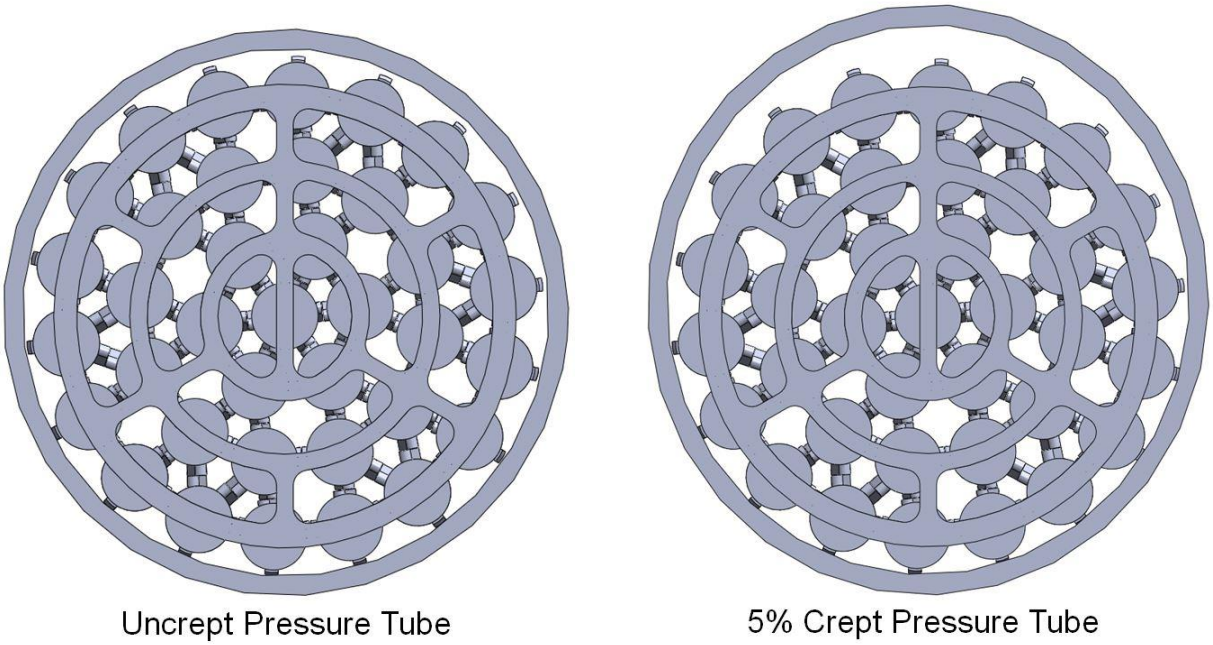

Figure 2-3: End view of a CANDU 37-element fuel bundle resting in an uncrept (left) and a 5% crept (right) pressure tube. The flow by-pass area for the crept pressure tube has increased allowing more coolant flow over the bundle rather than through the subchannels.

3 State-of-Art

Nuclear fuel performance codes are computer programs developed by the industry to predict fuel behaviour during operation. They are extremely important in safety analyses for determining appropriate operational safety margins. Fuel performance codes in Canada are tested and rigorously verified against experimental data in order to become Industry Standard Toolsets (IST's). In Canada, the CANDU performance codes ELESTRES and ELOCA have together successfully simulated CANDU fuel behaviour over a range of operating conditions for many years [15] [16]. Despite their prolonged success, the models used in these codes are fundamentally 1-dimensional, which limit their use for predicting fuel element deformation during upset and accident conditions. Alternative models designed specifically to assess deformation behaviour must be used.

3.1 Fuel Element and Bundle Deformation Models

A tool with the ability to predict fuel element bowing inside a reactor can be used to help demonstrate the integrity of a fuel bundle or its surrounding components, like the pressure tube, under different reactor conditions. In 1989, M. Tayal developed the BOW computer code to provide a fresh tool for predicting fuel element bow [17]. The code was developed based on the Veeder-Schankula model [13] for predicting fuel element bowing. Validation of this code is limited and it is not recognized as an Industry Standard Toolset. Since its inception, multiple improvements have been made to expand the codes capabilities in assessing performance parameters. However, solving requires the directional bending moments to be decoupled, essentially limiting the codes dimensionality to 1. More recently, the development of multidimensional and multiphysics models using commercial software have attempted to improve upon the limitations of the BOW code [18] [19] [20] [21] [22]. An overview of the

BOW code and other predictive fuel element deformation models developed with commercial platforms are discussed below.

3.1.1 Bow Code

The BOW code is a computer program developed at AECL Sheridan Park (now CANDU Energy Inc.) to simulate simultaneous elastic and elasto-creep deformations of all fuel elements within a fuel bundles under normal operating conditions. The code treats each fuel element as a composite beam made up of one-dimensional beam elements. BOW calculates deflections in both lateral directions due to temperature variations in the pellet and sheath, neutron flux gradient across the bundle radius, gravity, hydraulic drag force, and sheath creep. The code is based on linear elasticity theory of solid mechanics and utilizes the finite element method to numerically solve the governing equations. Although the BOW code has not been extensively validated, it has been verified against closed-form analytical solutions and other independent solutions for a total of 129 cases. As well, it has been benchmarked against two experimental post-irradiation measurements to demonstrate its accuracy for predicting in-reactor deformation behaviour under NOC [23].

The use of a composite beam formulation, as implemented in BOW, simplifies the fuel element geometry into an idealized form. This reduction in dimension and complexity removes features which would interact and contribute to the fuel element stiffness. In order to capture the important 3-dimensional phenomena that contribute to bowing, the BOW code includes two user defined factors to mimic and account for the loss of functionality. The first parameter introduced in BOW is the Curvature Transfer Factor (CTF), which describes the extent to which a pellet can transfer its curvature to the sheath. The flux gradient across a fuel pellet induces local curvature,

which differs across the pellet diameter. The CTF varies between zero, for the case where slipping occurs at the pellet-sheath interface allowing pellets to bend without bending the sheath, and a value of one when no slipping occurs and the total curvature of the pellet stack is imposed on the sheath. Next, a second parameter is introduced called the Rigidity Enhancement Factor (REF), which is a measure of the ability of the pellet stack to assist the sheath in resisting the bending moment. The REF varies between zero, for when pellets provide zero resistance to bending, and a value of one for when the sheath is fully capable of imposing its curvature on the pellet stack, and the flexural rigidities of the sheath and pellet stack both resist the applied bending moments. Also, BOW considers the ability of cracked pellets to partially resist bending of the sheath by adjusting the neutral axis of the pellet stack, in the moment of inertia term, when computing the flexural rigidity. Although these adjustment factors can be tuned to match the experiment of interest, they are unlikely to be predictable in any specific transient scenario. The limitation of guessing these empirical values in advance make the BOW code unreliable for predicting fuel element behaviour with the certainty required for safety analysis.

3.1.2 Multidimensional Multiphysics Models

In order to accurately model a real phenomenon, one requires an exact representation of the geometry and boundary conditions, which are present in the interacting system. Unfortunately, this type of precision is rarely possible and often simplifications are made during the development process. This can lead to the use of artificial assumptions in order to satisfy mathematical constraints (boundary conditions). The advancement of computer technology over the past few decades has provided an opportunity to progress multidimensional and multiphysics commercial software. The ability to better represent coupled systems with fewer simplifications has driven modelling research across many industries, aiding growth and interest for nuclear

applications. The applicability of these commercial software packages, e.g., ANSYS, ABAQUS and COMSOL, for predicting fuel element deformation has been investigated through research initiatives performed by different groups including AECL (now CNL), COG and RMCC. Some recent notable achievements in CANDU fuel modelling are outlined.

COMSOL Multiphysics is a commercial finite-element software that is capable of performing a coupled thermo-mechanical analysis. A full fuel bundle deformation model was developed by Bell et al. using a beam element representation, considering a "weak form" of the virtual work principle within the structural mechanics module of COMSOL [18]. Similar to BOW, a 1-dimensional composite beam model is used for both fuel pellets and sheath with short straight-beam segments to model endplate components. A 2-dimensional heat conduction analysis is performed on a pellet-sheath cross-section and coupled to the beam analysis. The endplate and fuel elements are assumed to form a continuous weld such that endplate deformations calculated by beam theory provide boundary conditions for the fuel elements. The time-dependent heat conduction analysis considers fuel burnup, heat generation accounting for radial flux depression, and burnup dependent fuel-to-sheath gap conductance. Average fuel and sheath temperatures evaluated with the heat conduction model are used as inputs for the temperature dependent material properties. An empirical "gripping" factor is use to specifically couple the bending moments of the sheath and pellets to account for pellet-sheath interaction effects, analogous to those used in BOW. The bundle model was successfully benchmarked against analytical formulae of stress and strain for the deformation of a simple beam, an out-reactor experiment and a BOW code simulation of a dryout patch analysis. This work demonstrates COMSOL's ability to couple a thermo-mechanical model to examine fuel and sheath deformation behaviour.

However, a more advanced pellet-sheath contact model is necessary to examine and predict bowing in FE-FE or FE-PT contact analysis.

An alternative approach to beam analysis for modelling CANDU fuel element bowing is to use a more complex numerical method such as 3-dimensional solid-element modelling. This technique offers an alternative solution to account for the influence of pellet-sheath interaction by physically representing the pellet and sheath as interacting components. The use of a contact algorithm to account for the solid body interaction between the pellet and sheath removes the need for tuneable "gripping" factors as the resulting frictional forces, contact pressure and contact area between two surfaces can be calculated directly. ANSYS is a commercially available finite element program used in a wide variety of engineering fields for its multiphysics simulation capability. Its ability to couple thermo-mechanical systems and solve physical contact problems [24] [25] makes it an ideal platform for investigating thermally driven fuel deformations. Over the past decade, development of an ANSYS fuel model to analyze bowing has been pursued by Williams at CNL. Initial work lead to the development of a 3-dimensional 43-element CANFLEX fuel bundle model [19], which included fuel elements composed of a monolithic fuel stack, sheath, bearing pads, and end caps attached to end plates. The solid model was used to perform a simple thermo-mechanical test to determine its capability and assess qualitative behaviour. The successful response verified the feasibility of ANSYS and lead to the development of a single fuel element model. The initial fuel pin model was benchmarked against a fuel element simulator experiment, which investigated thermally induced bow caused by a circumferential temperature variance. The motivation for this experimental comparison was to investigate solid-element bowing behaviour and assess the limits of the fuel model to determine

if individual pellets were necessary over a simplified monolithic stack, where pellet-pellet interactions could be ignored. The verification study demonstrated that when mechanical interactions between the fuel and sheath are high, a monolithic stack successfully emulates the structural response, under those experimental conditions. However, when the interaction is low, the fuel must be modelled as individual pellets to capture the correct fuel element response. This work provided useful insights for future solid-element modelling and offered an illustration of ANSYS's ability to capture the bowing phenomenon. Since this early work, Williams has advanced his single fuel model to a full 31-pellet fuel element with the use of two planes of symmetry. The model captures both the thermal and mechanical contact interaction between every pellet and sheath surface. Fuel and sheath material properties are entered via a temperature-dependent look-up table and are approximately equivalent to those used in ELESTRES and ELOCA. The model is capable of a transient analysis and includes time dependent features such as creep, pellet-sheath gap heat transfer and internal gas pressure [20]. The model has shown to be a useful tool for mimicking 3-dimensional fuel behaviour and has the potential ability to predict bowing and sagging under off-normal and accident conditions. Although success has been achieved with the model, there are limitations as with any computer code. Flexural rigidity testing of the fuel element model has shown how the precise dynamics of the pellet-sheath interaction can influence the 3-dimensional behaviour. Factors such as the coefficient of friction and initial pellet spacing were shown to contribute to the overall fuel element stiffness. These initial boundary conditions would likely be difficult to predict and therefore proper parametric studies are required to ensure that the uncertainties in the model predictions are appropriately characterized. Other limitations of the model arise from difficulties associated with obtaining a numerically converged solution. Although symmetry is used to

reduce complexity and assist convergence, quick changes in contact status between the pellets and sheath during a transient can cause instability for the large number of interacting contact surfaces. For example, simulating sheath detachment from the pellet surface during fuel element cooling cycles can lead to unconstrained motion of the pellets, which is numerically difficult to solve. The recent addition of a contact stabilization feature in ANSYS 14.5 has improved the stability to obtain convergence although its impact on the solution results has not been quantified.

Furthermore, a solid-element 3-dimensional model of a smaller size fuel element was developed on the ABAQUS platform by McCluskey [21]. Similar to Williams, solid modelling of the pellet and sheath geometries was used to simulate the pellet-to-pellet and pellet-to-sheath contact effects that influence fuel element deformation behaviour. The model was developed to investigate the ability of ABAQUS to simulate the dynamic nature of the fuel-to-sheath gap during power ramping. A single plane of symmetry was used to simplify the geometry, which included the following features; 11 fuel pellets, a sheath, internal heat generation, fuel-to-sheath gap conductance, internal gas pressure and temperature dependent material properties. The ABAQUS model was successfully benchmarked against an analytical beam calculation and a comparison of the predicted gap distance with the ELESTRES-IST code was performed for powers up to 30 kW/m. Convergence issues were encountered for higher power ratings which may have been the result of artificial constraints applied to the pellets. Also, an investigation into quantifying the Rigidity Enhancement Factor of BOW was performed although the inability of the model to handle contact effects at higher powers limited the characterization up to a linear

power of 30 kW/m. The effect of pellet cracking on the stiffness was not considered in this study.

Next, an assessment of using the state-of-the art Multiphysics Object Oriented Simulation Environment (MOOSE) framework, developed at Idaho National Laboratory, to simulate 3-dimensional deformation mechanisms of CANDU fuel elements was examined by Gamble [22]. MOOSE is a mathematical platform from which the LWR nuclear fuel performance code BISON is built. An independent fuel performance code named HORizontal nuclear fuel Simulation Environment (HORSE) was built upon the MOOSE framework to examine the capabilities and limitations of using the solid-element contact algorithms for modelling CANDU style fuel. The HORSE geometry utilized two planes of symmetry to produce a 31 pellet fuel element and included models for heat generation and transport, momentum conservation, temperature and burnup dependent material properties, fuel swelling and densification, sheath creep, sheath plasticity, pellet-to-pellet and pellet-to-sheath contact, and gas volume, pressure and composition. The various contact models available in MOOSE were tested and characterized to determine the optimal configurations for further bowing simulations. The contact algorithms behaved as expected for isolated contact analyses and fuel performance simulations when compared against analytical solutions and ELESTRES-IST. Element bowing behaviour was tested by performing flexural rigidity and thermal bowing simulations for predefined temperature gradients. The results of the stiffness simulation showed an unexpected fuel element response from lateral deflections indicating an underlying flaw in the glued contact algorithm. The results were presented to the BISON team for further investigation but until more testing is done the use of MOOSE for CANDU bowing analysis is not currently feasible.

Each model discussed has investigated a unique finite-element platform to determine whether improvements to current fuel element deformation models are possible. Success achieved in solid-element modelling has offered improvements over previous beam theory analyses. Employing physically based contact replaces the empirical approach used in BOW for coupling pellet-sheath interactions. Although a fully developed 3-dimensional fuel deformation model capable of simulating FE-FE and FE-PT contact is not readably available, the success achieved with previous models in simulating out-of-reactor bowing tests and fuel performance is promising for continued improvement and growth in deformation modelling. The ability to couple thermo-mechanical models, and simulate thermally driven deformation through multi-body contact interactions, make commercial finite-element software a viable option to model FE-FE and FE-PT contact in 3-dimensions. The development of a deformation model which is capable of simulating bundle behaviour in dryout conditions would provide a novel tool for aiding the understanding of fuel channel interactions.

4 Goals of Research

The computational complexity of 3-dimensional multiphysics models requires considerable resources to perform simulations. The development of a 3-dimensional CANDU fuel performance code with similar burn-up dependent physics to ELESTRES and ELOCA is still limited by computational requirements. The increase in the number of degrees of freedom between a 1-dimensional and 3-dimensional code can change the solving time from seconds to days. The models discussed in Chapter 3 are representative of current fuel deformation models and their limits in terms of the overall geometry scale and coupling of nuclear phenomena. Ideally, a full fuel bundle geometry resting inside a pressure tube that is capable of simulating all pellet-sheath interactions would most closely resemble the modelled reactor configuration. Unfortunately this level of detail would require software supporting high performance cluster computing, which is expensive and not easily accessible. However, a tool explicitly designed to investigate fuel channel interactions by thermally driven phenomena may only require a simplified geometry to represent the contact of interest. The relatively fast transient nature of fuel element bowing under dryout may allow certain nuclear phenomena, whose impact is expected to be small over a short time, to be excluded or coupled via an external code to reduce the model complexity. The development of a fuel deformation model is not intended to compete with a fuel performance code, but rather its intent is to utilize advanced numerical contact algorithms to mimic a fuel element response to mechanical and thermal loads that could lead to contact with the pressure tube or another fuel element. Although the possibility of developing a 3-dimensional model with the ability to predict fuel performance parameters and deformation is highly desirable, it is not being sought in this thesis.

The goal of the current work is to utilize the robust contact algorithms of ANSYS to investigate a fuel element's response to circumferential temperature differences in the ranges expected during post-dryout conditions. A model capable of simulating the bowing of a fuel element towards a pressure tube is chosen to offer insight into the associated knowledge gaps with FE-PT contact. The realized model is based on a 3-dimensional solid-element approach to account for pellet-sheath interactions and is used to:

1. Assess the effects of different fuel stack assumptions on the fuel element deformation profile through a flexural rigidity analysis. The relative contribution provided by the fuel stack to bowing deformation depends on several elements, such as pellet cracking and mechanical interaction with the sheath, which are generally unknown conditions. To understand these effects on fuel element bowing, the model must be characterized to account for these features. An Individual Fuel Pellet Model and Cracked-fuel Stack Model are investigated while considering different contact definitions such as frictionless and bonded.
2. Examine the thermal bowing of these different fuel models under predefined temperature gradients and compare against analytical solutions. Thermal loads can generate different moments than those produced by mechanical forces. It is necessary to characterize the different fuel element model behaviours to understand these differences.
3. Determine the ability of ANSYS to capture FE-PT contact under post-dryout heat transfer conditions. Drypatches can induce the necessary thermal loads to drive fuel element bow. Utilizing the characterized fuel element models, an assessment of the deformation magnitude and any potential contact with the pressure tube can be performed.

5 Finite Element Analysis

When nuclear fuel modelling codes first started being developed, FEA software was not utilized because computer resources were limited and the software was at a primitive stage. Fuel codes were developed on low-level programming languages and they required many conservative simplifications in the physics and spatial dimensions in order to run in a timely manner. Uncertainties in operational margins existed as these codes were at best only an approximation. As time progressed, computer technology advanced allowing FEA software to upgrade with an improved ability to handle complex problems. These days, FEA has become a very capable and popular means for research and development activities including engineering design, analysis and optimization. The simplicity of changing multiple variables in a computer code, and restarting a simulation, can be a competitive alternative to performing similar alterations in laboratory experiments. In addition, FEA can couple multiple physics together making it suitable for practical systems. For example, a thermal-structural analysis can first solve the thermal problem to acquire the temperature distribution, and then feed these results as inputs into a structural analysis for determining the total strain due to both mechanical and thermal loading. These multiphysics capabilities are now commonly available in commercial FEA programs. As discussed in Chapter 3, recent developments in coupled multiphysics nuclear fuel deformation modelling, utilizing commercial FEA software, has been underway at both the academic and industry level. The use of FEA offers a fresh approach to current day experimental design and safety analysis for nuclear applications. Performing modern day fuel bundle deformation experiments can be very expensive and obtaining the necessary regulatory approval to do so can be challenging. The work of this project builds on this modern FEA approach to produce a fuel

deformation model as a tool for providing insight into fuel channel interactions and potentially help guide future experiments.

5.1 Finite Element Method

The Finite Element Method (FEM) is the numerical technique used in FEA to solve engineering phenomena, expressed by governing equations and boundary conditions over a complex domain, for which closed-form solutions are not available. The physical interpretation of FEM can be described by the basic concept of subdividing a complex mathematical model into smaller disjoint components of a simple geometry, to create a new domain of individual pieces known as finite elements. The response of each element is expressed in terms of a finite number of degrees of freedom (DOF) characterized as the value of a field quantity at a set of connecting nodes. The field quantity is interpolated within elements by a polynomial function, which is explicitly evaluated at the shared nodes. The response of the mathematical model is determined by systematically assembling the individual responses of each finite element in a piecewise fashion. This technique is a powerful computational tool for performing engineering analysis on complex physical systems, governed by some underlying physics.

A characteristic feature of the FEM is it always provides an approximate solution to the partial differential equation governing the physical system. Replicating a physical system into a computer generated model requires artificial constraints and assumptions no matter the scale or intricacy of the system. The majority of these simplifications occur in the transfer of boundary conditions from the physical system to the model. Surfaces in reality are rough and continuous whereas FEM can only represent a surface with a finite number of nodes. This creates a

discretization error in the model which must be minimized in order to improve the representation of boundary conditions and calculation of gradients (stress, strain or temperature). The two techniques used to reduce this error are by increasing the number of nodes in the finite element mesh or increasing the order of the polynomial interpolation function. Increasing the number of nodes is accomplished by refining the mesh size in areas where boundary conditions and gradient results are of interest. If complex boundary conditions are not required and the model idealization error is small, higher order interpolation functions can provide greater accuracy with less sensitivity to the mesh spacing. As the discretization error is reduced, the results will converge on the correct solution for the system modelled. The model solution and the real physical solution will likely differ for complex domains as there will always be some inconsistencies in the model such as idealization of physical phenomena. Although each method to reduce error can be implemented to a certain degree, the computational expense may not be favourable. Therefore it is necessary to always be aware of potential limitations of the model and to recognize areas where results may not be precise. The goal is to approximate the exact solution as closely as possible or to the degree that is necessary for the analysis. This could mean simplifying the governing system to include only the relevant physics of interest that directly contributes to the desired output. For multiphysics systems, there may only be a few specific mechanisms which dominate the phenomenological system response being studied. This may permit the weakly coupled physics to be excluded without having a major influence on the results.

5.1.1 FEM Procedure

The Galerkin Method of Weighted Residuals is one numerical method used to approximate the solution to the differential equations being solved by FEM [26] [27]. The method is used to determine element formulations as well as global characteristic relationships as part of the FEM assembly. An illustrative example is given to demonstrate the solution process in FEA software like ANSYS.

Heat transport through a nuclear fuel bundle is a phenomenon governed by the heat conduction equation. Obtaining the temperature distribution in the bundle requires solving the boundary value problem. In this case, temperature is a field quantity and an approximate solution using the FEM can be found. A simple 2-dimensional triangle is used to represent the geometry under study. The first step is to break up the geometry into a finite number of elements. Depending on the shape and dimension of the problem, different shapes of elements may be used in this process. In general, 1-dimensional elements are represented by bars or beams, 2-dimensional planar elements are represented by quadrilaterals or triangular shells, and 3-dimensional solid elements are represented by hexahedrals or tetrahedrals elements. For some elements, a higher order version with more nodes is available for increased accuracy and use with complex geometries [26]. The choice of an element can be dictated by the shape of the geometry or the choice of the user. However, practise has indicated that hexahedral elements are favourable for representing larger structural geometries in 3-dimensions and should be incorporated when possible. In this example, a simple triangular domain can easily be broken into four discrete 2-D linear triangular elements with 3 connecting nodes (see Figure 5-1). This type of element is useful for illustrative purposes but their application is extremely limited as they can only represent constant stress or thermal distributions (or gradients) fields.

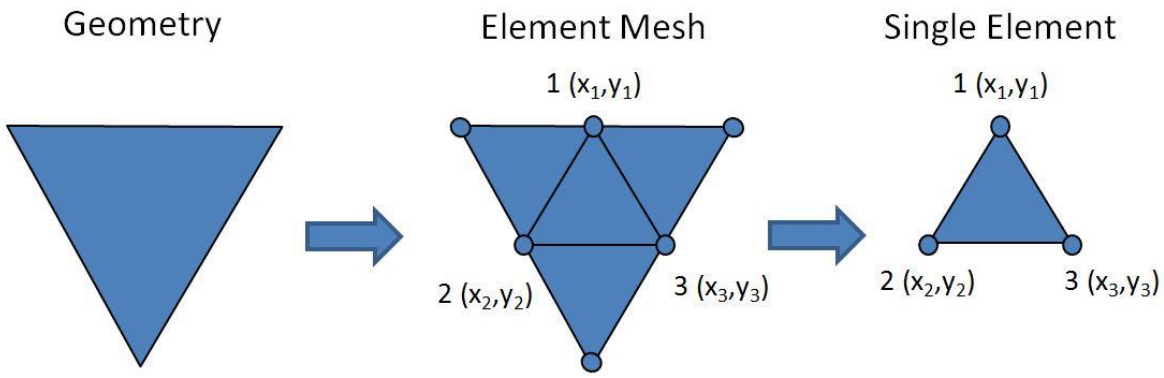

Figure 5-1: Finite element mesh. An initial geometry is partitioned into some finite number of elements which are defined by nodes.

The second step is to assign a polynomial function to represent the temperature distribution in the element. For a linear 2-D element with 3 degrees of freedom, the general algebraic equation describing the temperature at any node in the element can be written as:

$$T(x,y) = a_0 + a_1 x + a_2 y \tag{5-1}$$

where a_0, a_1 and a_2 are constants. This expression forms the basis for defining a set of three equations to describe the temperature at each node in an element. Assembling them into matrix form yields the following:

$$\begin{bmatrix} T_1 \\ T_2 \\ T_3 \end{bmatrix} = \begin{bmatrix} 1 & x_1 & y_1 \\ 1 & x_2 & y_2 \\ 1 & x_3 & y_3 \end{bmatrix} \begin{bmatrix} a_0 \\ a_1 \\ a_2 \end{bmatrix} \tag{5-2}$$

In order to solve for the unknown constants in terms of the spatial variables, the matrix is inverted to give:

$$\begin{bmatrix} a_0 \\ a_1 \\ a_2 \end{bmatrix} = inv\left(\begin{bmatrix} 1 & x_1 & y_1 \\ 1 & x_2 & y_2 \\ 1 & x_3 & y_3 \end{bmatrix}\right) \begin{bmatrix} T_1 \\ T_2 \\ T_3 \end{bmatrix} \tag{5-3}$$

These constants can be substituted into Equation 5-1 and relabelled to form Equation 5-4.

$$T(x,y) = N_1(x,y)T_1 + N_2(x,y)T_2 + N_3(x,y)T_3 \tag{5-4}$$

$N_i(x,y)$ are called shape functions or interpolation functions and they are used to define an expression for the field variable in terms of the nodal variables. In this case, the field variable is temperature, but in general it is the dependent variable of the boundary value problem. It was mentioned that the FEM gives only an approximate solution to the differential equation being solved. Therefore Equation 5-4 should be written as follows:

$$\tilde{T}(x,y) = [N_1(x,y)\ N_2(x,y)\ N_3(x,y))]\begin{bmatrix} T_1 \\ T_2 \\ T_3 \end{bmatrix} = [N]\begin{bmatrix} T_1 \\ T_2 \\ T_3 \end{bmatrix} \tag{5-5}$$

The third step is to apply these algebraic equations to the element formulation. Starting with the steady state heat conduction equation as our boundary value problem,

$$\nabla \cdot (k\nabla T) + Q = 0 \tag{5-6}$$

where k is the thermal conductivity, Q is internal heat generated and T is the temperature, the temperature given by Equation 5-5 can be substituted into Equation 5-6. The combined expression yields a statement that is no longer valid. This implies that the right hand side of Equation 5-7 must be represented by some nonzero residual function called $R(x,y)$.

$$\nabla \cdot \left(k\nabla \tilde{T}\right) + Q = R(x,y) \tag{5-7}$$

The resulting expression requires a numerical method called the Galerkin Method of Weighted Residuals to solve [27]. The method utilizes the polynomial shape functions as a set of basis functions to minimize the residual by determining the constants, T_i, by the following relation.

$$\int_A N_i(x,y)R(x,y)dA = 0 \tag{5-8}$$

This expression forms a system of linear equations, which can be solved to find the temperatures at the nodal locations of the 2-D linear triangular element [27]. However, an additional step must be executed before the calculation can be complete. Starting with the strong formulation given by Equation 5-9,

$$\int_A N_i(x,y)\left(\nabla\cdot\left(k\nabla[N]\begin{bmatrix}T_1\\T_2\\T_3\end{bmatrix}\right)+Q\right)dA=0 \tag{5-9}$$

the divergence (Green-Gauss) theorem is used to convert this complicated expression into a solvable form called the weak formulation [27]. This theorem is useful for converting a differential operator into an integral. Its application converts the surface integral of Equation 5-9 into a simpler form with a line integral as shown in Equation 5-10.

$$\int_A N_i(x,y)\left(\nabla\cdot\left(k\nabla\tilde{T}\right)\right)dA=\oint_\Omega N_i(x,y)\cdot\left(\left(k\nabla\tilde{T}\right)\cdot\vec{n}\right)d\Omega-\int_A \nabla N_i(x,y)\cdot\left(k\nabla\tilde{T}\right)dA \tag{5-10}$$

Substituting Equation 5-10 into Equation 5-9 and rearranging leads to the weak form representation of the 2D heat flow problem (Equation 5-11).

$$\int_A \nabla N_i(x,y)\cdot\left(k\nabla\tilde{T}\right)dA=\oint_\Omega N_i(x,y)\cdot\left(\left(k\nabla\tilde{T}\right)\cdot\vec{n}\right)d\Omega+\int_A N_i(x,y)\cdot Q\,dA \tag{5-11}$$

In this form, the left hand side represents the element's conductivity matrix, the first term on right represents the boundary load vector and the second term on right hand side is the internal load vector, which corresponds to the internal heat generated. A numerical integration method called Gauss Quadrature is typically used to approximate the integral of the elements conductivity matrix and force/load vectors [27]. It approximates the integral as the sum of Gauss weights multiplied by the function evaluated at the Gauss points. The 2-D summation is given by

$$I=\int_{-1}^{11}\int_{-1}^{11} f(\xi,\kappa)\,d\xi\,d\kappa\approx\sum_{i=1}^{n}\sum_{j=1}^{m}W_iW_jf\left(\xi_i,\kappa_j\right) \tag{5-12}$$

where W_i and W_j are the weight factors and ξ_i and κ_j are the sampling point locations, and is only valid over the range of -1 to 1. The accuracy of the approximation improves as more Gauss points are used and an exact solution may be obtained for a polynomial of degree 2*n*-1 for *n* integration points.

This process of assembly continues across each element in the geometry until all element conductivity matrices are collected. The next step is to build the global conductivity matrix and apply the known boundary conditions. The global conductivity matrix represents a nodal set of simultaneous algebraic equations that provide the value of the field quantity when solved. For linear static problems, a direct solver can be used to directly eliminate equations by backwards and forwards substitution. If nonlinear behaviour is present, an iterative solver must be used because the information needed to construct the conductivity matrix is not known in advance. The simple triangular geometry example is a trivial model to solve with a linear solver. However, in the thermal-mechanical model being developed in this thesis, the linear thermal analysis is coupled with a non-linear structural analysis, which requires the iterative solver. Therefore, a description of non-linear analysis is provided.

Nonlinear structural behavior can be classified under three principle categories: changing status, geometric and material [26]. Changing status nonlinearity occurs when the stiffness of the system depends on the interacting status. This behaviour is most commonly observed in contact problems due to changes in contact status. Geometric nonlinearities refer to the nonlinearities in components due to changing geometry as it deflects. The stiffness matrix is a function of the displacements and therefore large displacements and/or rotations require the equilibrium equations to be written in terms of the deformed geometry. Stresses within the deformed component cannot be determined because the final shape is not initially known. Material nonlinearity develops when stress is a nonlinear function of strain or material properties are functions of other constitutive variables and/or their derivatives. These complex materials follow a nonlinear constitutive law and their behaviour depends on the current deformation state and

possibly past history of the deformation. The implicit nature of these nonlinearities increases the model complexity and requires a different approach for solving the equilibrium system equations.

The Newton-Raphson (N-R) method is an iterative way to solve nonlinear problems in ANSYS [26] [27]. The method utilizes an incremental approach to find a solution to the nonlinear governing equations. Applied loads are subdivided into a series of load increments, which are applied over several substeps. The incremental form of the nonlinear governing equations is of the form:

$$[K(u)]\{u\} = [F^a] \tag{5-13}$$

By dividing the load vector, the solution can be constructed through a series of smaller linear steps, which converge in the appropriate direction, in order to closely approximate the exact solution. The incremental form of the governing equations can be expressed as

$$\left[{K_i}^t(u_i)\right]\{\Delta u_i\} = [F^a] - [{F_i}^{nr}] \tag{5-14}$$

where $\left[{K_i}^t\right]$ is the Jacobian matrix (tangent stiffness matrix), $\{\Delta u_i\}$ is the unknown incremental field quantity vector, $[F^a]$ is the incremental applied load vector and $[{F_i}^{nr}]$ is the restoring load vector (the loads corresponding to the element stresses) [26]. An initial guess of the solution vector, $u = u_0$, is used to determine the initial stiffness and begin the iterative process. The full load is applied and a linear approximation is made to calculate the magnitude of the incremental step using the initial stiffness.

$$\Delta u_1 = [K_0^t(u_0)]^{-1} F_a \tag{5-15}$$

Based on the first step, the equilibrium force, F_1, is determined with the updated stiffness matrix.

$$F_1 = K(u_1)u_1 \tag{5-16}$$

For a converged solution, the equilibrium force would be exactly equal to the applied load. Since the nonlinear equilibrium conditions are solved approximately, there will be some out-of-balance force between the two. This residual force vector is calculated by,

$$\Delta R_i = F_a - K(u_i)u_i \tag{5-17}$$

which provides the difference between the applied load vector and the equilibrium force vector based on the assumed solution. The residual load vector provides feedback on the appropriateness of the steps taken towards the exact solution, which satisfies the equilibrium equations. The residual load is checked for convergence against the specified tolerance to determine if further iterations are required. If the convergence criteria are not satisfied, the trial solution is updated with an incremental step,

$$u_{i+1} = u_i + \Delta u_{i+1} \tag{5-18}$$

which requires an updated solution vector given by an incremental change in load and an updated tangent stiffness matrix.

$$\Delta u_{i+1} = \left[{K_i}^t(u_i)\right]^{-1}([F^a] - [F_i]) \tag{5-19}$$

This leads to the computation of the new residual load vector given by

$$\Delta R_{i+1} = F_a - K(u_{i+1})u_{i+1} \tag{5-20}$$

This iterative process is repeated until the imbalance between the internal forces, given by the equilibrium load, and the applied force is less than a specified amount ($|\Delta R_{i+1}| < Tolerance$).

5.1.2 3-D Solid Element Contact

The biggest advantage of using FEA for simulating fuel element deformation is the ability to explicitly model pellet-sheath contact interactions. This offers an alternative method to the

empirical approach currently employed in beam analysis. Modelling the pellet and sheath as separate components permits multi-body contact between pellet-to-pellet and pellet-to-sheath to better predict the stiffness of the system. In addition, solid element modelling can incorporate irregular features like pellet dishing and sheath appendages to more accurately represent the fuel design. When these features are included, fuel element phenomena like sheath bambooing and pellet hourglassing become inherently simulated in the model. Contact can also simulate macroscopic behaviour such as surfaces separating or frictional forces on the relatively small scale of a fuel element. The importance of contact modelling in a fuel deformation model is an obvious, yet difficult requirement. Several commercial FEA software packages are capable of simulating the mechanical and thermal interaction necessary for a FE-PT contact analysis. However, ANSYS is selected for this investigation because it possesses very strong contact modelling capabilities, robust solving algorithms, strong coupling between thermal and mechanical solutions and has been demonstrated as a successful candidate for CANDU fuel element deformation studies by Williams [19] [20]. To gain an understanding of the solid element contact behaviour in ANSYS, a description of a penalty-based contact algorithm is discussed.

In ANSYS, contact is a changing-status nonlinearity because the stiffness of the system depends on the contact status, which is determined by whether bodies are touching or separated [24]. This must be determined in the analysis as the position of bodies can change with applied loads. When physical systems come into contact, they do not interpenetrate because they are continuous. It was previously mentioned that surfaces in FEM are not truly continuous because they are composed of discrete nodes. In order to enforce the constraint that bodies in contact do

not penetrate each other in the model, ANSYS employs a contact algorithm to enforce compatibility in a contact region. The algorithm establishes a relationship between the two surfaces to prevent them from passing through one another when close. This can be accomplished with a numerical penalty-based contact formulation. The idea is to use artificial springs to resist penetration by generating stiffness between surfaces. The artificial springs are activated once penetration occurs. A counter pressure is applied by the springs to the surfaces to try and achieve a penetration of zero (Figure 5-2). The contact force is given by

$$F_{contact} = k_{normal} \cdot x_{penetration} \tag{5-21}$$

where k_{normal} is the contact stiffness normal to the Target surface and $x_{penetration}$ is the interpenetration depth between solid surfaces [28]. The solution iterates until no significant change in the contact force occurs. The contact stiffness is a user defined value which can be related to the modulus and size of the material in contact. As the contact stiffness is increased, the amount of penetration will decrease.

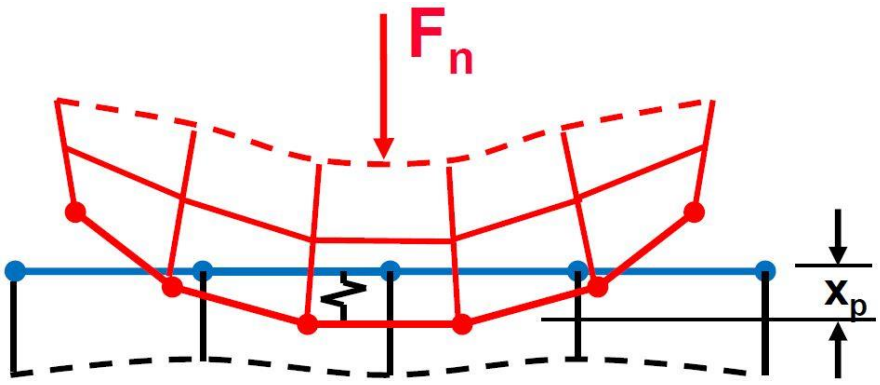

Figure 5-2: A finite normal force brings two bodies into contact where interpenetration occurs. The counter contact force is determined by the normal stiffness and penetration distance shown as x_p [28].

Ideally, an infinite contact stiffness would result in zero penetration but numerically this is unstable. Some interpenetration is required for the algorithm to enforce compatibility. As long as the penetration is small or negligible, the solution results will be accurate. To minimize the penetration sensitivity to the magnitude of the contact stiffness, an extra term, λ, can be added to Equation 5-21 to augment the contact force calculation. This augmented method requires more iterations than the pure penalty method, but is more robust in general friction or frictionless problems [28]. The Augmented Lagrange method is given by

$$F_{contact} = k_{normal} \cdot x_{penetration} + \lambda \tag{5-22}$$

The contact equations have been presented assuming contact in the normal direction. If friction or bonded contact is defined, a similar situation exists in the tangential direction. The penetration distance is changed to a sliding distance and the pure penalty formulation (Equation 5-21) must be followed.

Furthermore, surfaces expected to come into contact are defined with a Target and Contact surface designation. The Target and Contact surfaces constitute a "Contact Pair". In asymmetric contact, only the Contact surface is prevented from penetrating the Target surface. The technique is computationally less expensive than symmetric contact, which prevents both surfaces from penetrating one another. A Pinball radius is defined to monitor the position and motion of a Contact element relative to its associated Target surface. The surface integration point method detects penetration between surfaces at the gauss points (Figure 5-3). This radius is used to differentiate between elements in 'near-field' contact versus 'far-field' contact. The difference affects how closely the contact is monitored which is associated to the computational demand. The most complex calculations occur when the elements are in actual contact. For example, in

the thermal analysis only those Contact elements, which lie within the Pinball radius, may exchange heat when bonded contact is defined.

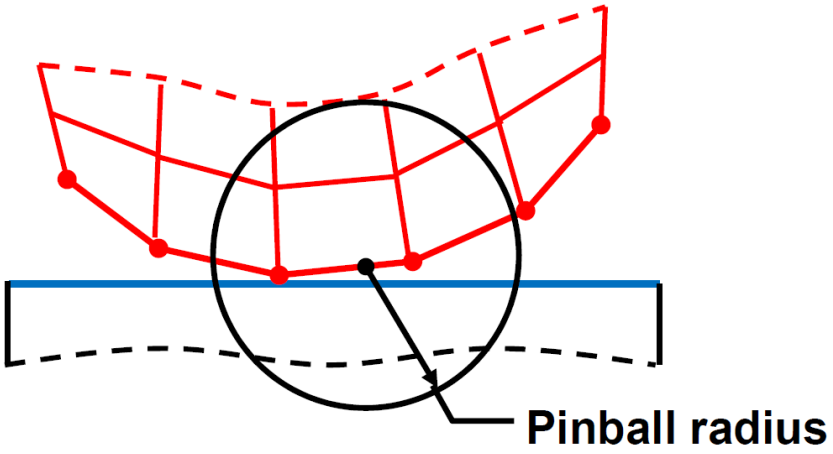

Figure 5-3: The Pinball radius is a contact element parameter that differentiates between far field open and near field open status. The Pinball radius should be on the order of the Contact pair gap size to prevent dramatic changes in contact status and help convergence.

In multi-body contact problems, it is possible for an individual component to only be constrained through contact with another component. If this part is unconstrained before contact is initiated, the part may be subjected to free translation or rotation known as Rigid Body Motion (RBM). RBM is numerically unstable and will prevent a solution from being found. Inside a fuel element, fuel pellets are free to move laterally within the sheath causing a potential problem for RBM. In reality, friction and gravity offer constraint to the pellets, but if frictionless contact is assumed, an artificial constraint must be imposed. Therefore, parts subjected to free motion in reality must always be constrained in static analyses to prevent RBM, but must still represent the physical system.

6 Model Capability and Implementation

The commercially available ANSYS software provides physics-based packages, which incorporate the necessary governing relationships to perform basic thermo-mechanical analyses. The packages are extensively verified and validated against numerous benchmarks to ensure they are properly functioning [29]. Custom physics and model specific parameters may be integrated within the framework to enhance its capability for a certain analysis. The use of ANSYS for a nuclear fuel deformation study requires some fuel-specific additions in order to simulate realistic behaviour. Although the software is not as flexible as others for nuclear applications, it is fully capable of achieving the objectives defined by the scope of this project.

The main objective for this deformation model is to analyze FE-PT contact under post-dryout heat transfer. It was mentioned that sophisticated multiphysics systems can often be simplified in FEA models to reduce the complexity in order to capture the underlying event(s) of interest. This directly applies to nuclear fuel modelling where many phenomenological processes are actively present and influence fuel bundle behaviour in the reactor. Since this deformation model is research oriented and not meant to compete with a fuel performance code, accurate prediction of all performance parameters is not a priority. However, it is important to identify the key phenomena that contribute to the results of interest. In this thesis, thermally driven deformation is the main bowing mechanism investigated. The phenomenon is governed by differential axial strain in the sheath, which requires material specific thermal expansion to be included. Although mechanical mechanisms such as creep or plasticity often contribute to fuel element deformation, they are not included here. Specifically, creep is known to play an important role in driving fuel element deflection at high temperatures and over long periods of time. For this analysis, the

temperature and duration of post-dryout conditions are assumed to be low enough that its relative contribution is eclipsed by the thermal mechanism. In addition, sheath plasticity can influence the deformation by affecting sheath strain at high stresses. Again, an assumption is made to investigate thermally driven processes as the dominant mechanism. Any deformation resulting from sheath plasticity and creep prior to dryout are assumed small and not specifically investigated. This section describes the inherent and added features of ANSYS that are used as part of the fuel deformation study.

6.1 Thermal Analysis

Modelling the thermal response of a fuel element requires accurately solving for the temperature profile across the entire body. Heat is generated from fission within the fuel and transferred to the coolant through the fuel-to-sheath gap and across the sheath by conduction. Accurately predicting the heat transport is an essential step as most fuel characteristics are dependent on temperature. The ability to change the heat transfer coefficient around the sheath to mimic drypatches is necessary for analyzing post-dryout conditions. These non-uniform temperature variations over a fuel element will influence how thermal phenomena like bundle deformation develop. This model takes advantage of the steady-state thermal analysis package in ANSYS to solve for the temperature distribution.

6.1.1 Heat Transport

The distribution of heat after it has been generated by fission is governed by the heat conduction equation. The steady-state heat equation is given by

$$\nabla \cdot (k \nabla T) + Q = 0 \tag{6-1}$$

where *k* is the thermal conductivity, *T* is the temperature, and *Q* is the volumetric heat generation rate [26]. The source term, *Q*, accounts for the heat generated by fission within the pellet and is derived from the linear fuel element rating. The conversion is given by

$$\mathrm{Q} = \frac{P_{linear}}{2\pi a_p} \tag{6-2}$$

where P_{linear} is the linear power rating of the fuel element (kW m^{-1}) and a_p is the pellet radius. It is assumed that the internal heat generated by fission is uniform within the fuel. In reality, asymmetric heat generation occurs because the neutron flux profile across a fuel element decreases towards the bundle center. Flux depression is one of the thermal mechanisms responsible for fuel element deflection and can have the largest contribution under NOC. For the current analyses performed under post-dryout conditions, this contribution becomes insignificant compared to relative deflection generated by drypatches. As a result, its inclusion as a thermal deformation mechanism is not pertinent.

In addition, convection heat transfer is the primary heat transfer mode responsible for the exchange of energy between the fuel sheath and bulk coolant. It accounts for the combined effects of conduction and bulk fluid motion. This mode is accounted for through a convective boundary condition given by

$$\mathrm{q}''_{conv} = h_{sc}(T - \bar{T}_c) \tag{6-3}$$

where q''_{conv}, the convective heat flux (W m^{-2}), is proportional to the difference between the surface and bulk coolant temperatures T, and $\bar{T}_c$, respectively [26]. The proportionality constant, h_{sc}, is termed the sheath-to-coolant convective heat transfer coefficient (W m^{-2} K^{-1}) [26].

6.1.2 Thermal Contact

Heat exchange between the fuel and sheath gap is typically modelled as a combination of three components; radiative, fluid and solid. The solid component is due to heat transfer through points of solid-solid contact and the fluid component is due to conduction across the gas-filled regions. The work of Ross and Stoute [30] has provided a standard model for representing fuel-to-sheath heat transfer by incorporating the effects of surface roughness, interfacial pressure and gas composition on the gap heat transfer coefficient. Under NOC, the sheath will collapse on to the fuel stack and the gap heat transfer becomes dominated by the solid component. For the short transients of interest in this study, it is assumed that the fuel and sheath will remain in close contact throughout the deformation process. This is a typical assumption for Anticipated Operational Occurrence (AOO) analysis when there is still an effective trip (primary or backup). In ANSYS, the amount of heat flow across a contact interface is defined by the contact heat flux expression given by

$$\mathrm{q}_{interface} = \mathrm{TCC} \cdot \left(T_{target} - T_{contact}\right) \tag{6-4}$$

where T_{target} and $T_{contact}$ are the temperatures of the Target and Contact surfaces respectively, and TCC is the thermal contact conductivity (W m^{-2} K^{-1}) [31]. The thermal contact conductivity is the input variable used to incorporate the impedance of the fuel-to-sheath gap in the thermal contact definitions. There are two types of contact definitions applied to this analysis: Frictionless and No Separation. The Frictionless contact definition in ANSYS allows heat to transfer between components only if they are in physical contact. The No Separation contact definition forces the Target and Contact surfaces to remain together irrespective of initial gap, penetration and loading but allows relative motion between the surfaces. This forced contact may be used in the thermal analysis to transfer heat across a gap, but must be replaced in the

mechanical analysis with a Frictionless contact connection in order to allow the Target and Contact surfaces to physically interact.

6.2 Mechanical Analysis

Modelling the mechanical response of the fuel elements can give an indication of the structural integrity based off the induced stress and strain. There are a number of physical processes that can cause strain and each contribution can be added individually to give the cumulative total. In this model, elastic and thermal strains will be investigated with the aid of the steady-state mechanical analysis package.

6.2.1 Stress-Strain Relationships

The response of a component to external forces is determined by the constitutive relation between stress and strain. For linear materials, the relationship is governed by Hooke's law

$$\{\sigma\} = [D]\{\varepsilon^{el}\} \tag{6-5}$$

where $\{\sigma\}$ is the stress vector $[\sigma_X\ \sigma_Y\ \sigma_Z\ \sigma_{XY}\ \sigma_{YZ}\ \sigma_{XZ}]^T$ and $\{\varepsilon^{el}\}$ is the total strain vector $[\varepsilon_X\ \varepsilon_Y\ \varepsilon_Z\ \varepsilon_{XY}\ \varepsilon_{YZ}\ \varepsilon_{XZ}]^T$, which includes elastic plus thermal strain [26]. The elastic stiffness matrix, $[D]$ is given by

$$[D] = \begin{bmatrix} 1/E_X & -\nu_{XY}/E_X & -\nu_{XZ}/E_X & 0 & 0 & 0 \\ -\nu_{YX}/E_Y & 1/E_Y & -\nu_{YZ}/E_Y & 0 & 0 & 0 \\ -\nu_{ZX}/E_Z & -\nu_{ZY}/E_Z & 1/E_Z & 0 & 0 & 0 \\ 0 & 0 & 0 & 1/G_{XY} & 0 & 0 \\ 0 & 0 & 0 & 0 & 1/G_{YZ} & 0 \\ 0 & 0 & 0 & 0 & 0 & 1/G_{XZ} \end{bmatrix}^{-1} \tag{6-6}$$

where a typical term E_X is the Young's modulus in the X direction, ν_{XY} is major Poisson's ratio and G_{XY} is the shear modulus in the XY plane [26]. These three quantities are dependent on each other by the following relation

$$G = \frac{E}{2(1+\nu)} \tag{6-7}$$

For an isotropic material model, the directional components of Young's modulus and Poisson's ratio are the same [26].

6.2.2 Thermal Strain

Materials subjected to a thermal load experience a change in volume that is proportional to its original size and change in temperature. The constant of proportionality is a characteristic material property called the thermal expansion coefficient [26]. Inside a fuel channel, the high operating temperatures contribute to thermal expansion of both the fuel and sheath. It was previously mentioned that when asymmetric cooling is present, differential axial growth can lead to fuel element bowing. The present investigation uses this phenomenon as the primary mechanism responsible for driving fuel element deformation.

The thermal strain generated by thermal expansion is calculated by the following expression:

$$\varepsilon_{th} = \alpha(T - T_{ref}) \tag{6-8}$$

where α is the linear thermal expansion coefficient of the material (K^{-1}), T_{ref} is the reference temperature at which no strain is assumed and T is the temperature in the deformed state [28].

6.3 Material Models

The fuel elements under assessment are composed of two materials, UO_2 for the fuel and Zircaloy-4 for the sheath and pressure tube. In reality, the pressure tube is made from a different Zirconium alloy that contains 2.5 wt% of niobium (Zr-2.5 Nb). For the purpose of being solely a support in this analysis, the tube is approximated as Zircaloy-4. In order to include both materials in ANSYS, specific properties must be specified in the material library. Extensive research has

been conducted on these materials and expressions describing their properties are referenced in nuclear specific libraries. MATPRO is a library of nuclear material properties developed at the Idaho National Engineering and Environmental Laboratory [32]. Many material properties have been studied through laboratory experiments which have produced semi-empirical correlations. When possible, theoretical considerations are used to derive relations but occasionally empirical elements are added to give agreement with experimental data. In order to transfer these correlations to ANSYS, the equations must be discretized and populated into a lookup table since multi-variable, spatially varying equations are not easily implemented. This method is used to add temperature-dependent material properties, with values between entry points interpolated by the software. The material library in ANSYS provides all the characteristic properties required by the finite elements during the analysis.

6.3.1 Fuel Model

As part of the heat conduction equation, Fourier's Law describes the heat flux through a material as a function of its thermal conductivity. The expression given for UO_2 by MATPRO is:

$$k_{UO_2} = \left[\frac{D_1}{1 + (6.5 - 0.00469T')(1 - D_1)}\right]\left[\frac{C_v}{(A + BT'')(1 + 3\varepsilon_{th})}\right] + 5.2997 \times 10^{-3} Te^{\left(\frac{-13358}{T}\right)}\left\{1 + 0.169\left[\left(\frac{13358}{T}\right) + 2\right]^2\right\} \quad (6\text{-}9)$$

where D_1 is the fraction of theoretical density (unitless), C_v is the phonon contribution to the specific heat at constant volume (J kg^{-1} k^{-1}), ε_{th} is the linear strain caused by thermal expansion, T is the fuel temperature (K), T' is a porosity correction factor for temperature ($T' = 6.5 - T(0.00469),\ T < 1364\ K$ and $T' = -1,\ T > 1834\ K$) and T'' is a correction factor given by $T'' = T,\ T < 1800$ and $T'' = 2050\ K,\ T > 2300\ K$ [32]. The parameter A is a factor proportional to the point defect contribution to the phonon mean free path given by 0.339 + 12.6*x* (m s kg^{-1} K)

where *x* is the deviation from stoichiometry. The parameter B accounts for phonon self-scattering given by 0.06867 (m s kg^{-1} K^{-1}) [32]. The parameter C_v is given by the analytical expression

$$C_v = \frac{Y_1 \theta^2 e^{(\theta/T)}}{T^2[e^{(\theta/T)} - 1]^3} \tag{6-10}$$

where Y_1 is 296.5 (J/kg K) and θ is 535.285 (K). In ANSYS, the correlation is implemented for 95% dense UO_2.

MATPRO's correlation for thermal strain was developed for unirradiated fuel pellets and reported as

$$\varepsilon_{th} = 1.0 \times 10^{-5}T - 3.0 \times 10^{-3} + 4.0 \times 10^{-2}e^{\left(-\frac{6.9\times10^{-20}}{kT}\right)} \tag{6-11}$$

where T is the temperature of the fuel and *k* is Boltzmann`s constant [32]. The reference temperature for this equation is 300 K and remains valid as long as the fuel is in a solid state. The thermal strain is converted to a thermal expansion coefficient using Equation 6-8 for input into the ANSYS model.

The sintering of UO_2 pellets forms a ceramic material that is assumed to follow an isotropic elasticity model. Young's modulus and Poisson's ratio for UO_2 are given by

$$E_{UO_2} = 2.334 \times 10^{11}[1 - 2.752(1 - D_1)][1 - 1.0915 \times 10^{-4}T] \tag{6-12}$$

$$\upsilon_{UO2} = 0.316 \tag{6-13}$$

where T (K) is the fuel temperature and D_1 is the fraction of theoretical density (unitless) [32] which is taken as 95%.

Increasing the temperature of the fuel will induce thermal strains which will consequently change the density. These changes are given by

$$\rho = \rho_0(1 - 3\varepsilon_{th}) \tag{6-14}$$

where ρ is the theoretical density, ρ_0 is the initial density of the fuel at 300 K and ε_{th} is the linear strain caused by thermal expansion [32]. The initial fuel density is taken as the maximum theoretical density of 10980 kg m^{-3} [32].

6.3.2 Sheath Model

Similar material properties to the fuel are needed for Zircaloy-4 in ANSYS. Unlike UO_2, Zircaloy is a metal which is manufactured through a cold working and stress-relieved process. This process strengthens the metal by causing dislocation movements and generation within the crystal structure. As a result of cold working, Zircaloy exhibits anisotropic material properties. The correlations for thermal expansion are selected from MATPRO and were developed for as-fabricated Zicraloy-4. Different thermal strains are expressed for the radial and axial directions by

$$\varepsilon_{11} = \varepsilon_{22} = \begin{cases} 4.95 \times 10^{-6}T - 1.485 \times 10^{-3}, & 300 < T < 1083\ K \\ \left[2.77763 + 1.09822\cos\left(\dfrac{T - 1083}{161}\pi\right)\right]10^{-3}, & 1083 \leq T < 1244\ K \\ 9.7 \times 10^{-6}T - 1.04 \times 10^{-2}, & 1244 \leq T < 2098\ K \end{cases} \tag{6-15}$$

$$\varepsilon_{33} = \begin{cases} 1.26 \times 10^{-5}T - 3.78 \times 10^{-3}, & 300 < T < 1083\ K \\ \left[8.76758 + 1.09822\cos\left(\dfrac{T - 1083}{161}\pi\right)\right]10^{-3}, & 1083 \leq T < 1244\ K \\ 9.7 \times 10^{-6}T - 4.4 \times 10^{-3}, & 1244 \leq T < 2098\ K \end{cases} \tag{6-16}$$

where the arguments of the cosines are in radians and $\varepsilon_{11}, \varepsilon_{22}$ are the radial and circumferential thermal expansion (m/m) and ε_{33} is the axial thermal expansion (m/m) [32].

MATPRO provides a simplified temperature-dependent thermal conductivity for Zircaloy which neglects secondary effects such as texture, irradiation and defect density [32]. The following correlation is valid up to 2098 K and is in units of W m^{-1} K^{-1}.

$$k_{Zr-4} = 7.51 + 2.09 \times 10^{-2}T - 1.45 \times 10^{-5}T^2 + 7.67 \times 10^{-9}T^3, \qquad T < 2098\ K \tag{6-17}$$

The correlation for Young's modulus is given by MATPRO as a temperature-dependent step function [32]. The model is presented without modifications for effects due to oxidation, cold work and fast neutron fluence. Therefore the material is assumed dislocation free and an isotropic elasticity model can be used. The approximation for Young's modulus and Poisson's ratio is

$$E_{Zr-4} = \begin{cases} 1.088 \times 10^{11} - 5.47 \times 10^{7}T, & T \leq 1090\ K \\ 1.017 \times 10^{11} - 4.827 \times 10^{7}T, & 1090 < T < 1240\ K \\ 9.21 \times 10^{10} - 4.05 \times 10^{7}T, & 1240 \leq T < 2030\ K \\ 1.0 \times 10^{10}, & T \leq 2030\ K \end{cases} \tag{6-18}$$

$$\upsilon_{Zr-4} = 0.32 \tag{6-19}$$

where T is the temperature (K) and the modulus is presented in units of Pa.

The change in Zircaloy density due to thermal strains is less than the correlation uncertainty over the analysis temperature range. Therefore the density can be taken as a constant value of 6550 kg m^{-3}.

6.4 Model Implementation

The material models presented in this chapter describe the various modelling capabilities and enhancements made to ANSYS in order to perform a fuel deformation study. Their implementation and incorporation in the analysis is discussed in this section to give an understanding of the techniques used to obtain results.

ANSYS offers a one-way coupled methodology for analyzing thermomechanical systems. The direct coupling between the thermal and mechanical system is achieved through exporting the temperature results, acquired through the thermal analysis, into the mechanical analysis as a thermal load. The final results are derived from a combination of both systems since the results of the mechanical analysis depend on the solution to the thermal analysis. Figure 6-1 presents an illustrative flow chart of the sequential one-way coupling.

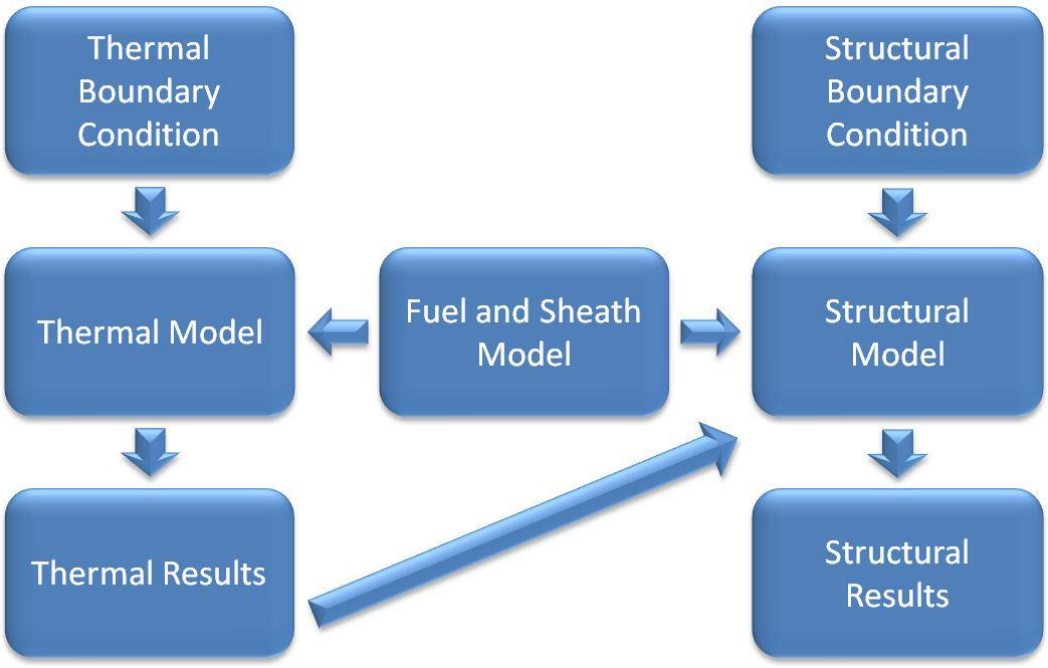

Figure 6-1: Sequential coupling between the steady-state thermal analysis and static structural analysis.

The general coupling procedure starts by using a steady-state thermal analysis to solve for the fuel element temperature profile, which will represent the response at one specific point in time. To satisfy a steady-state energy balance, the heat supplied must be equal to the heat removed. For this thesis, the internal heat generation within the UO_2 fuel must be matched by the

convective heat transfer occurring along the outer sheath surface to the coolant. Two different approaches are available to simulate convective heat transfer between a solid and fluid domain. The first approach utilizes a prescribed heat transfer coefficient to account for the thermal dissipation along the solid boundary. The second approach extends the model to include the fluid domain to describe the heat transfer and flow in the surrounding area. To avoid the complexity of modelling two-phase fluid flow, the first approach is used where the heat transfer coefficients for the relevant thermalhydraulic conditions are applied. Changing thermal conditions can be represented by a series of individual steady-state analyses, where different thermal loads are applied to each model to represent the conditions at a given point in time. Each solution represents a converged solution that may be exported into the structural model. Next, a static structural analysis is linked to the thermal analysis to compute the induced stress, strain and overall deflection from both thermal and structural loads. Mechanical loading caused by external coolant pressure on the sheath and gravity are added as boundary conditions to the elastic analysis. Contact is established between interacting components to account for solid-solid interaction effects. The fuel element is properly constrained to prevent RBM, while closely representing physical conditions. Multiple load steps may be defined to incorporate changing boundary conditions and fluctuating thermal loads. The static solution is solved for the integrated mechanical response based on the thermal and mechanical properties of the individual components. The stress and strain values in the fuel stack and sheath are computed for the particular analysis. Displacement of the finite element nodes describe the deformation profile, whereas the contact statuses provide information related to the contacting components.

7 Characterizing the Fuel Element

The development of a fuel deformation model, in this thesis, with the ability to simulate FE-PT contact requires a two-phase approach. The first phase seeks to characterize the stiffness of a fuel element where the fuel stack is represented by various assumptions between a monolithic cylinder and individual pellets. The motivation to investigate different fuel stack assumptions is driven by the possibility of simplifying the fuel element model when fuel-to-sheath interaction is high. The characterization was assessed through separate mechanical and thermal studies, which included a flexural rigidity analysis, thermal bowing analysis, and comparison with known fuel element bowing formulations and analytic equations. This chapter focuses on the first phase work to determine the best fuel element representation to pursue for the fuel deformation model. A detailed description of the different fuel model assemblies, their performance in the characterization studies and their potential use as part of the deformation tool is provided in this chapter.

7.1 Fuel Element Models

When a fuel bundle is resting inside the fuel channel, the outer most elements will be the first to contact the pressure tube if sufficient outward bowing were to occur. In a 37-element fuel bundle, outer ring elements contain 3 bearing pads and 3 or 4 spacer pads each. For the purposes of studying this contact interaction, a typical outer element with 4 spacer pads and 3 bearing pads was chosen. It will be shown in Section 7.2.2 that the effect of the different numbers of pads on the flexural rigidity is negligible. An illustration of the outer element type used in Phase 1 is provided in Figure 7-1 as a quarter fuel element geometry. Although the outer element type remained the same throughout the analysis, different fuel stack representations were investigated;

individual pellets, a monolithic fuel stack and a cracked-fuel stack. Each assembly was built as a CAD model in Solidworks and imported into the ANSYS environment via a Parasolid format. A detailed description of each model is given in the following sections.

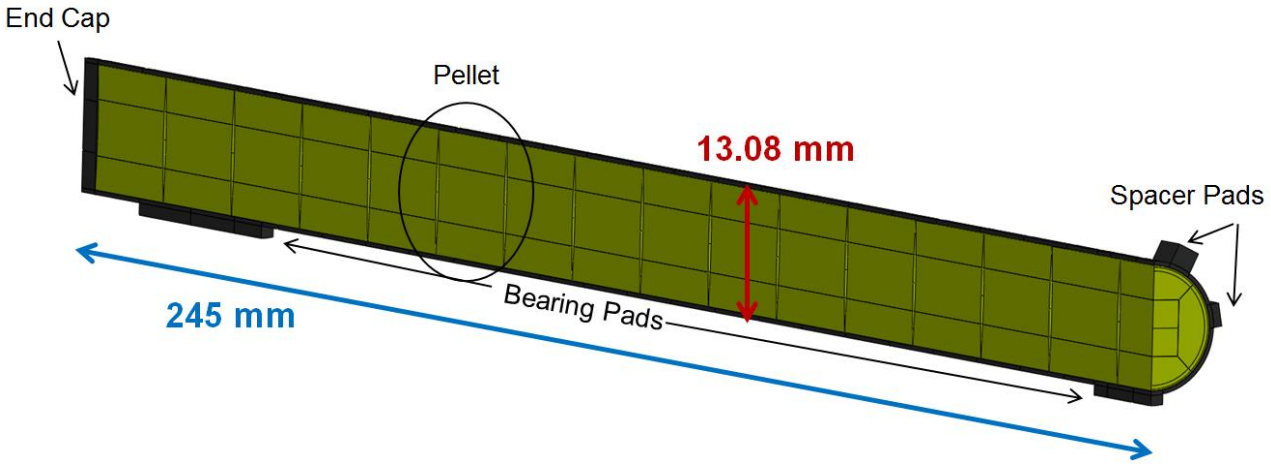

Figure 7-1: One quarter of a full length outer fuel element. The horizontal lines passing through each pellet are partition cuts from the CAD model.

7.1.1 Individual Fuel Pellet Model

The Individual Fuel Pellet Model represents the fuel stack as separate solid fuel pellets. Each pellet is free to contact a neighboring pellet and the sheath. This representation most closely depicts the physical geometry of a reactor fuel element.

7.1.1.1 Geometry

The fuel characterization studies performed in Phase 1 incorporate symmetric boundary conditions which allow two planes of symmetry to be exploited in the outer fuel element model. The realized geometry includes 15.5 pellets which are placed concentrically inside the fuel sheath to maintain an even fuel-to-sheath gap distance of 0.04 mm. The pellets are set axially end-to-end with a separation of 0.094 mm to give a total axial gap of 1.5 mm across the entire

fuel stack length. A simple 3 mm cylindrical end cap is attached to the end of the fuel sheath to seal the fuel stack inside. The physical geometry imported into ANSYS with the symmetry planes highlighted in red is shown in Figure 7-2.

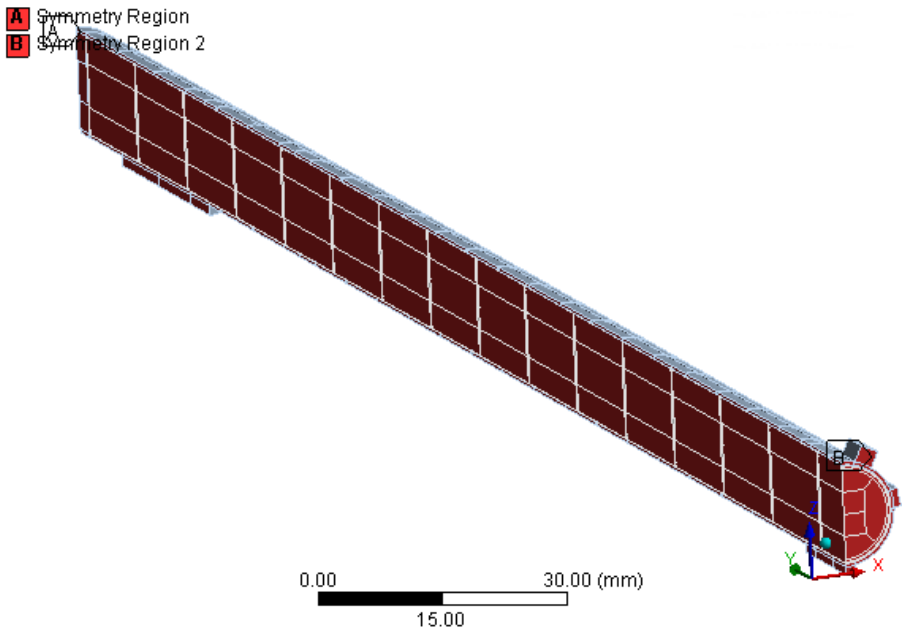

Figure 7-2: Physical geometry of fuel element in ANSYS with symmetry plane indicated.

The level of detail included in the geometry was selected to suit the needs of this specific study. The pellets were modelled as individual components and included normal features such as a land width, chamfered edges and dished faces. The pellet and sheath dimensions as specified in the model are listed in Table 7-1.

Table 7-1: Typical Pellet and Sheath dimensions were used in the fuel element models.

Pellet Features	Dimension [mm]	Sheath Features	Dimension [mm]
Pellet radius	6.09	Sheath outer radius	6.54
Pellet length	15.52	Sheath thickness	0.41
Land radius	5.58	Total diametral gap	0.08
Dish depth	0.25		
Chamfer	0.15		

The sheath was assembled with spacer and bearing pads bonded to the outer surface to mimic a single solid component. In reality, these appendages are brazed to the sheath during fabrication and the spacers are angled to prevent contact between FE-FE. For this analysis, the appendages were included because the same geometry is used later in the FE-PT study. The dimensions for these appendages are provided in Table 7-2.

Table 7-2: Appendage dimensions used in the fuel element model.

Appendages	Length [mm]	Width [mm]	Height [mm]
Center bearing pad	26	2.54	1.02
End bearing pad	28	2.54	1.2
Spacer pad 1	8.26	2.29	0.8
Spacer pad 2	8.26	2.29	2

Also, it is assumed the end cap is a perfect cylinder that is tightly bonded with the sheath to simplify the weld connection. All components attached to the sheath are treated with the Zircaloy-4 material model and the fuel pellets are represented with the UO_2 fuel material model.

7.1.1.2 Element Type and Mesh

In Solidworks, the full fuel element geometry was partitioned in such a way that a sweep method utilizing higher order hexahedral elements (SOLID 186) could be used along the entire length of each pellet and sheath. This allowed full control over the mesh spacing and total number of elements. An illustration comparing the partitioned fuel pellet along with the corresponding mesh distribution generated in ANSYS is given in Figure 7-3. Each pellet mesh contains 1680 elements and 7886 nodes.

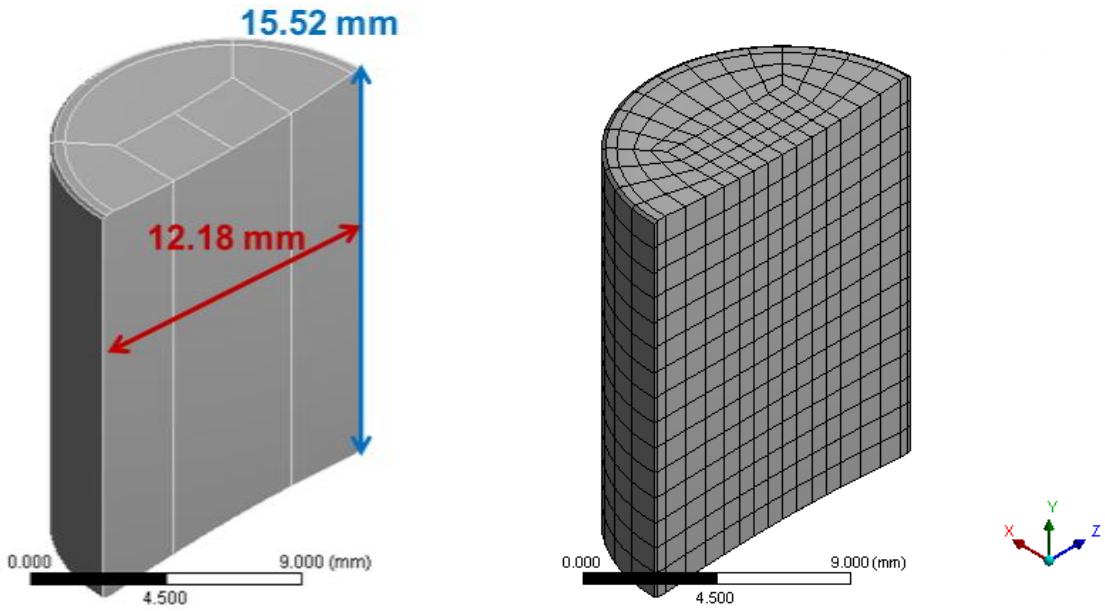

Figure 7-3: (Left) Partitioned fuel pellet from Solidworks. (Right) Fuel pellet meshed in ANSYS.

Greater consideration was given while partitioning the sheath in order to incorporate the appendages and accommodate certain boundary conditions in the model. Three finite elements were set across the fuel sheath thickness and the length was divided into axial segments of roughly 10 mm for fine mesh control. The sheath partitions and corresponding mesh in ANSYS are displayed in Figure 7-4. The sheath mesh contains 26715 elements and 136409 nodes.

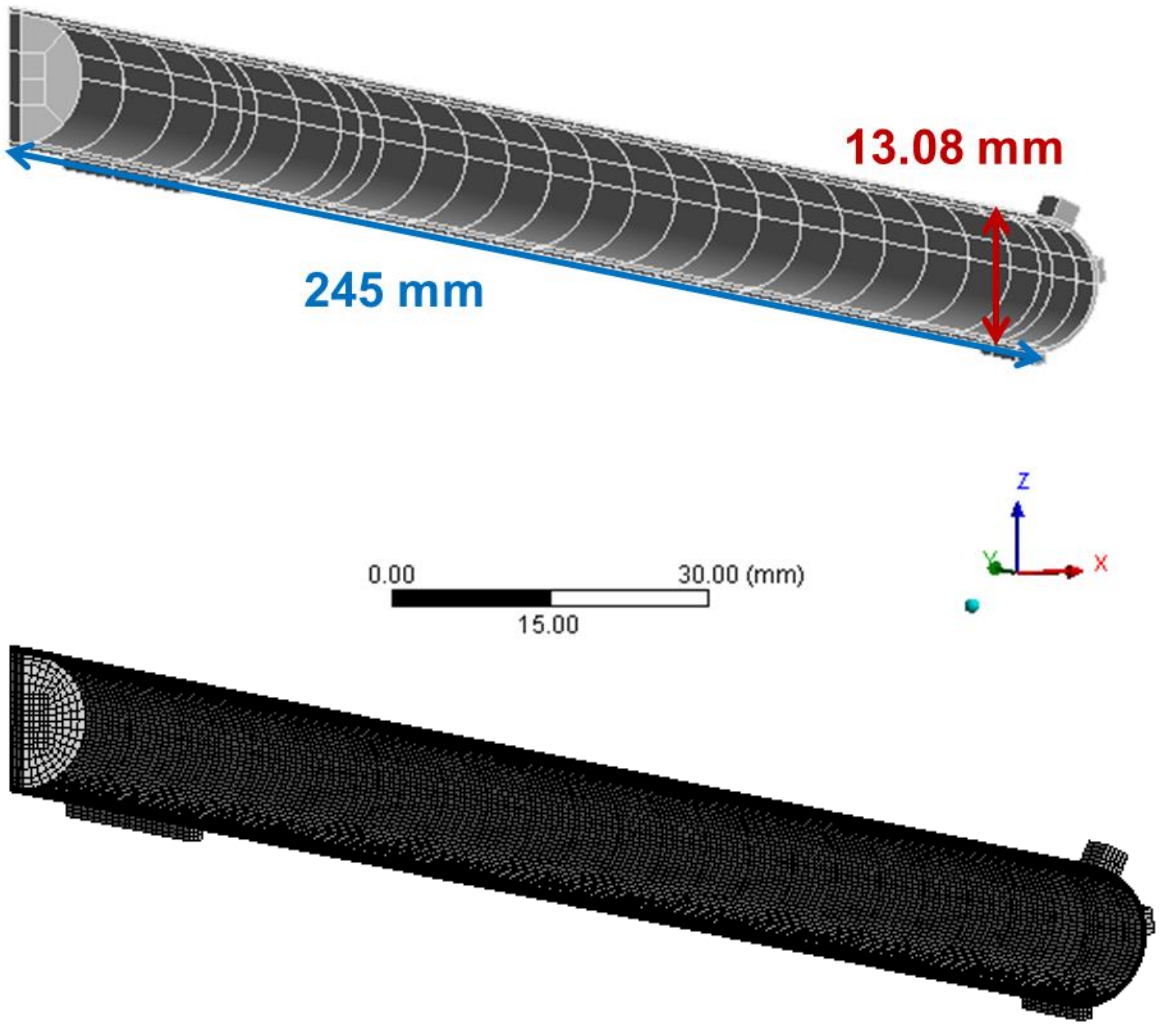

Figure 7-4: (Top) Partitioned fuel sheath from Solidworks. (Bottom) Finite element mesh of sheath and end cap in ANSYS.

7.1.1.3 Thermal Loading and Boundary Conditions

Contact connections are established to define the Target and Contact surfaces which allow heat to transfer between separate components. Pellet-to-pellet contact was established through 15 separate contact definitions, which correspond to the 15 gaps between pellets within the half-length element (See Figure 7-5).

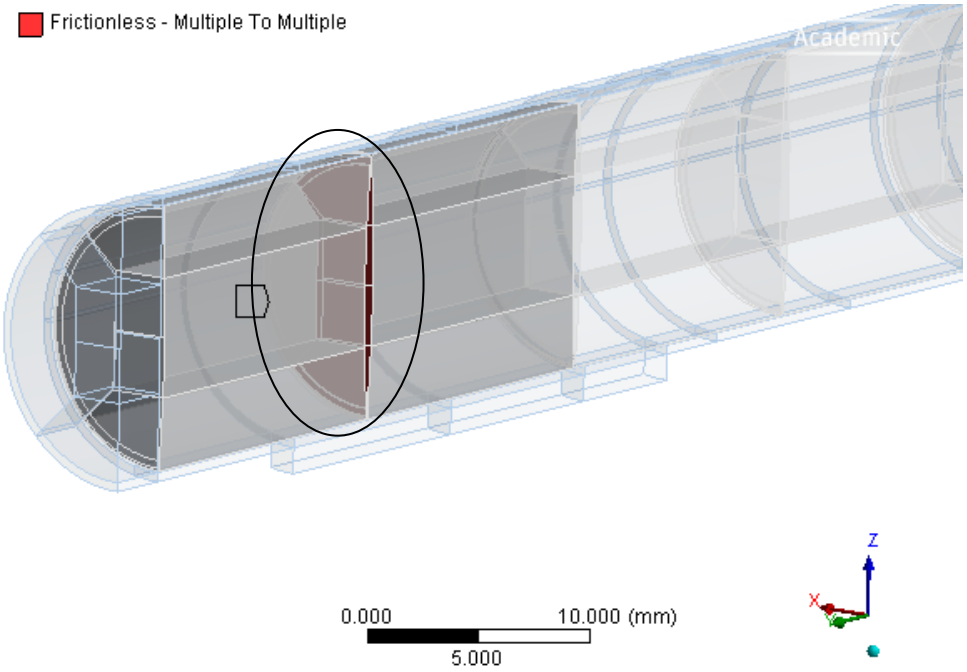

Figure 7-5: Frictionless contact definition established between two neighboring fuel pellets.

Each pellet-to-pellet contact was set to Frictionless with the Target and Contact surfaces defined the same way for each gap. Since the pellets are separated by a gap (in the thermal analysis), the choice of the Frictionless contact definition does not allow any heat to transfer axially between pellets. This is a good assumption as the pellet boundaries are close to periodic. However, this same assumption cannot be made between the pellet-to-end cap connection (see Figure 7-6).

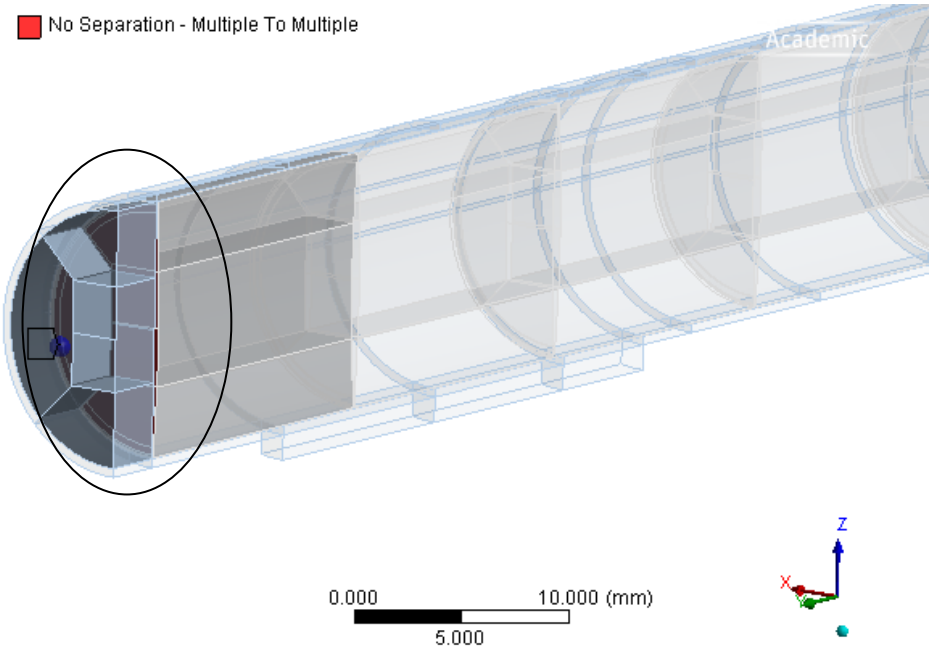

Figure 7-6: A No Separation contact definition established for pellet-to-end cap contact.

At this location, coolant surrounding the end cap will increase the heat removal from the pellet face. A No Separation contact connection between these components is needed to permit heat transfer across the empty gap. The ceramic properties of the fuel pellets make it an easy choice for the Target surface, due to its stiffer properties, which leaves the inner sheath as the Contact surface. These same contact surface choices are used for the final contact connection required between the pellets and sheath. For the pellet-to-sheath contact connection, all pellet sides are included in the same Target definition even though they are not initially together (see Figure 7-7).

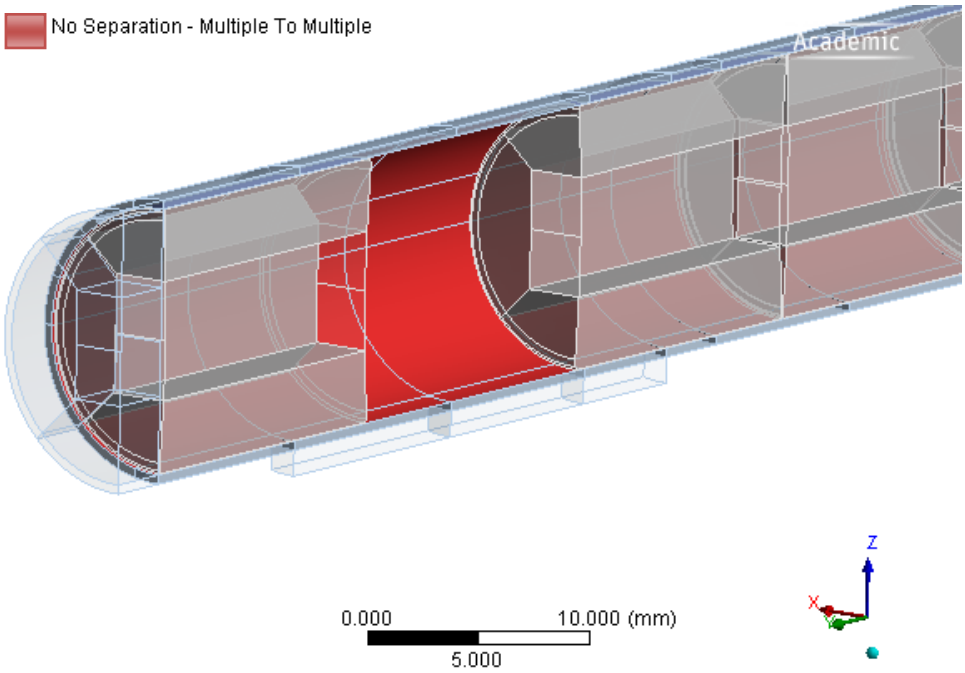

Figure 7-7: A No Separation contact connection established for pellet-to-sheath contact. A single pellet is hidden to distinguish the contact surface.

The contact finite elements used in the model are CONTA174 and TARGE170. The pinball radius is set to 0.5 mm for all contact connections and the thermal contact conductance, TCC, is assumed to have a constant value of 9500 W m^{-2} K^{-1} representing solid contact between the fuel and sheath.

Next, the thermal loading conditions for the fuel element include a uniform internal heat generation load to account for the heat generated by fission and a convective heat transfer boundary condition on the surface of the sheath to account for heat transfer to the coolant (see Figure 7-8).

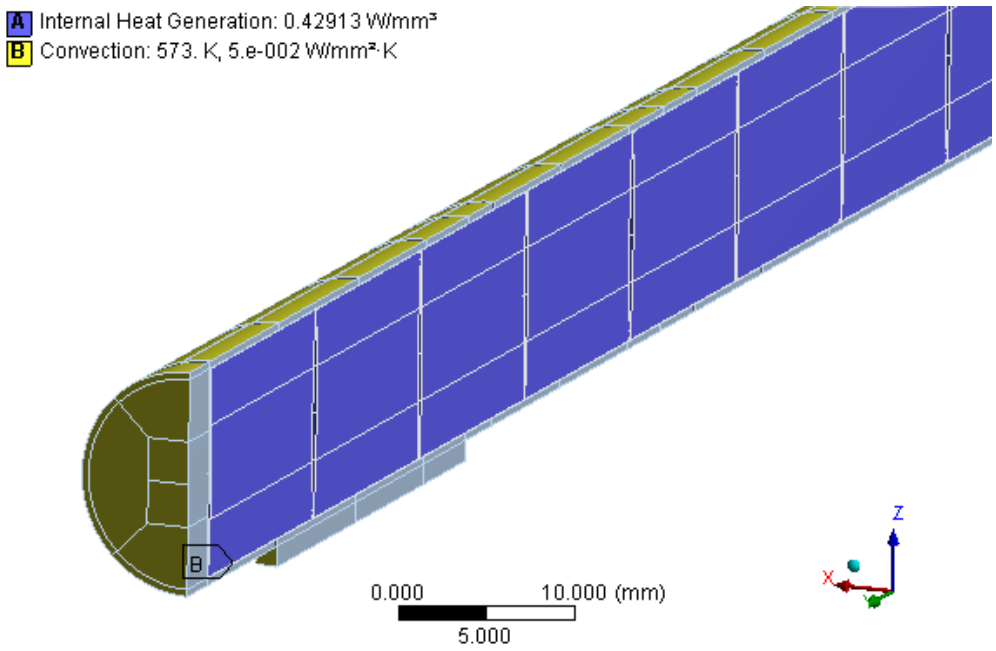

Figure 7-8: Thermal boundary conditions including internal heat generation in the pellets and convective heat transfer on the sheath.

The internal heat generation is applied as a volumetric source term to all individual fuel pellets, which is determined by the specified fuel element linear power through the conversion given in Equation 6-2. For the current analysis, normal operating conditions assume a high linear fuel element power rating of 50 kW m^{-1}. The NOC heat transfer coefficient for heavy water is taken as the nominal value of 50 kW m^{-2} K^{-1} and participates fully around the sheath surface. The fluid temperature of the coolant is set at 573 K. An illustration of the temperature profile generated under NOC is displayed in Figure 7-9.

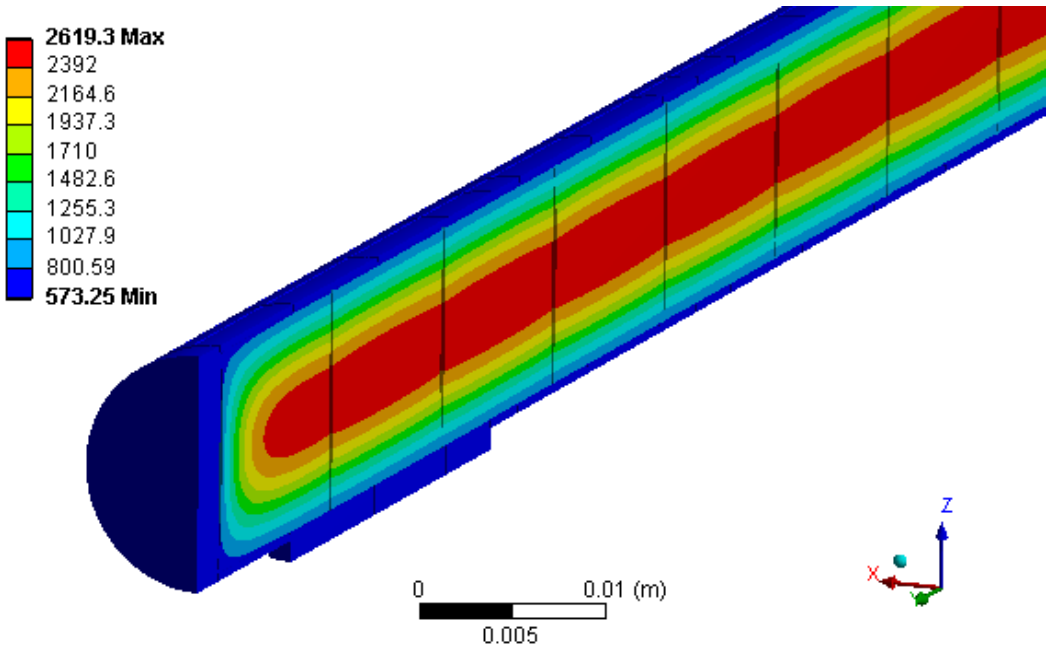

Figure 7-9: Sample temperature distribution of the Individual Fuel Pellet Model under normal operating conditions. Temperature is reported in Kelvin.

The parameters set for NOC in the thermal analysis are summarized in Table 7-3.

Table 7-3: Parameters specified under the thermal analysis normal operating conditions.

Parameter	Value
Initial System Temperature [K]	300
Linear Fuel Rating [kW m^{-1}]	50
Thermal Contact Conductance [kW m^{-2} K^{-1}]	9.5
Sheath-to-coolant heat transfer coefficient [kW m^{-2} K^{-1}]	50
Bulk Coolant Temperature [K]	573

7.1.1.4 Structural Loading and Boundary Conditions

The second half of the coupled analysis requires the necessary structural loading and boundary conditions to be defined on the fuel element. In order to simulate the closure of the fuel-to-sheath gap and account for physical contact between the two, the No Separation contact definitions in

the thermal analysis are replaced in the structural analysis. Once the thermal solution is solved and transferred to the structural analysis, the contact finite elements are deleted and a new set of Frictionless contact pairs are defined in their place. This new contact definition assumes the coefficient of friction between Target and Contact surfaces is zero, but the surfaces are still able to come in and out of contact in the normal direction. All contact definition settings are set to asymmetric behavior, Augmented Lagrange formulation, and a normal contact stiffness of 1, which is the recommended value [31].

Furthermore, the symmetry of the system prevents the sheath from translating in the X and Y directions as well as rotating about any axis. The Z translational DOF for the sheath is constrained by preventing the outer end cap face from translating in the Z direction. This is applied to the square partition on the end cap shown in Figure 7-10.

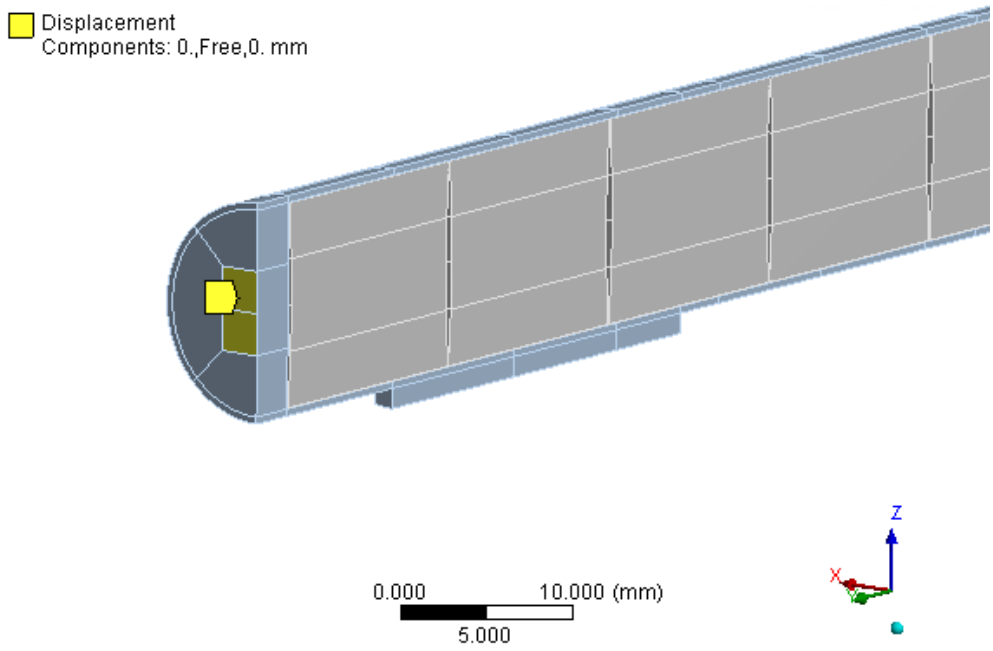

Figure 7-10: Hinged boundary constraint applied to the end cap.

The spatial constraint still allows the end cap to rotate which represents a hinged boundary condition. This constraint has shown to be good approximation for an endplate restraint on a fuel element through experiments [13]. This spatial constraint remains active throughout all load steps.

Although the pellets are prevented from translation in the X direction and rotation about the Y and Z axes from the geometric symmetry constraints, the initial gap between components offers no physical constraint between interacting bodies. Additional spatial constraints must be attached to the pellets to prevent RBM, in the Y and Z direction and about the X axis, until they come in contact with each other. The same constraints are required for the initial gap between the end cap and last pellet. A series of 3 load steps, as described below, are used to apply artificial boundary conditions until all contacts are engaged, then they are removed. This is strictly a modelling technique to prevent RBM and does not affect the results of the steady-state solution. The constraints are applied to the inside square faces of the pellet dishes as shown in Figure 7-11. In the first load step, the full thermal load is applied and the pellet faces are fixed from translation in all three spatial directions. The high coolant pressure and thermal expansion of the fuel pellets is enough to close the fuel-to-sheath gap and initiate contact in this step. The second load step is used to fully engage pellet-to-pellet contact along the land width by removing the Y direction translation constraint. In the third load step, the two remaining spatial constraints on the pellets dishes are removed and the pellet is only constrained through contact with neighboring pellets and the sheath.

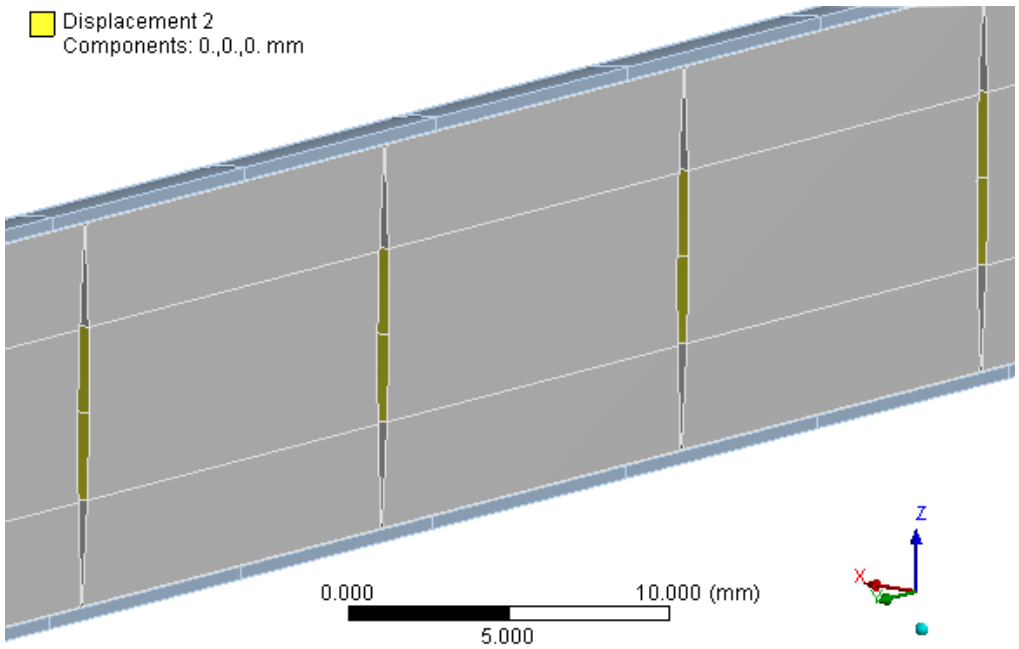

Figure 7-11: Spatial constraints imposed on the pellet dishes to prevent RBM before engaged in contact with the sheath.

The structural analysis handles the coolant pressure as a boundary condition applied to the same surfaces that are selected for the sheath-to-coolant convective heat transfer condition as shown previously in Figure 7-8. A PHTS pressure of 10 MPa is applied to the fuel element model. Also, gravity is included as a body force applied to all components in the structural model. These are both activated during the first structural load step. Once the pellets are fully engaged after the third load step, the fuel element is considered brought to NOC and any further loads applied during the characterization tests may be implemented.

7.1.1.5 No-Separation Individual Fuel Pellet Model

A slight variation to the Individual Fuel Pellet Model is made to investigate the effect of the fuel-to-sheath contact constraint on the flexural rigidity. Instead of replacing the fuel-to-sheath contact definition with Frictionless in the structural analysis, the No Separation definition used in

the thermal analysis is kept for the structural analysis. The No Separation contact maintains the initial spacing between the fuel pellets and sheath but allows sliding to occur. This contact definition provides an alternative way to ensure close pellet-to-sheath contact.

7.1.2 Monolithic Fuel Stack Model

The Monolithic Fuel Stack Model considers a fuel stack representation where the fuel pellets are bonded together to form one continuous piece of UO_2. Although the physical geometry remains similar to a real fuel element, constraining the pellets together is an assumption which removes individual pellet freedom.

7.1.2.1 Geometry

The geometry of the Monolithic Fuel Stack Model is identical to the Individual Fuel Pellet Model except for the initial spacing between fuel pellets. In the Monolithic Fuel Stack Model, the axial gap is concentrated at the end cap and the fuel pellets are bonded together at their land width. Connecting the fuel pellet together forms a monolithic pellet stack inside the fuel element. This geometry is illustrated in Figure 7-12.

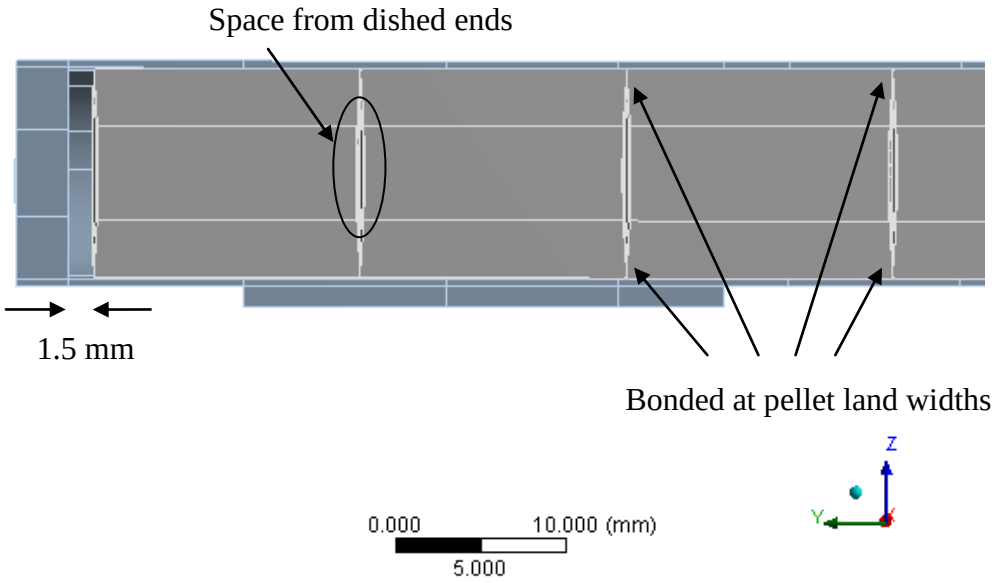

Figure 7-12: Axial gap in fuel stack is concentrated between the end cap and last fuel pellet. Pellets are bonded to their land widths within the CAD geometry.

7.1.2.2 Element Type and Mesh

Since the physical geometry is the same as the Individual Fuel Pellet Model, the partitions and mesh for the pellet, sheath and end cap remain the same.

7.1.2.3 Thermal Loading and Boundary Conditions

The thermal loading and boundary conditions for the Monolithic Fuel Stack Model remain identical to those described in the Individual Fuel Pellet Model. However, some alterations are required to the contact definitions to account for the change in fuel pellet positions. The monolithic pellet stack assumption removes the need for pellet-to-pellet contacts to be established. The fuel pellets are physically bonded together at their land width. The No Separation pellet-to-sheath contact connection remains the same as the Individual Fuel Pellet Model. The No Separation pellet-to-end cap connection requires an increase in the pin ball radius

to 2 mm in order to transfer heat across the larger gap distance. These small changes have a negligible impact on the NOC temperature profile.

7.1.2.4 Structural Loading and Boundary Conditions

Similarly to the Individual Fuel Pellet Model, the No Separation contact definitions are replaced with Frictionless contact pairs. By forming a monolithic pellet stack, the possibility for RBM of the pellets is removed. However, the initial spacing between the fuel pellets and sheath can present trouble when seeking contact convergence in the first load step. To assist the fuel with 'settling' into its equilibrium contact state, artificial spatial constraints are used to control the contact engagement process at the pellet-end cap frictionless connection. The spatial constraints are applied to the square partition on the pellet next to the end cap (see Figure 7-13).

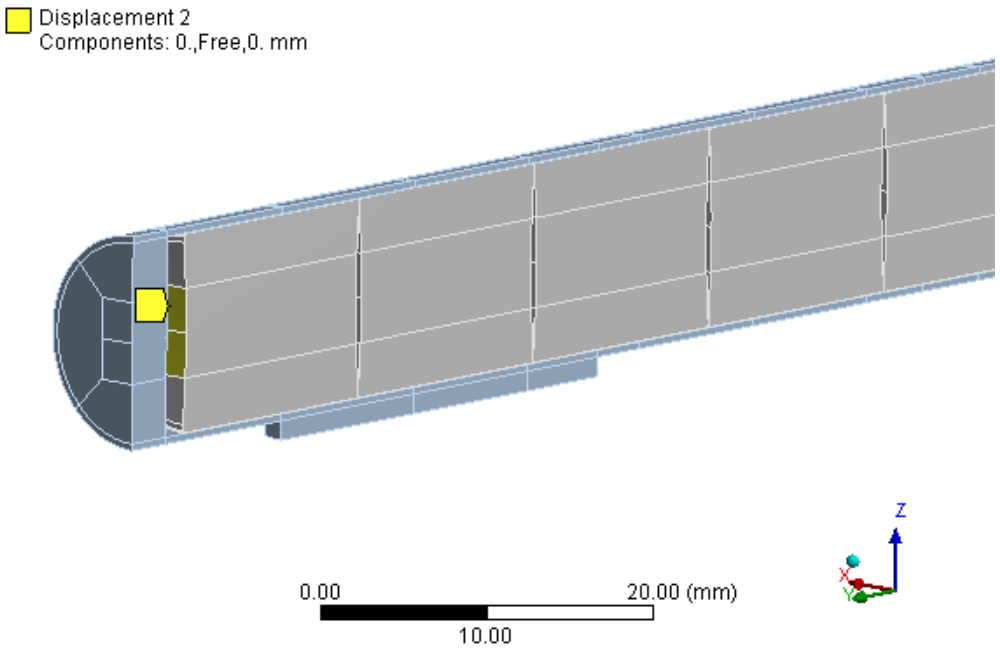

Figure 7-13: Spatial constraint on the monolithic pellet stack in the Monolithic Fuel Stack Model.

Two load steps are required to bring the fuel element to NOC conditions. During the first load step, the full thermal load is applied and the monolithic pellet stack end is constrained to the axial Y direction. Also, the coolant pressure of 10 MPa and gravity load are activated. This engages contact with the end cap which allows the remaining two translational DOFs in the X and Z directions to be removed during the second load step.

7.1.3 Cracked-Fuel Stack Model

The Cracked-fuel Stack Model accounts for pellet cracking in a similar manner to the single element BOW Code beam model. The fuel and sheath are represented as a composite beam with no fuel-to-sheath gap and the fuel is treated as a simple cylinder.

7.1.3.1 Geometry

The BOW code employs an analytic treatment for the fuel element's flexural rigidity based on a composite beam model. The code considers the ceramic nature of the fuel, which has a very low strength against fracture in tension. When a fuel element is subjected to a transverse load produced by either a thermal or mechanical mechanism, the fibres in the top portion of the fuel element contract in length generating a compressive stress, whereas the fibres near the bottom extend in length creating a tensile stress. If the maximum tensile stress in the fuel exceeds the flexural tensile strength of UO_2, the fuel fibres will crack, causing that portion to become ineffective at resisting any further tensile stress. As a result, the effective fuel section is reduced and the tension resisted by the UO_2 just prior to cracking is transferred to the sheath at that location. This will cause a sudden increase in sheath strain and lead to an upward shift of the neutral axis (the axis where fibres do not change length), and a further increase in curvature.

Tayal [17] notes the shift in the location of the neutral axis can be estimated by solving the transcendental equation given by

$$\mathrm{E}_p\left[\frac{1}{3}(a^2-\eta^2)^{1/2}(2a^2+\eta^2)-\eta a^2 cos^{-1}\frac{\eta}{a}\right]-\mathrm{E}_s\eta\pi(b^2-a^2)=0 \tag{7-1}$$

where E_p and E_s are the Young's modulus for the pellet and sheath respectively, b and a are the outer and inner radii of the sheath and η is the distance of the neutral axis from the centroid. The flexural rigidity of the fuel element is then given by

$$\mathrm{EI}=E_s\left[\frac{\pi}{4}(b^4-a^4)\right]+G_{ps}\mathrm{E}_p\left[\frac{a^4}{4}cos^{-1}\frac{\eta}{a}+\frac{\eta}{12}(a^2-\eta^2)^{1/2}(2\eta^2-5a^2)\right] \tag{7-2}$$

where G_{ps} is the pellet-to-sheath 'gripping factor' [17]. In order to compare the fuel model to the BOW formulation, another fuel element model is made using the same geometric assumption for the shift in neutral axis. This requires the fuel pellets to be represented as a simple cylinder stack which consumes the diametral gap in order to sit in direct contact with the sheath. The cylinder is partitioned at the neutral axis with the purpose of specifying a lower Young's modulus in the tensile portion. In order to calculate the axis location change for a full power element using Equation 7-1, a nominal value for the Young's modulus was taken to simplify the temperature dependent material model. A value of 166 GPa was selected for the fuel and 77.2 GPa was chosen for the sheath as typical average values at NOC. Using those values, the shift in the neutral axis from the center of the fuel element was determined to be 3.26 mm. The cracked fuel region will offer no tensile resistance in the flexural rigidity analysis, however, the physical fuel is included so that the same model can be used for the FE-PT analysis. An illustration of the pellet partition used to specify separate material properties is shown in Figure 7-14.

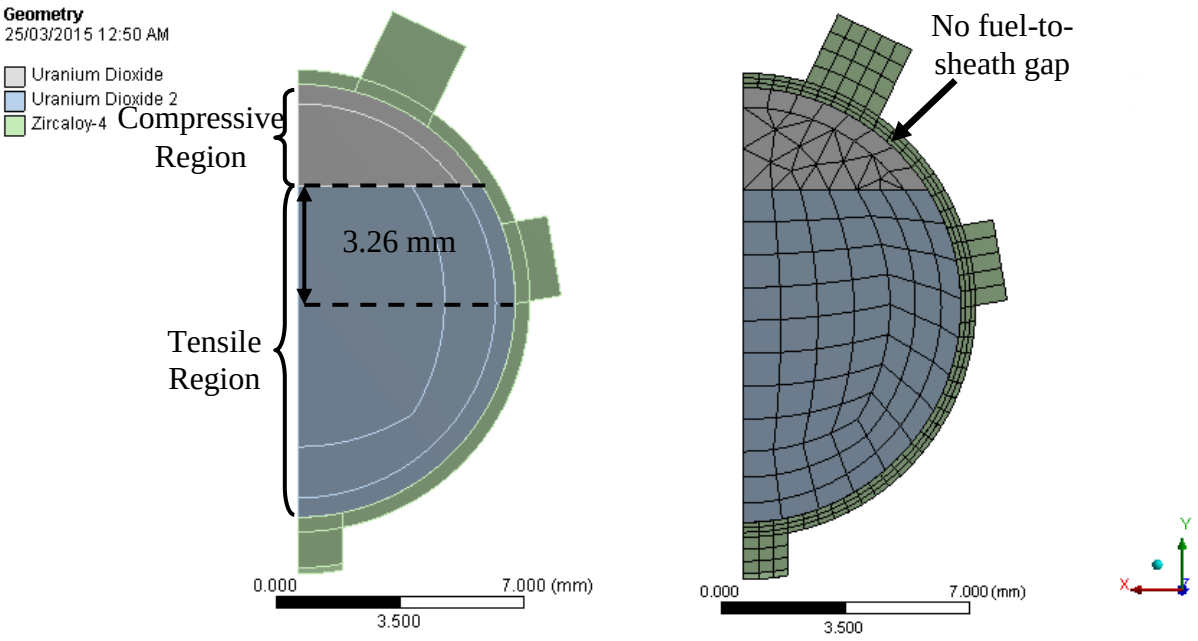

Figure 7-14: (Left) The fuel pellet is effectively separated into two halves with the top portion forming the compressive region and the bottom portion the tensile. (Right) A composite finite element mesh which incorporates both hexahedral and tetrahedral elements is used on the pellet face and swept through the stack length.

The change in fuel stack geometry has no impact on the end cap or sheath used in the prior two models. This allows the monolithic pellet stack in the Monolithic Fuel Stack Model to be swapped with the cracked-fuel stack to form a new geometry. The Cracked-fuel Stack Model maintains an axial gap of 1.5 mm between the fuel stack and end cap.

7.1.3.2 Element Type and Mesh

Identical meshing is used on the sheath geometry to that specified in the Monolithic Fuel Stack Model. In contrast, the fuel stack requires a different mesh and element type. Since the geometry is a simple cylinder, the face mesh shown in Figure 7-14 can be swept through the entire fuel

stack length. The swept mesh applied to the cracked-fuel stack is illustrated in Figure 7-15. It contains 7800 elements and 32344 nodes.

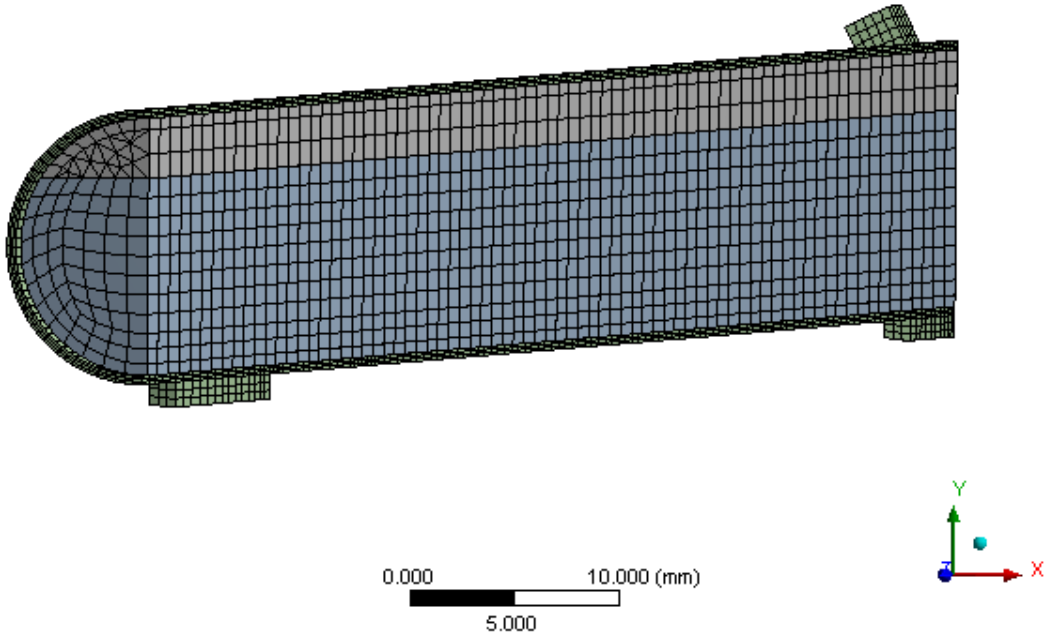

Figure 7-15: Cracked-fuel stack geometry and mesh. The end cap has been hidden for clarity.

7.1.3.3 Thermal Loading and Boundary Conditions

The intimate contact between the cracked-fuel stack and sheath permits a Frictionless contact definition to be used in the thermal analysis. The concentrated axial gap between the fuel and end cap requires a No Separation contact definition similar to that employed in the Monolithic Fuel Stack Model. The internal heat generation load is applied to the entire cracked-fuel stack body instead of the individual fuel pellets in the other models. The same NOC thermal conditions specified in Table 7-3 are used to generate a NOC temperature profile.

7.1.3.4 Structural Loading and Boundary Conditions

The same loading and boundary conditions applied in the Monolithic Fuel Stack Model are used to bring the Cracked-fuel Stack Model to normal operating conditions.

7.2 Mechanical Studies

The first set of studies investigates the fuel element response to mechanically applied loads. The fuel element models described above are subjected to mechanical loading in order to characterize the flexural rigidity of the various representations. The methods and results are presented in the following sections.

7.2.1 Flexural Rigidity

A fuel element can be thought of as a composite beam made of two materials one inside another. If the two materials were bonded together, the stiffness of the element would be determined by the sum of their flexural rigidities. However, in a fuel element, the fuel is not a discrete monolithic stack and a gap separates the pellets and sheath. Chapter 3 discussed how an empirical ‘gripping factor’ is used in beam analysis to estimate the fuel stacks contribution to the fuel element’s stiffness. Examining the flexural rigidity of the fuel element will provide an indication of this stiffness enhancement via a solid element contact approach. An analysis is performed by treating the fuel element as a simply-supported beam and applying a point load at the centre of the beam. The induced mid-plane deflection is characteristic of the beam’s stiffness given by the following relation

$$\delta = \frac{-PL^3}{48EI} \tag{7-3}$$

where δ is the vertical mid-plane deflection, *P* is the applied load at the mid-plane, *L* is the length between supports and *EI* is the flexural rigidity. To give an indication of how modelling the fuel stack affects the fuel element's stiffness at high powers, three separate models are simulated. These models include: the Individual Fuel Pellet Model (Section 7.1.1), the Monolithic Fuel Stack Model (Section 7.1.2) and the No-Separation Individual Fuel Pellet Model (Section 7.1.1.5). Also, two additional models are investigated called the empty sheath and monolithic pellet stack to assist in characterizing the different fuel element models. The empty sheath is simply the fuel sheath used in the different fuel element models but without any fuel inside (Figure 7-16).

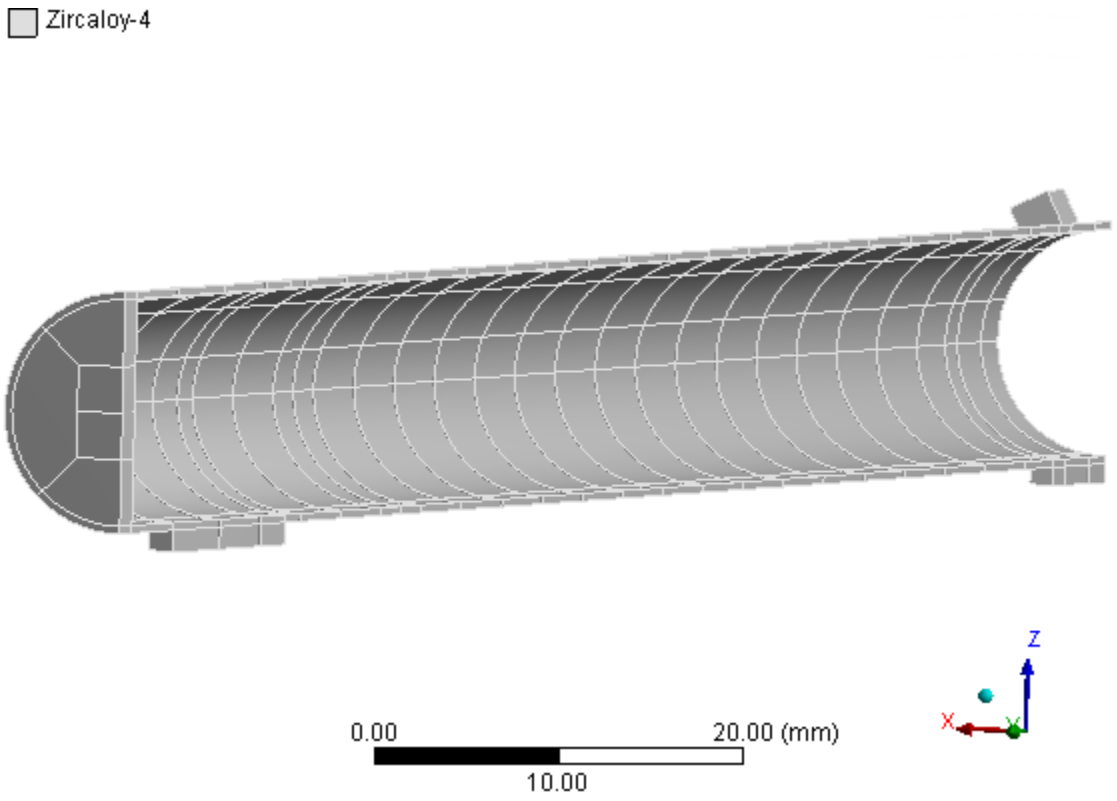

Figure 7-16: Empty sheath model.

The monolithic pellet stack is the same fuel stack used in the Monolithic Fuel Stack Model where each pellet is bonded together at their land width (Figure 7-17).

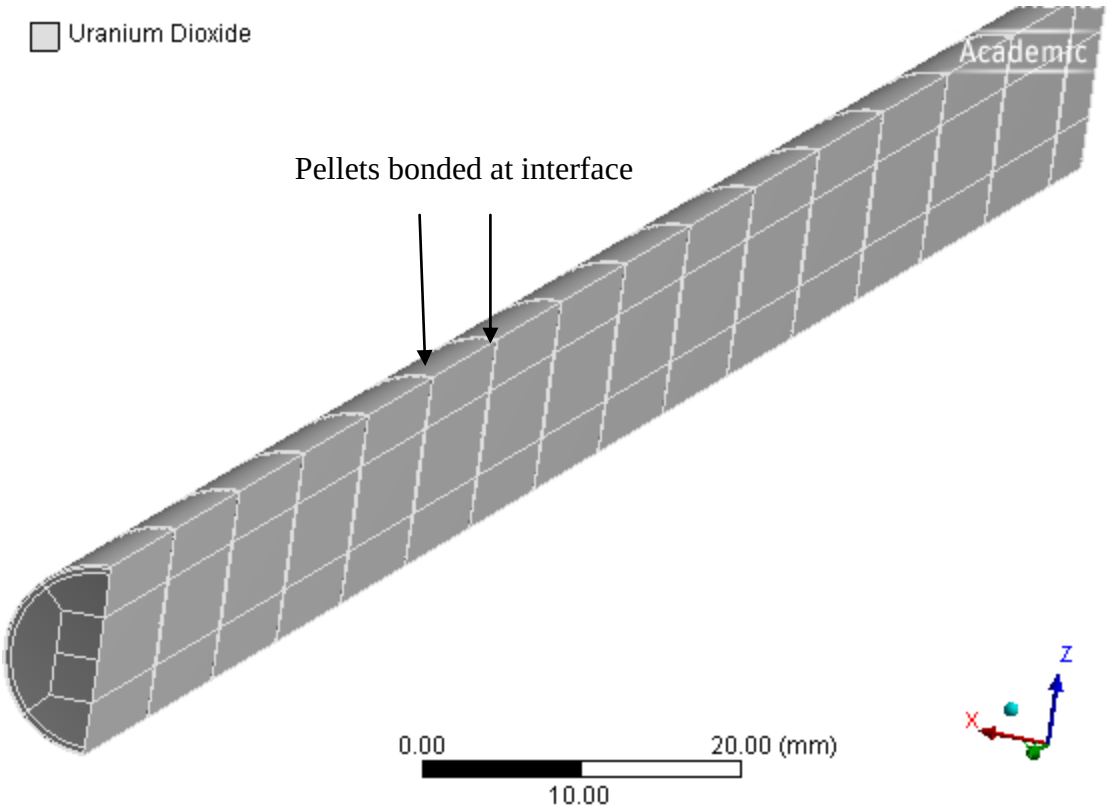

Figure 7-17: Monolithic pellet stack model. The fuel pellets are bonded together at their land widths.

The empty sheath and monolithic pellet stack simulations are performed at a temperature of 573 K in order to compare with analytical methods whereas the fuel element models were performed at NOC. A vertical load of 50 N is applied as a surface boundary condition on the sheath's face along the half-length symmetry plane (See Figure 7-18) resulting in a total of 200 N on the full fuel element. The load is activated incrementally in substeps after NOC equilibrium is reached.

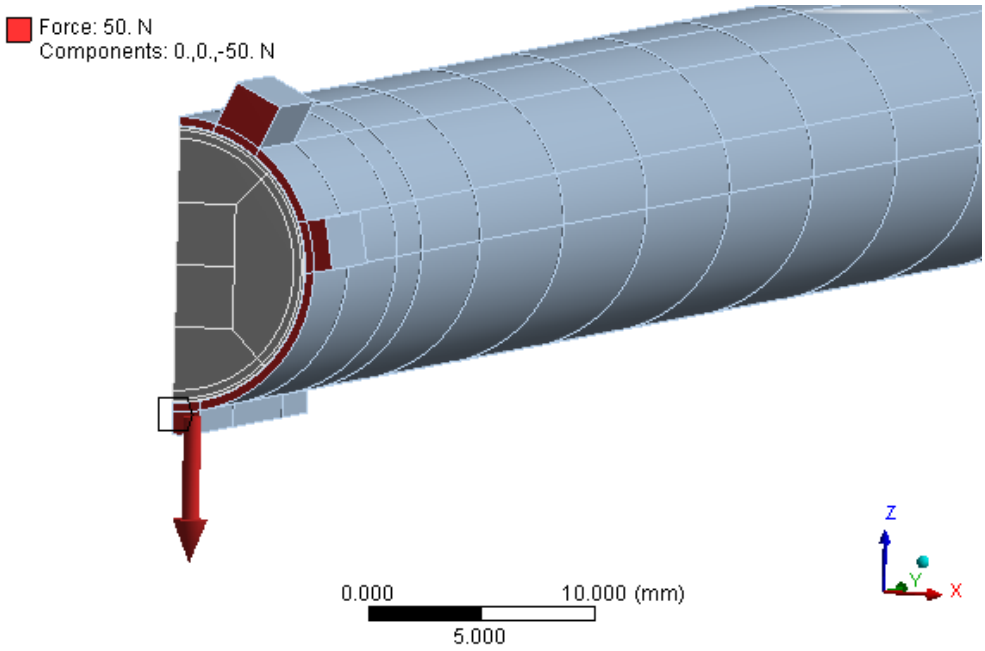

Figure 7-18: Vertical force applied to the sheath mid-plane as a surface boundary force.

7.2.2 Flexural Rigidity Results

The flexural rigidity simulations were performed to characterize the stiffness of the fuel element using different modelling assumptions to represent the fuel stack. The flexural rigidity may be individually calculated for fuel and sheath by idealizing their geometry as a solid and hollow cylinder, respectively. Unfortunately, the complex interaction between the fuel and sheath does not permit one to simply add their individual stiffness to estimate that of a fuel element. As part of the stiffness characterization study, an empty sheath and the monolithic pellet stack were simulated to provide bounding estimates for the fuel element's flexural rigidity, while also offering a benchmark against an analytical solution. The results of the simulations are summarized and compared in Table 7-4.

Table 7-4: Flexural rigidity results for the empty sheath and monolithic pellet stack simulations in ANSYS compared against analytical solutions.

Component	ANSYS [N m^2]	Analytical [N m^2]
Empty Sheath	25.6	25.4
Monolithic Pellet Stack	154.8	204.9

Comparisons of the flexural rigidities for both components show good agreement for the empty sheath and poorer agreement for the monolithic pellet stack. The empty sheath simulation was expected to predict a slightly higher flexural rigidity than the analytical calculation due to the additional support provided by the appendages. This minor contribution is observed by the small positive difference between the simulated and analytical value. The result verifies the initial outer element assumption that appendages offer a relatively minor contribution to sheath stiffness and subsequently may be positioned straight as assumed in the CAD geometry. It also indicates there is likely a negligible difference in stiffness between a 3 and 4 spacer pad outer element, confirming the original choice. It is unfortunately not possible to provide a quantitative estimate of the stiffness contribution as the magnitude is on the same order of the finite element error. Next, the solid cylinder assumption, used in the moment of inertia term for computing the monolithic pellet stack analytical value, predicted a larger flexural rigidity than was simulated. This substantial difference occurred because a solid cylinder does not accurately depict the simulated monolithic pellet stack. The physical gaps from chamfers and dished ends in the UO_2 along the bonded pellet stack create spaces, which are not captured in the solid cylinder assumption. The true moment of inertia would be smaller in those regions because there is physically less material. Despite this difference, these simulated results provide an expected range for the fuel element's flexural rigidity, which will fall somewhere between an empty

sheath (25.6 N m^2) and the combination of the monolithic pellet stack and empty sheath (180.4 N m^2).

In order to determine the fuel element's stiffness, the flexural rigidity analysis was extended to three different fuel element models. 1) The Individual Fuel Pellet Model includes individual pellets that are free to move vertically and horizontally into contact with other pellets and the sheath, 2) The No-Separation Individual Fuel Pellet Model includes individual pellets that are free to move axially into contact with other pellets but maintain the initial gap distance between the sheath and 3) The Monolithic Fuel Stack Model includes pellets bonded together so they expand axially together and move vertically into contact with the sheath as one piece. The stiffness results for each representation are provided in Table 7-5, where the deflection was taken as the maximum vertical displacement at the mid-plane. A typical vertical deflection profile for the flexural rigidity simulation is shown in Figure 7-19.

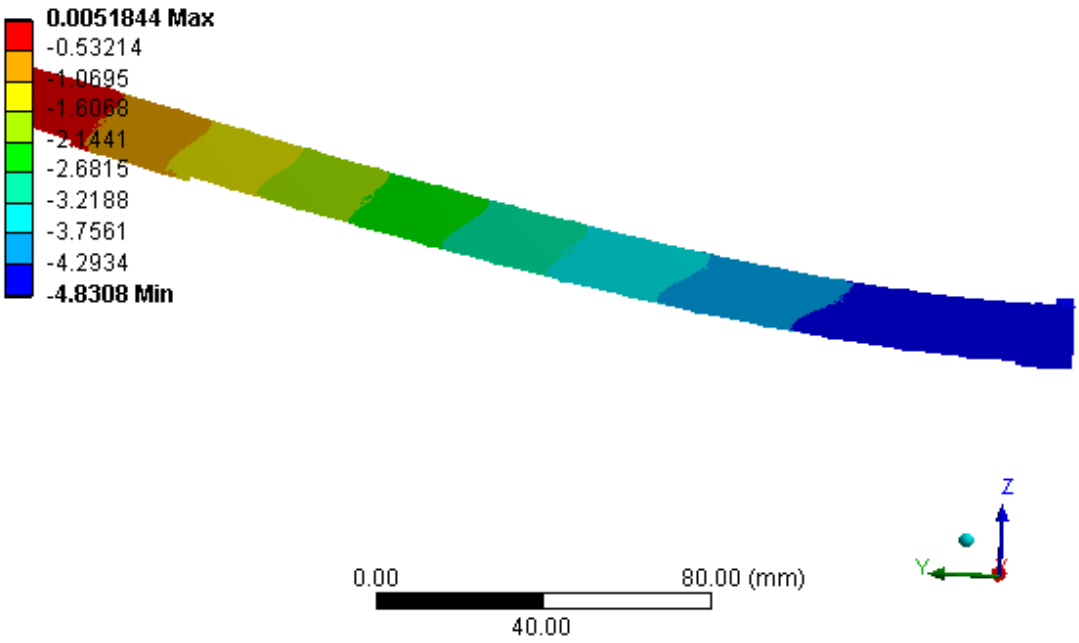

Figure 7-19: Flexural rigidity simulation of the Individual Fuel Pellet Model showing the fuel element deflection for a 200 N load. The deflected profile has been magnified by 10x to emphasize the shape. It is not to scale.

Table 7-5: Flexural rigidity results for the fuel element simulations performed with ANSYS.

Fuel Element Model	ANSYS [N m^2]
Individual Fuel Pellet Model	102.9
No-Separation Individual Fuel Pellet Model	147.4
Monolithic Fuel Stack Model	163.9

As expected, the flexural rigidity for all models was determined to be less than that of an empty sheath and monolithic pellet stack together (180.4 N m^2). The choice to investigate these three different models was motivated by the possibility of simplifying the interacting fuel pellets as a monolithic pellet stack inside the fuel element at high linear powers (50kW m^{-1}). In this power range, the fuel pellets expand axially to close any initial spacing between them, and it was thought that they essentially form a monolithic fuel stack. However, the flexural rigidity analysis

found the true monolithic assumption to be much stiffer than the other fuel representations at the same linear power. The largest flexural rigidity was recorded for the Monolithic Fuel Stack Model. The high stiffness can likely be attributed to the forced bonding between pellets. A similarly high flexural rigidity was observed when the monolithic pellet stack was simulated by itself in Table 7-4. The second largest flexural rigidity was recorded for the No-Separation Individual Fuel Pellet Model. This model was run to simulate a similar monolithic assumption with different contact constraints for comparison. In this case, the fuel pellets were held in contact with the sheath through a constant fuel-to-sheath gap distance but pellet-to-pellet contact with sliding was allowed with the frictionless connection. Allowing the pellets to slide past one another appears to result in a slightly lower flexural rigidity. If the pellets can slide vertically with respect to each other, then they can make the entire element bend by shifting vertically and looking like stair steps (offset vertically from each other). The Individual Fuel Pellet Model is the least stiff representation which recorded a substantial change in flexural rigidity compared to the other two models. Permitting frictionless contact between all interacting components provided the most pellet freedom and consequently led to the least resistance to sheath bending. This model should also be the most realistic if some friction had been included. The result of this study implies the monolithic fuel stack assumption is overly stiff even though the axial gap is fully consumed in each model. Without an analytical model for direct comparison with the different fuel stack representations, it is difficult to quantify which model provides a closer resemblance to an actual fuel element's flexural rigidity. In reality, all components in contact will experience some form of friction, which will impact the overall behaviour. Since none of the present models capture this exactly, there is expected to be some inaccuracy in the results. The analysis indicates that properly capturing the fuel stack behaviour is important to predicting

mechanically induced deformation. It is noted that the least stiff model is also the most similar to an actual fuel element's physical geometry. These features make it the best candidate of the three to use in a FE-PT contact model as it will provide the most conservative estimates for deflections without over simplifying the fuel stack assembly. To support this choice for further analysis, and possibly gauge the accuracy of the Individual Fuel Pellet Model, the results are compared against reported values acquired with Williams' friction model [20].

Williams investigated the impact of friction on the stiffness of the fuel element by performing a sensitivity study with the coefficient of friction for pellet-to-sheath contact. It is known Williams' model includes additional time-dependent parameters, such as a fully coupled dynamic gap conductance, which presents some discrepancy in comparison. However, both models used individual pellets to represent the fuel and were obtained under steady conditions at high power (45 kW m^{-1} and 50 kW m^{-1}). At this power, the pellet-to-sheath interaction should be comparable which would yield similar flexural rigidities. The results of Williams' study showed that as the coefficient of friction increased, the flexural rigidity decreased (Table 7-6).

Table 7-6: Flexural rigidity of a fuel element for different coefficients of friction between the fuel and sheath. Values are reported by Williams using ANSYS [20].

Williams' Models	ANSYS [N m^2]
Fuel-to-Sheath Friction 0.05	149.3
Fuel-to-Sheath Friction 0.9	138.8
Fuel-to-Sheath Bonded	83.8

Williams' explanation is that when the sheath and pellets are tightly gripped, the gap between adjacent pellets isn't able to close and results in less axial interaction and therefore more flexibility in the element. A further investigation of this phenomenon is being pursued by

Williams [20] but the current results are interesting to compare. It was expected that the flexural rigidity of the Individual Fuel Pellet Model would be comparable to Williams' lowest coefficient of friction model. Surprisingly, the flexural rigidity of the Individual Fuel Pellet Model related closer to Williams' Bonded model, which forbids sliding between the fuel and sheath. The flexural rigidity of the No-Separtion Individual Fuel Pellet Model was most similar to Williams' 0.05 coefficient of friction model. These comparisons add further evidence to the importance of properly capturing fuel-to-sheath and pellet-to-pellet contact to estimate fuel element stiffness. The overlap of flexural rigidity results with different contact definitions provides an indication of how sensitive the fuel element stiffness can be under different conditions. A detailed comparison between the two models would be fascinating, but would require a more thorough investigation of the model parameters and contact definitions in Williams' model. Nevertheless, the flexural rigidity of the Individual Fuel Pellet Model has been characterized and appears to be in the typical range for a fuel element.

7.2.3 Flexural Rigidity Comparison with BOW Code

The flexural rigidity comparison between the different fuel stack models and Williams' friction models [20] showed the stiffness of the fuel element models are within the same range. In an attempt to better quantify a fuel element's stiffness, a comparison between an ANSYS simulation and an analytical beam model was performed. This led to the development of the Cracked-fuel Stack Model, which could be directly compared with the BOW code formulation. The same loading conditions, shown in Figure 7-18, were applied to the sheath after the Cracked-fuel Stack Model was brought to NOC equilibrium. Three separate simulations were performed corresponding to the Young's modulus being reduced by a factor of 10, 100 and 1000 in the cracked-fuel region.

7.2.4 Results of Flexural Rigidity Comparison with BOW Code

The flexural rigidity of the Cracked-fuel Stack Model was characterized for comparison with the BOW code formulation. The results of the simulations are presented in Table 7-7.

Table 7-7: Flexural rigidity calculations for the cracked-fuel stack model.

Cracked Pellet	ANSYS [N m^2]	Analytical G_{sp}=0 [N m^2]	Analytical G_{sp}=0.5 [N m^2]	Analytical G_{sp}=1 [N m^2]
Young's Modulus Reduced by 10	29.2	25.3	35.4	45.5
Young's Modulus Reduced by 100	28.4	25.3	35.4	45.5
Young's Modulus Reduced by 1000	27.7	25.3	35.4	45.5

The results of the ANSYS simulations indicate consistent flexural rigidities despite changing the Young's modulus. The ANSYS values indicate that a gripping factor between 0.12 and 0.2 is needed to match the analytical values obtained with the BOW code methodology. This is much lower than expected for a fuel element in this power range [17]. The discrepancy can be explained through an understanding of how the flexural rigidity calculation is evaluated in the BOW code. Equation 7-2 provides the flexural rigidity formula used to obtain the analytical values. The equation can be generalized as

$$EI = J_s + G_{sp} \cdot J_p \tag{7-4}$$

where J_s is the flexural rigidity of the sheath, J_p is the flexural rigidity of the pellet stack and G_{sp} is the sheath-to-pellet gripping factor also known as the REF [17]. The analytical values reported in Table 7-7 show the range of possible flexural rigidities for various pellet-to-sheath gripping factor assumptions. The ANSYS simulations were performed for a frictionless pellet-to-sheath contact definition, which reduces the mechanical interaction between the fuel and sheath. Therefore, the ANSYS results were expected to predict a lower flexural rigidity corresponding to

a smaller sheath-to-pellet gripping factor, since the interaction was minimized through the frictionless contact definition. By reducing the cracked-fuel stack's ability to resist the bending moment, it is expected that the fuel element's flexural rigidity would lie closer to that of an empty sheath. This is indeed what is indicated by the small gripping factor required to match the results. This behaviour indicates that the frictionless contact definition provides a conservative estimate for the maximum deflection a fuel element can experience under mechanical loading. The minor shift in flexural rigidity, when the Young's modulus was changed by several orders of magnitude in the tensile region, supports this finding. The behaviour provides additional support for selecting the Individual Fuel Pellet Model as a potential candidate over the Monolithic Fuel Stack Model for further deformation studies. Although the Cracked-fuel Stack Model predicts a much lower flexural rigidity than expected in this power range, pursuing this model for further studies provides a bounding value for an actual fuel element's flexural rigidity. The lower bound is advantageous for this analysis as it will provide a conservative estimate for fuel element deformation. This model is therefore selected for further analysis studies.

7.2.5 Effect of Power

An attempt was made to quantify the REF in the Individual Fuel Pellet Model and Cracked-fuel Stack Model in order to better understand the influence of the UO_2 fuel on the overall fuel element's flexural stiffness. This was accomplished by evaluating the flexural rigidity at different linear powers. To perform this analysis, a series of sequential thermal loads steps were used to lower the linear power rating from 50 kW m^{-1} down to 10 kW m^{-1} in steps of 10 kW m^{-1}. Each thermal solution was transferred to the structural analysis to be activated in sequential load steps. For example, the first decrease in power is activated in the 5^{th} load step of the Individual

Fuel Pellet Model after the 4th load step activates the transverse force applied for the flexural rigidity study.

7.2.6 Effect of Power Results

Decreasing the fuel element power reduces the interaction between the fuel and sheath because less thermal expansion occurs. It was expected that as the linear power rating was lowered, the flexural rigidity would approach a value roughly equal to the empty sheath or slightly offset due to reduced interaction between the fuel and sheath. The results of the Individual Fuel Pellet Model are shown in Figure 7-20.

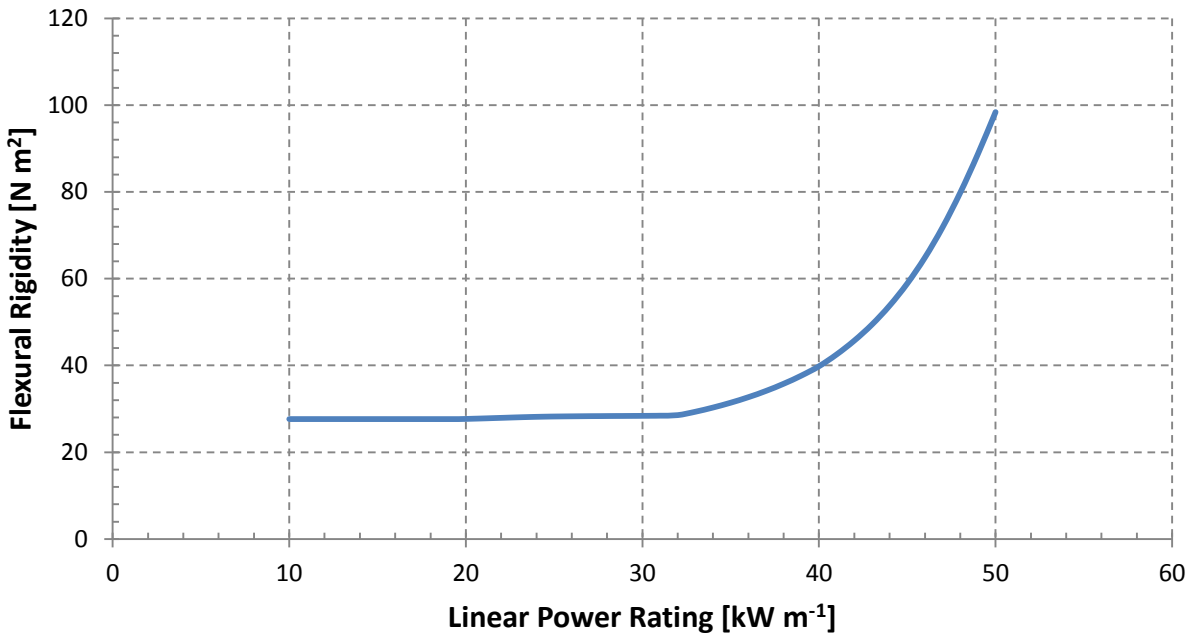

Figure 7-20: Flexural rigidity of the Individual Fuel Pellet Model as a function of linear power. At low linear powers the flexural rigidity is approximately equal to that of the empty sheath (25.6 N m^2).

The flexural rigidity of the Individual Fuel Pellet Model follows the expected trend as the linear power changes. At low power, the pressure between the pellet and sheath are low and the fuel

stack provides little resistance to the bending moment in the sheath. The flexural rigidity approaches a steady value, which is slightly higher than an empty sheath. As the power increases, the pellet-sheath interaction increases, even with frictionless contact, and the overall fuel element stiffness increases. This behaviour is representative of the REF applied in the BOW code. Quantifying the REF value from this analysis is difficult because the total fuel stack contribution is not known. In reality, it is expected that a high linear power of 50 kW m^{-1} would maximize the enhancement factor. However, the analysis shows that the enhancement factor continues to increase beyond 50kW m^{-1} and would have to be greater than 1. This discrepancy could be derived from the absence of pellet cracking in the Individual Fuel Pellet Model, which would likely saturate the enhancement. Although an equivalent 'gripping factor' cannot be determined for the Individual Fuel Pellet Model, the shape of the stiffness profile across the power spectrum suggests the solid-element contact is behaving as expected.

Furthermore, the analysis was also performed on the Cracked-fuel Stack Model to determine if the fuel stack remained ineffective at resisting bending at lower powers. The results of this analysis are shown in Figure 7-21.

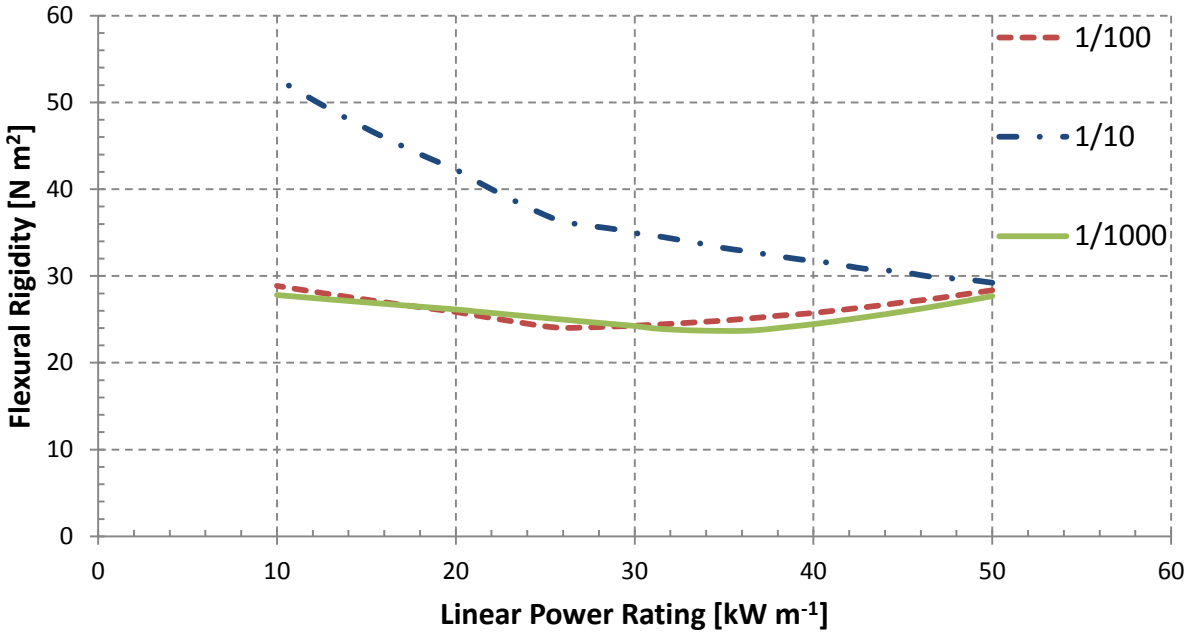

Figure 7-21: Flexural rigidity results of the Cracked-fuel Stack Model as a function of linear power. The separate lines represent the reduction factor of the Young's modulus in the cracked-fuel region.

The behaviour of the Cracked-fuel Stack Model is dependent on the Young's modulus reduction factor in the cracked-fuel region. When the Young's modulus is reduced by a factor of 10, the flexural rigidity continues to increase as the linear power is lowered. For larger reductions such as 100 and 1000, the flexural rigidity remains fairly consistent at a value resembling an empty sheath along the entire power ramp. The reason for this behaviour can likely be attributed to the contact interaction between the fuel and sheath. At low powers, the fuel is forced to remain in close contact with the sheath because there is no fuel-to-sheath gap present. In the Individual Fuel Pellet Model, the gap size is seen as an important feature which limits the sheath-to-pellet interaction in this power range. This is not possible in the Cracked-fuel Stack Model because the fuel stack fills this region as part of the composite beam formulation. This interaction leads to higher stiffness at low power if the Young's modulus is not reduced sufficiently. The similarities

between the flexural rigidity profiles when the Young's modulus is reduced by a factor of 100 and 1000 indicate a proper range to reduce the cracked-fuel region in further deformation analyses. The slight offset in flexural rigidity from the empty sheath value is almost identical to that observed in the Individual Fuel Pellet Model, which indicates some minimal interaction exists between the fuel and sheath under the frictionless conditions.

7.3 Thermal Bowing

Thermal bowing is the primary mechanism being investigated for driving FE-PT contact under post-dryout heat transfer. The mechanical studies provide an indication of the fuel element's stiffness through a mechanically applied load. Similar to characterizing the fuel element models to mechanically generated bending moments, it is necessary to understand the response of a fuel element to thermally generated moments. The thermal study performed in this section evaluates the Individual Fuel Pellet Model and Cracked-fuel Stack Model behaviour under a thermal gradient. The deformation results and a comparison with two fuel element bow formulations are presented.

7.3.1 Effect of Thermal Gradient

It was mentioned that thermally driven deformation can result from large temperature gradients across the fuel sheath. During a transient such as Loss of Flow (an AOO event), dryout of the fuel sheath can create the necessary thermal gradients for this deformation to occur. A thermal bowing analysis is performed to further characterize the fuel element to investigate the impact of the fuel stack when a thermal temperature gradient is applied. A linear temperature gradient of 100 K, 200 K and 300 K is used to represent the typical increase in temperature caused by drypatches. Similar to the flexural rigidity analysis, an empty sheath and monolithic pellet stack

simulation are used to provide a benchmark for comparison against analytical solutions. Accurately predicting the individual component responses to thermal loads offers greater confidence in their combined behaviour when assembled together in a fuel element model. For the empty sheath and monolithic fuel model, the thermal gradients were prescribed through a linearly varying thermal body load across their diameter (see Figure 7-22).

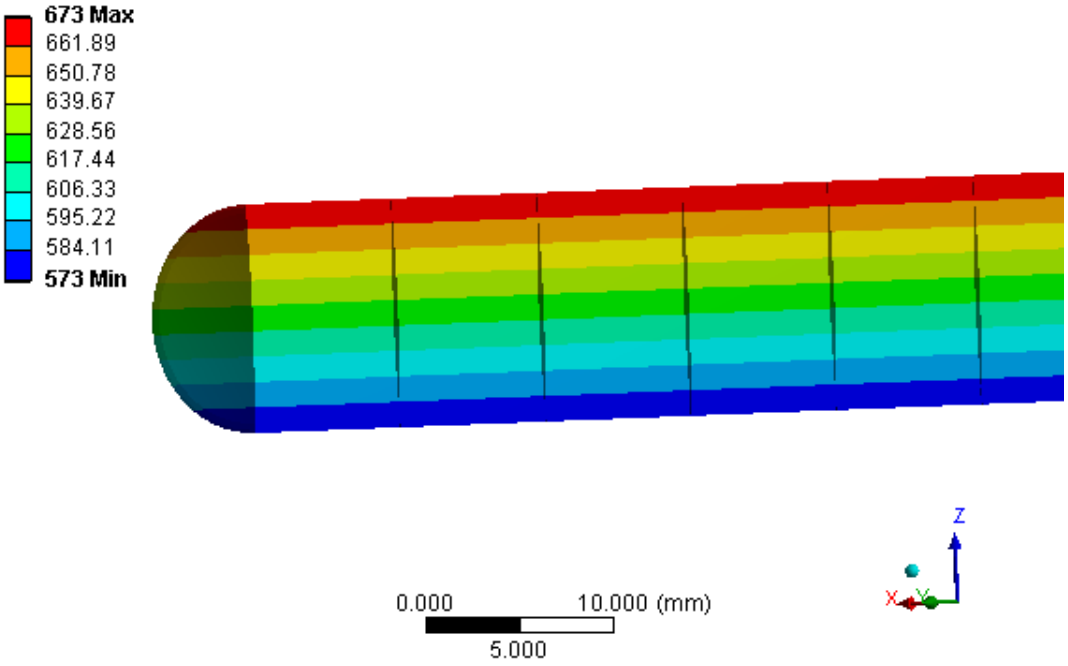

Figure 7-22: Linear temperature gradient across the monolithic pellet stack.

An estimate for the extent of bowing in the empty sheath and monolithic pellet stack can be made with the following deflection relation

$$\delta = \frac{-\alpha L^2}{16b}(\Delta T_i) \tag{7-5}$$

where δ is the vertical midplane deflection, α is the coefficient of thermal expansion of the material, L is the length between supports of the beam, b is the outer sheath radius (or pellet

radius, a_p) and ΔT_i is given by the linear difference between the maximum and minimum temperature applied across the body, $\Delta T_i = \{T_{Max} - T_{Min}\}$.

For the Individual Fuel Pellet Model and the Cracked-fuel Stack Model, the linear gradient is manipulated through the convective heat transfer coefficient from the sheath-to-coolant by varying the bulk coolant temperature across the sheath surface (see Figure 7-23).

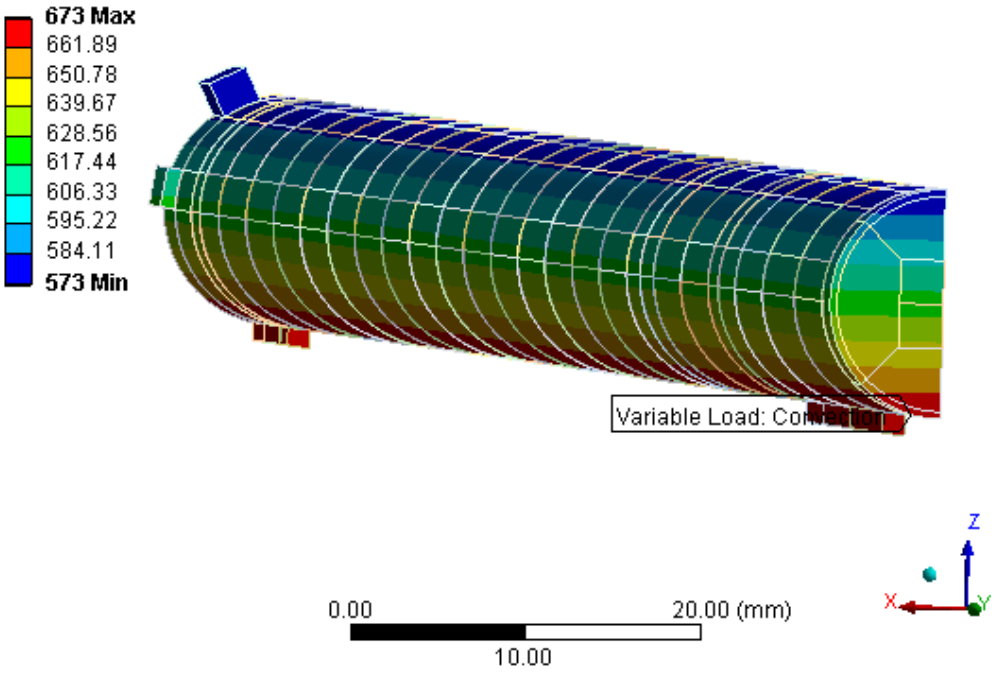

Figure 7-23: Linear bulk coolant temperature increase of the sheath-to-coolant heat transfer boundary condition to induce a temperature gradient.

The gradient is applied from top to bottom of the fuel sheath so that downward bowing of the fuel element occurs. Thermal gradients of 100, 200 and 300 K were applied by varying the nominal coolant temperature from 573 K to 673, 773 and 873 K respectively. For the fuel element models, the thermal load was applied in a sequential load step after NOC was reached.

When estimating the total deflection of a fuel element under operating conditions, Veeder and Schankula [13] suggests the temperature gradient, ΔT_i, which arises due to non-uniform coolant temperatures is given by

$$\Delta T_i = \frac{2\beta \bar{T}_c}{1 + \frac{h_{ps}}{h_{sc}}\left(\frac{k_p}{k_p + a h_{ps}}\right)} \tag{7-6}$$

where

$$\beta = \frac{T_c(\max) - T_c(\min)}{T_c(\max) + T_c(\min)} \tag{7-7}$$

and h_{ps} is the pellet-to-sheath gap conductance, h_{sc} is the sheath-to-coolant convective heat transfer coefficient, $\bar{T}_c$ is the average coolant temperature around the element and k_p is the thermal conductivity of the pellet. Also, the mechanical interaction between the bowed fuel stack and the sheath must be considered. To account for the ability of the fuel to grip the sheath, the equivalent temperature gradient, which would produce a deflection equal to that caused by the pellet-sheath interaction is

$$\Delta T_i = \mathrm{G}_{ps} \frac{2q'D}{\pi a\left(1 + \frac{k_p}{aH}\right)}\left[\frac{\frac{\alpha_p}{\alpha_s} - 1}{H} + \frac{1}{h_{ps}}\right] \tag{7-8}$$

where G_{ps} is the pellet-to-sheath 'gripping factor', q' is the power per unit length of the element and *D* is a factor determined by the flux depression through the fuel bundle [13]. *H* is the total thermal impedance between the fuel surface and coolant given by

$$\frac{1}{H} = \left(\frac{1}{h_{ps}} + \frac{1}{h_{sc}} + \frac{b - a}{k_s}\right) \tag{7-9}$$

The combined bowing from both interactions can be estimated by substituting the total thermal gradient from Equation 7-6 and Equation 7-8 into Equation 7-5.

Furthermore, Suk et al [33] re-derived the bowing analysis model of Veeder and Schankula [13] by considering an alternate formulation for estimating the effects of coolant temperature variation and film heat transfer coefficient on element bowing. The analytical formulation is derived through two separate considerations. The first evaluates the bowing of an empty sheath without mechanical interaction between the fuel and sheath by only considering bending moments generated through peripheral temperature gradients. The second evaluates the bending due to the interaction between the pellet stack and sheath caused by induced mechanical strain when the fuel grips the sheath. The generalized equivalent temperature gradient [33] caused by the combined effects of the empty tube bending and pellet-sheath interactions is given by

$$\Delta T_i = \frac{2\left\{aK_1\left(\bar{h}_{sc}(1-\gamma^2)\beta\bar{T}_c - \gamma\bar{w}\right) - 2b\bar{w}D\right\}}{K_2} + \frac{2G_{ps}b}{a\alpha_s}\left\{\beta\bar{T}_c\left(K_3 - \frac{K_4\bar{h}_{sc}k_p(1-\gamma^2)}{K_2}\right) + \frac{K_4\bar{w}\left(k_p\gamma - 2\bar{h}_{sc}(1-\gamma^2)bD\right)}{K_2}\right\} \tag{7-10}$$

where

$$K_1 = 1 + \frac{k_p}{ah_{ps}} + \frac{k_p(b-a)}{ak_s} \tag{7-11}$$

$$K_2 = k_p + a\bar{h}_{sc}(1-\gamma^2)\left(1 + \frac{k_p}{ah_{ps}} + \frac{k_p(b-a)}{ak_s}\right) \tag{7-12}$$

$$K_3 = \alpha_p - \alpha_s \tag{7-13}$$

$$K_4 = \left(\alpha_p - \alpha_s\right)\left(\frac{1}{h_{ps}} + \frac{1}{\bar{h}_{sc}} + \frac{b-a}{k_s}\right) + \frac{\alpha_s}{h_{ps}} \tag{7-14}$$

and

$$\bar{w} = \frac{q'}{2\pi b} \tag{7-15}$$

$$\gamma = \frac{h_{sc}(\max) - h_{sc}(\min)}{h_{sc}(\max) + h_{sc}(\min)} \tag{7-16}$$

The presented analytical models for predicting fuel element bow due to non-uniform coolant conditions are used for comparison with the solid-element models.

7.3.2 Effect of Thermal Gradient Results

The thermal gradient analysis was first completed for the empty sheath and monolithic fuel stack. The analytical solution was computed using Equation 7-5 with the axial thermal expansion coefficient evaluated at the average temperature between 573 K and the maximum given by the gradient. For example, a value of 723 K was chosen for the 300 K temperature gradient. The maximum deflections calculated in ANSYS are compared with analytical solutions in Table 7-8.

Table 7-8: Deflection results of the empty sheath and monolithic pellet stack for the prescribed thermal loads. The analytical solutions are provided for comparison.

Temperature Gradient Across Diameter [K]	Maximum Bow [mm]					
	Empty Sheath			Monolithic Pellet Stack		
	ANSYS	Analytical	Error (%)	ANSYS	Analytical	Error (%)
100	2.914	2.891	0.79	2.441	2.384	2.39
200	5.821	5.782	0.66	4.913	4.779	2.79
300	8.727	8.673	0.62	7.450	7.191	3.60

The simulation results show very good agreement with the analytical solutions. The longer free length of the empty sheath and larger axial thermal expansion coefficient of Zircaloy results in a larger deflection for the empty sheath model compared with the monolithic pellet stack. Slight differences in values can be associated with the temperature dependent material models and the selection of an averaged thermal expansion coefficient. The relative errors in the empty sheath model decrease as the thermal gradients are increased, which is opposite to the trend observed

for the monolithic pellet stack model. Also, the monolithic pellet stack produces slightly larger errors than the empty sheath, which likely occurs from assuming these geometries behave as simple beams, when in fact spaces between pellets and appendages on the sheath could have minor influences.

Next, the successful thermal benchmark of the individual components allowed the fuel element models to be investigated. The Individual Fuel Pellet Model and Cracked-fuel Stack Model were selected for further characterization. Unlike the component analysis, the thermal gradient was applied in the convective heat transfer boundary conditions by varying the bulk coolant temperature around the sheath. The Cracked-fuel Stack Model was simulated under three different conditions corresponding to the Young's modulus in the cracked-fuel portion being reduced by a factor of 10, 100 and 1000 times. The maximum vertical deflections calculated in the simulations are displayed in Figure 7-24.

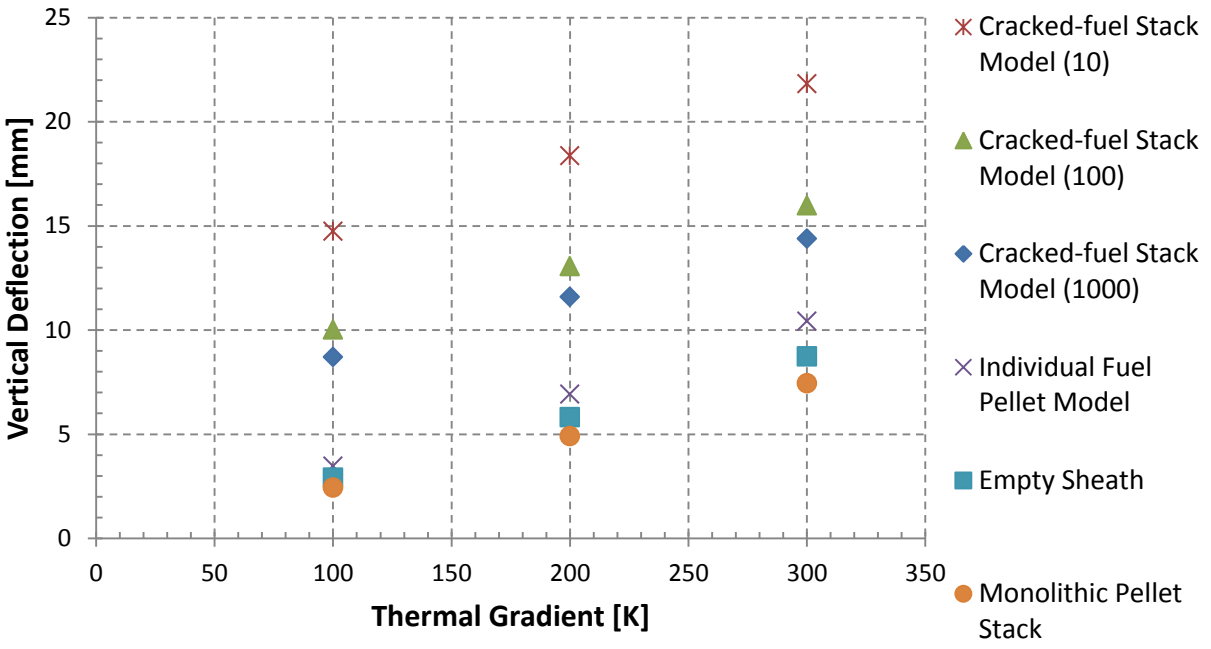

Figure 7-24: Vertical deflections of the Individual Fuel Pellet Model and the Cracked-fuel Stack Model with the Young's modulus reduced by a factor of 10, 100 and 1000. The empty sheath and monolithic pellet stack are also included for comparison.

The linear relationship between the thermal gradient and maximum deflection given in Equation 7-5 appears to hold true for the fuel element simulations. As the thermal gradient was increased across the fuel sheath, the total deflection increased in a linear proportion. An illustration of the Individual Fuel Pellet Model deflection is given in Figure 7-25.

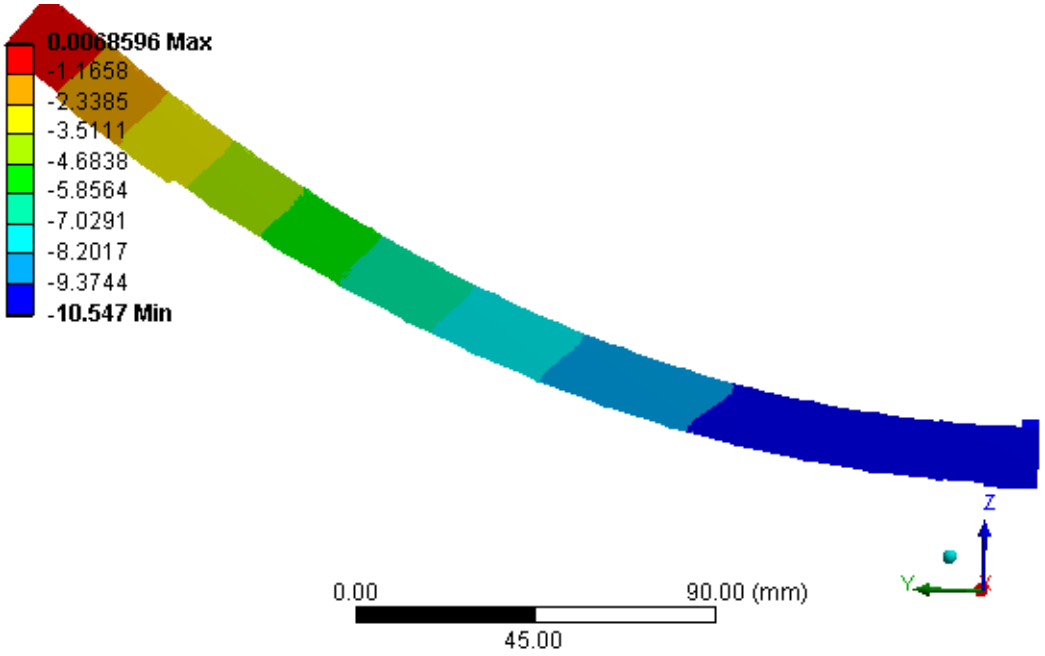

Figure 7-25: Vertical deflection from a 300 K thermal gradient induced on the Individual Fuel Pellet Model. The deflected profile has been magnified by 10x to emphasize the shape. It is not to scale.

The deflections recorded for the Individual Fuel Pellet Model were consistently higher than the empty sheath and monolithic pellet stack model for each thermal gradient. Although the linear thermal gradients were applied differently for the two sets of simulations (body load vs convective), they were each set to the same magnitude. As well, this deformation behaviour is observed to be more pronounced with the Cracked-fuel Stack Model. In contrast to the flexural rigidity analysis, the vertical deflection in the fuel element models is always greater than the empty sheath model. This is only possible if the fuel stack is a positive contributor to the overall bowing. When the fuel sheath is subjected to a thermal gradient, a similar gradient develops in a portion of the fuel. As a result, the applied thermal load generates a bending moment in both the sheath and fuel stack. In this case, rather than helping resist the applied bending moment on the sheath, the fuel stack contributes to the deformation and causes an overall larger bowing

response. This behaviour, where pellet bending is transferred to the sheath, is captured in the BOW code via the CTF value.

Furthermore, the thermal gradient analysis found the Cracked-fuel Stack Model to have a larger deflection than the Individual Pellet Model for each applied gradient. This result coincides with the flexural rigidity analysis, which found the stiffer Individual Fuel Pellet Model deflected less under the same mechanical loading. The relative difference in deflection magnitude between both models remained roughly the same for all three thermal gradients. This indicates both models respond almost linearly to an increase in gradient. One of the most intriguing results of this analysis surrounds the behaviour of the Cracked-fuel Stack Model, when the Young's modulus was lowered in the cracked-fuel region. The results show a consistent decrease in vertical deflection by about the same proportion under each thermal gradient. The trend shows a sharp decrease in deflection but begins to steady at a deflection which is still greater than the Individual Fuel Pellet Model. Based on the initial deflections of both the Individual Fuel Pellet Model and Cracked-fuel Stack Model, it was expected that a lower stiffness would increase the amount of thermal bowing for a fuel element. Surprisingly, the simulations revealed the opposite behaviour. To explain why the vertical deflection decreased, one has to note the observation made above, which is that the fuel stack contributes to the total thermal bow. When the stiffness is reduced in the cracked-fuel region, the ability of the UO_2 to transfer its bending moment to the sheath is reduced and the majority of the remaining deflection is caused by the bending moment in the sheath. Applying this logic to the Individual Fuel Pellet Model implies the disjoint pellets inside the sheath are only able to transfer a small amount of bending to the sheath. The degree of fuel stack contribution in both models is derived by how the pellet and sheath interact. In the

Cracked-fuel Stack Model, the fuel is a solid component and lies directly in contact with the sheath. This permits a high degree of transfer even with frictionless contact. In the Individual Fuel Pellet Model, the gap between the fuel and sheath along with pellet-to-pellet contact interactions does not present optimum conditions for transfer.

In addition, a comparison of the Individual Fuel Pellet Model with the analytical formulations provided by Veeder and Schankula [13], and Suk et al. [33] is made for the thermal gradient analysis. In order to present a direct comparison, the material properties in the ANSYS model were changed to constant parameters to match those used in the calculations. A sample calculation is provided in the Appendix. The results of these analytical models along with the Individual Fuel Pellet Model are provided in Table 7-9. The non-uniform coolant deflection is calculated with Equation 7-6 for V&S and the left hand term of Equation 7-10 for Suk et al. The Pellet/Sheath interaction deflection is calculated using Equation 7-8 for V&S and the right hand term of Equation 7-10 for Suk et al. Since the ANSYS model inherently captures both effects, the deflection is presented as a single value.

Table 7-9: Thermal bowing estimates based off the Veeder and Schankula model for non-uniform coolant temperature around a fuel element.

Thermal Gradient	**100 [K]**		**200 [K]**		**300 [K]**	
	Non-uniform Coolant [mm]	Pellet/Sheath Interaction [mm]	Non-uniform Coolant [mm]	Pellet/Sheath Interaction [mm]	Non-uniform Coolant [mm]	Pellet/Sheath Interaction [mm]
V&S	2.635	-	4.878	-	6.810	-
Suk et al.	2.635	-0.663	4.878	-1.227	6.811	-1.713
ANSYS	3.465		6.572		9.506	

Although both models are based on the work of Veeder and Schankula, the derivation provided by Suk et al. did not include the neutron flux gradient factor in the pellet-sheath interaction term, which allowed an estimate for its contribution to resist thermal bow. The values were calculated for a pellet-to-sheath gripping factor, G_{ps}, of 1. The Individual Fuel Pellet Model predicted higher values than both analytical formulations. Although a similar linear trend was observed across the thermal gradients, a closer agreement between values was expected. The over prediction is surprising because the characterization of the Individual Fuel Pellet Model showed the equivalent REF to be greater than 1(Figure 7-20). A larger stiffness would yield less deflection, which should lead to an under prediction. The fact that over prediction was observed suggests there may be 3-dimensional effects, such as the observed fuel stack bending contribution, which is not captured in the 1-dimensional formulations. Nevertheless, fuel element model seems to respond reasonably to the applied gradient indicating a properly behaving solid-element contact connection.

7.4 Summary of Characterization Results

Multiple fuel element models were used as part of the solid element approach to modelling fuel element deformation behaviour. These models were characterized through a flexural rigidity study, a thermal bowing analysis and compared with analytical formulae when possible. Accurately predicting fuel behavior under simple loading conditions allows further extensions to be studied with added confidence in the qualitative results. These types of studies are necessary when simulating fuel deformation behaviour because limited experimental information has been correlated to provide quantitative predictions about fuel bowing for complex loading conditions like drypatch formations. Without experimental or correlated results, modelling can only offer

qualitative insight into these complex systems, which can be used to guide further studies. Solid element modelling offers advantages over beam theory models for analyses requiring 3-dimensional loading conditions and/or contact modelling between interacting components. The work of this chapter has characterized the Individual Fuel Pellet Model and Cracked-fuel Stack Model as two distinct fuel element representations with diverse fuel-to-sheath contact behaviour which both show potential. The limited quantity of published results for the bending stiffness of a fuel element has made it difficult to characterize the REF in the Individual Fuel Pellet Model in order to compare the effectiveness of the different fuel element representations. A search in the literature for other reference values found a flexural rigidity value of 103 N m^2 reported by Jiang et al. [34] based on a 3-dimensional fuel element beam bending simulation performed with Martec's VAST finite element program suite. This value is most closely associated with the Individual Fuel Pellet Model (102.9 N m^2) and is assumed to fall within the typical range for expected fuel element stiffness. For the purposes of developing a fuel deformation model, pursuing a model with the lowest flexural rigidity will provide some conservatism in estimating fuel element deflection. The Cracked-fuel Stack Model was found to represent a lower bound for the stiffness, which was not much higher than that of the empty sheath. This behaviour was also found at lower powers when the Young's modulus was reduced by a factor of 100 and 1000 in the tensile fuel region. Unlike the Individual Fuel Pellet Model, the cracked-fuel stack was observed not to resist any mechanically generated bending moment in the sheath, despite using the same frictionless contact connection. The behaviour was attributed to the physical geometry representation, which saw the Individual Fuel Pellet Model use individual interacting pellets separated by a diametral and axial gap verses the Cracked-fuel Stack Model, which used a solid cylinder with no gaps. This difference in behaviour offers two extremes for what the stiffness of

an actual fuel element at high power may be in reality. To investigate this assumption further, both models were subjected to a thermal gradient analysis. The results of the thermal bowing analysis indicate the Cracked-fuel Stack Model was again the most conservative fuel element model to use in a FE-PT deformation study. The fuel stack was found to transfer a large portion of its own bending moment to the sheath to effectively increase the total deformation. Reducing the Young's modulus in the cracked-fuel region was found to decrease the amount of thermal bow due to less curvature transfer. Similarly, the Individual Fuel Pellet Model was observed to contribute a portion of the bending moment generated in the pellet stack to the sheath but was much smaller in magnitude. The difference in behaviour was again attributed to the fuel-to-sheath representation, where the absence of a physical gap led to a larger transfer in bending moment compared to having interacting components with a gap. The various studies performed within this chapter allowed a lot of information to be gathered about both fuel element representations. However, neither one can confidently predict the real nature of a fuel element without experimental comparison. As a result, exploring both the Individual Fuel Pellet Model and Cracked-fuel Stack Model as the fuel element representation in a FE-PT contact deformation model would provide a useful indication of what specific modelling characteristics are the most important for capturing overall behaviour under post-dryout thermal conditions. The Cracked-fuel Stack Model pursued for further investigation uses a reduced Young's modulus of 100 times, which maintains its conservative nature.

8 Post-dryout Fuel Element Deformation

The development of a fuel deformation model, in this thesis, with the ability to simulate FE-PT contact requires a two-phase approach. The first phase investigated potential candidate fuel element models to use within the FE-PT contact study. Distinct models were characterized under separate mechanical and thermal loading analyses to determine the best choices moving forward. The second phase seeks to expand upon the realised models developed in the first phase by extending their geometry to full length, and subjecting them to a FE-PT contact study under complex heat transfer conditions. The study investigates 3-dimensional drypatches to generate large temperature gradients across the sheath in order to induce the necessary deformation. This chapter describes the second phase work, which focuses on using the Individual Fuel Pellet Model and Cracked-fuel Stack Model as potentially viable options for analysing FE-PT contact and deformation under post-dryout conditions. A detailed description of the drypatch analysis along with a discussion related to the findings and implications is provided in this chapter. Also, a multi-drypatch benchmark case, similar to the one used as part of the BOW Code verification studies, is simulated with the fuel element models.

8.1 Fuel Element Models

Predicting CHF locations (i.e., subchannel and direction) and induced drypatch geometries for given operating conditions and element design is extremely difficult. Typical dryout locations tend to form downstream of the fuel bundle along the ¾ length plane. In order to simulate the asymmetric generation of drypatches and their spreading post-dryout along a fuel element, a full length fuel element representation is required. Fuel element bowing caused by a drypatch formation will bend towards the direction of higher temperature. Therefore, the most challenging

location for dryout to occur and result in the fuel element contacting the pressure tube would be in the subchannel of an outer ring fuel element facing towards the pressure tube. Representing a uniform drypatch in this region of the sheath allows the fuel element geometry to be simplified by one plane of symmetry down the axial length. Also, a section of pressure tube is needed to support the fuel element and account for the important support provided from the bearing pads. Descriptions of the modifications made to the Individual Fuel Pellet Model and Cracked-fuel Stack Model for use in the second phase are given below.

8.1.1 Individual Fuel Pellet Model

8.1.1.1 Geometry

The geometry required for the drypatch analysis is derived by simply mirroring the Individual Fuel Pellet Model at the half-length symmetry plane to create a full length fuel element with only one plane of symmetry. A section of a pressure tube is added to the geometry and positioned so that the fuel element is supported by resting directly on top. The remaining symmetry plane on the fuel element is aligned with pressure tube as shown in Figure 8-1.

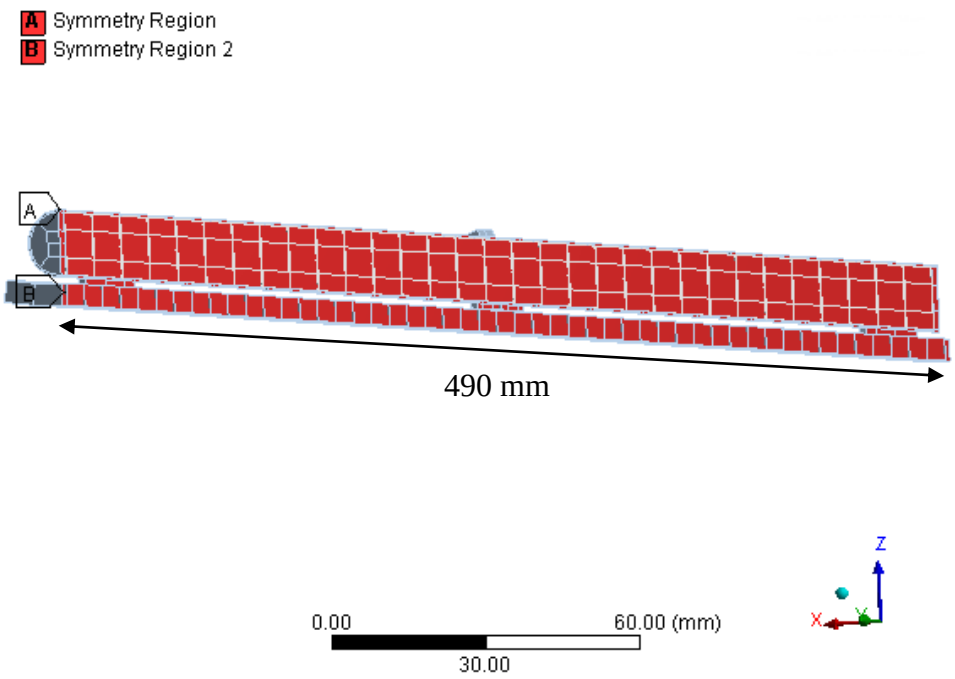

Figure 8-1: Symmetry region applied to the full length Individual Fuel Pellet Model.

The single plane of symmetry results in a fuel element that is twice the size with 31 pellets, 3 bearing pads and two end caps. The updated dimensions for the fuel element and the pressure tube section are provided in Table 8-1.

Table 8-1: Specified dimensions for the full-length Individual Fuel Pellet Model and associated pressure tube section.

Full Length Fuel Element Features	**Dimension [mm]**
Element length including End Caps	490
End Cap thickness	3
Total axial gap	3
Axial gap between pellets	0.094
Pressure Tube Features	
Pressure tube OD	112.36
Pressure tube thickness	4.3
Arc angle	12.5 Degrees

8.1.1.2 Element Type and Mesh

The full geometry utilized in this phase is shown in Figure 8-2. The element mesh is composed of 111,902 elements (52,080 Pellets, 52,830 Sheath, 1680 End Caps and 5312 Pressure tube) for a total of 642,618 nodes. By utilizing the same physical components, a similar mesh discretization is applied to the individual pieces.

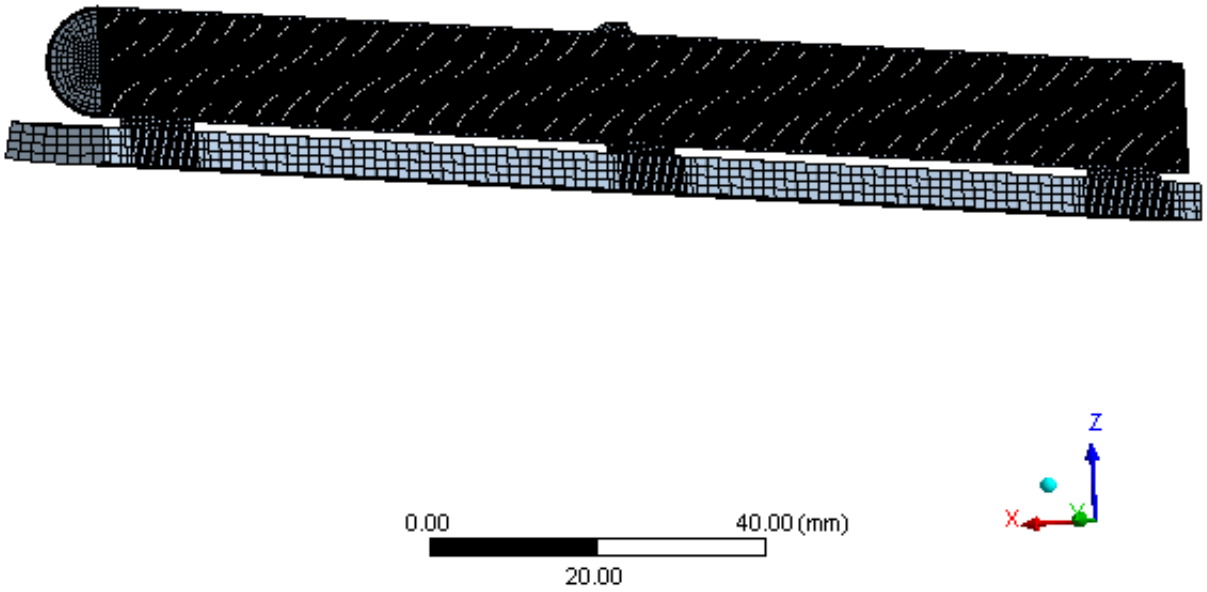

Figure 8-2: Full length fuel element resting on a section of pressure tube.

8.1.1.3 Thermal Loading and Boundary Conditions

Similar to Phase 1, the fuel element model is brought to the normal operating conditions specified in Table 7-3 before the analysis is performed. The incorporation of the pressure tube geometry requires additional boundary conditions to be considered. In the reactor, the pressure tube is exposed to the PHTS coolant on the inside surface and the annulus gas system on the outside. A convective heat transfer boundary condition is applied on both sides of the pressure tube to capture these conditions. The inside surface is specified with the same 50 kW m^{-2} K^{-1}

sheath-to-coolant boundary condition, while the outside is prescribed a convective coefficient of 320 W m^{-2} K^{-1} with a bulk moderator temperature of 353 K. These parameters were selected to maintain the pressure tube wall temperature at roughly 573 K. To allow heat transfer between the bearing pads and the pressure tube, the two outside bearing pads are given a No Separation contact connection. The pressure tube surface is taken as the Target surface and the bearing pads are the Contact surfaces (see Figure 8-3).

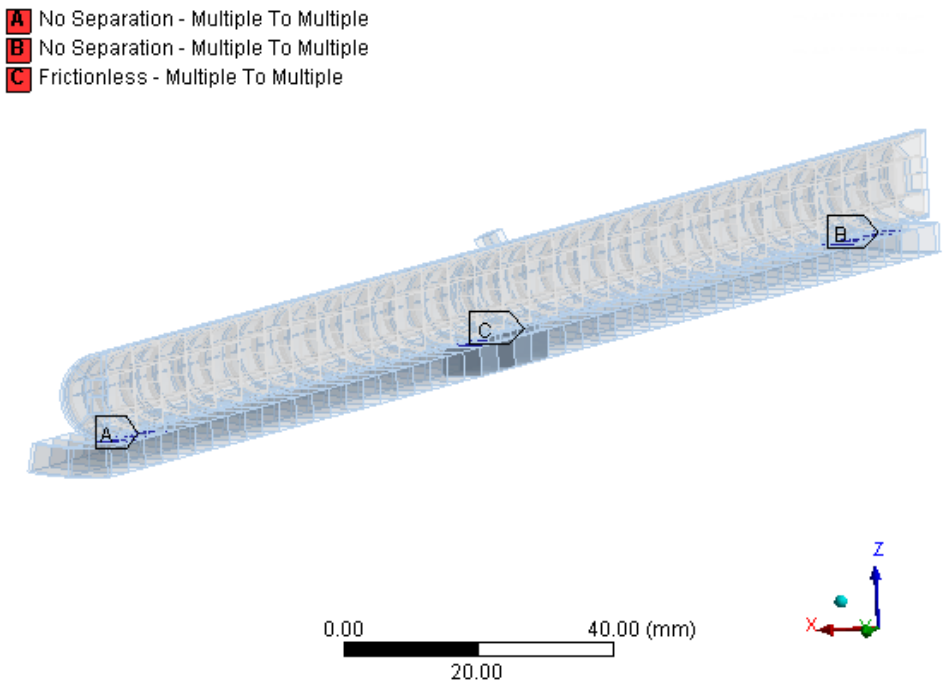

Figure 8-3: Bearing pad contact connections established with the pressure tube. The outer bearing pads are specified as No Separation and the center pad is Frictionless.

The previously established fuel-to-sheath contact connections are updated to reflect the reduction in symmetry. In addition, the single pellet-to-end cap connection is duplicated for the opposite end.

8.1.1.4 Structural Loading and Boundary Conditions

Similarly to the thermal analysis, many structural loads and boundary conditions remain the same in the full length model. A coolant pressure of 10 MPa is applied to the full surface area of the sheath and a gravity body load is applied to all components. Also, the previous structural contact connections are updated to account for changes in symmetry, while the end bearing pad connections do not require changes. The No Separation bearing pad contacts force the fuel element to stick with the pressure tube in the normal direction but do not restrict its movement axially. The center bearing pad is slightly shorter in height than the other two (Table 7-2) so a Frictionless contact connection is established between it and the pressure tube. This allows the center bearing pad to come in and out of contact with the pressure tube in the normal direction. Spatial constraints applied to the pellet dishes remain active to engage contact between components for NOC. In addition, the hinged boundary condition applied to the end cap is kept for one side of the fuel element, but the same spot on the opposing end cap is constrained from moving axially. This is necessary to prevent the entire fuel element from sliding along the pressure tube. These boundary conditions are a simplification for the effect of an end plate. For the current analysis, the section of pressure tube is treated as a rigid body and does not exhibit any deflection. In reality, the pressure tube is held at one end of the reactor and allowed to strain axially at the other, due to internal fluid forces causing axial growth. For the purposes of being a support and contact surface in this analysis, a rigid body assumption is acceptable.

8.1.2 Cracked-Fuel Stack Model

The changes required for the Cracked-fuel Stack Model are external to the fuel stack and were captured in the Individual Fuel Pellet Model section above. The Cracked-fuel Stack Model is updated accordingly for participation in the drypatch analysis.

8.2 Drypatch Analysis

An attempt to characterize the CHF and post-dryout performance of 37-element fuel under steady state and transient conditions has been conducted by the CANDU industry through experimental research [35]. Drypatch maps have been analyzed to understand the extent of fuel element patchy dryout, such as patch sizes, temperature ranges, spread trends and locations in the bundle, under postulated overpower or loss of flow events [35]. Results from the literature have indicated a wide distribution among variables with no direct correlations established. For the purposes of a FE-PT contact study, the most severe location for a single drypatch to occur is midway between two adjacent supporting points or half the free span length. The amount of fuel bowing will be determined by both the circumferential temperature gradient and drypatch width. An analysis is performed to evaluate fuel element bowing caused by the formation of a drypatch between the center and end bearing pad (location to be shown in Figure 8-5). The extent of bowing is restricted through the inclusion of bearing pad contact with the pressure tube. An additional Frictionless contact definition is applied between the sheath and pressure tube at the dryout location to capture any physical FE-PT contact interaction (see Figure 8-4).

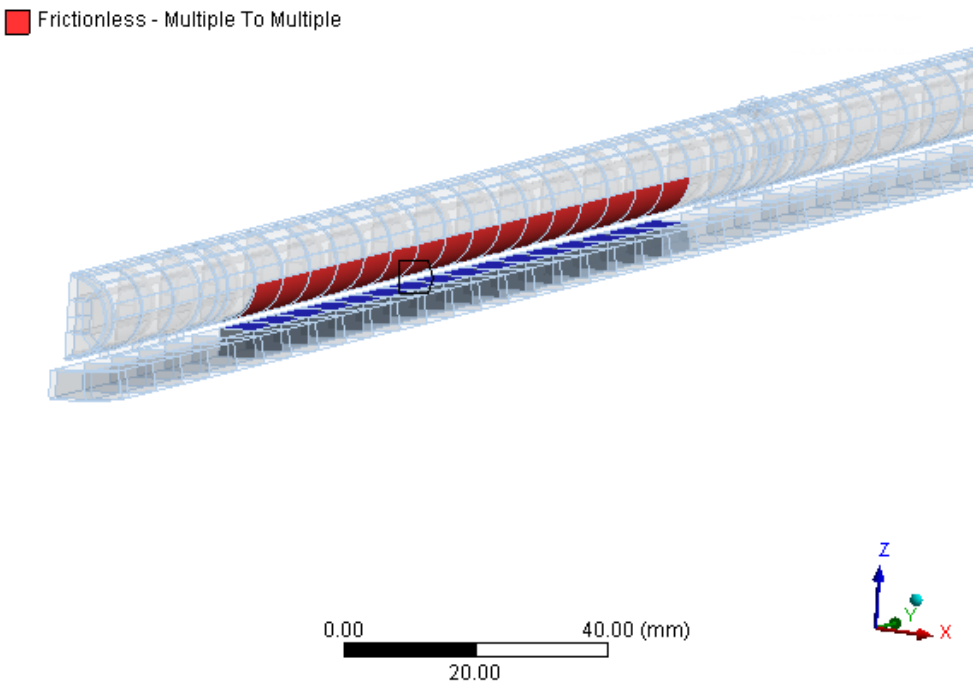

Figure 8-4: Frictionless contact connection established between the sheath and pressure tube for FE-PT contact.

Outer ring fuel elements are designed with three planes of bearing pads to avoid direct contact with the pressure tube under NOC. The placements of the bearing pads are chosen to reduce the free span length of the fuel element to limit outward deflection. The current trip parameters specified in G-144 are to prevent the sheath temperature from operating above 600°C to preclude any possible pressure tube interaction. The purpose of the drypatch analysis is to investigate the deformation behaviour of a fuel element whose sheath temperature surpasses this temperature limit and analyze the FE-PT contact behaviour, if any. Above 800 °C, high temperature creep becomes an important mechanism, which is responsible for increasing fuel element deformation. Below 800 °C, thermal gradients will likely be the largest contributor to fuel element deformation during upset conditions of short durations. Since the analysis focus is on transients

of this nature, specifying a drypatch temperature close to 800°C would provide the most severe thermal gradient to possibly cause FE-PT contact.

The drypatch analysis is conducted by bringing the fuel element model to NOC and then activating the drypatch in a following load step. The drypatch is formed halfway between the center and end bearing pad with a length of 10 mm and circumferential arc length of 100 degrees from the symmetry plane. This angle was found to correspond to the largest induced sheath temperature gradients from over 220 drypatch map results [35]. The temperature rise is applied by increasing the bulk coolant temperature of the convective heat transfer coefficient in the local area to 1073 K. This causes the inner sheath temperature to reach approximately 1120 K. An illustration of the induced temperature profile on the sheath is shown in Figure 8-5.

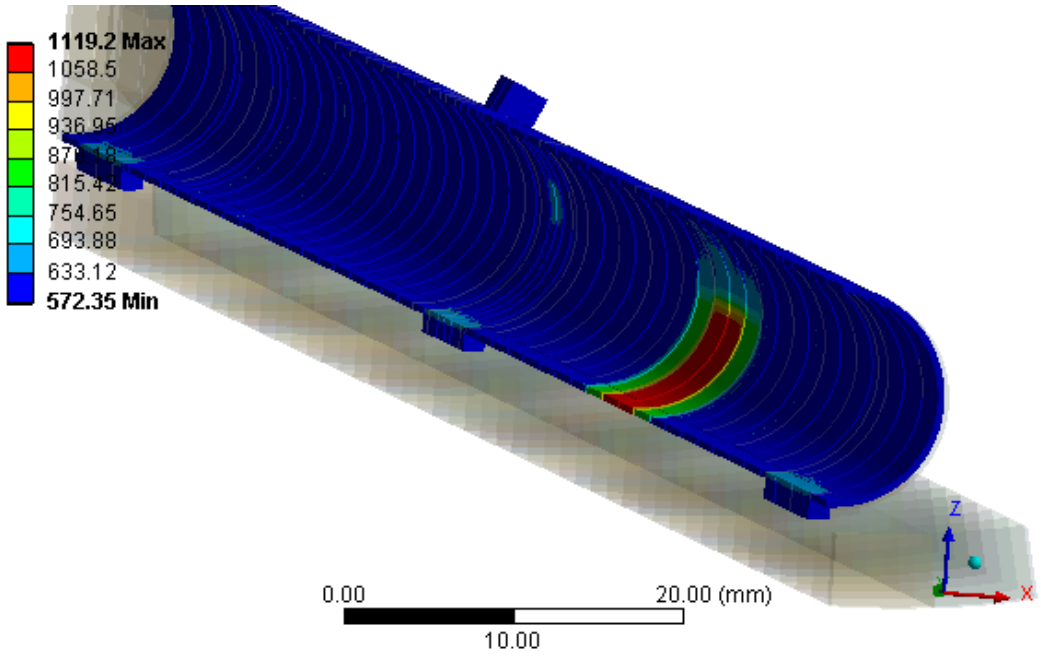

Figure 8-5: 10 mm drypatch on the bottom sheath surface facing the pressure tube.

A series of load steps are used to grow the drypatch axially between the bearing pads in increments of 20 mm, split evenly on either side. A total of eight load steps are used to create an expanded drypatch length of 150 mm (Figure 8-6).

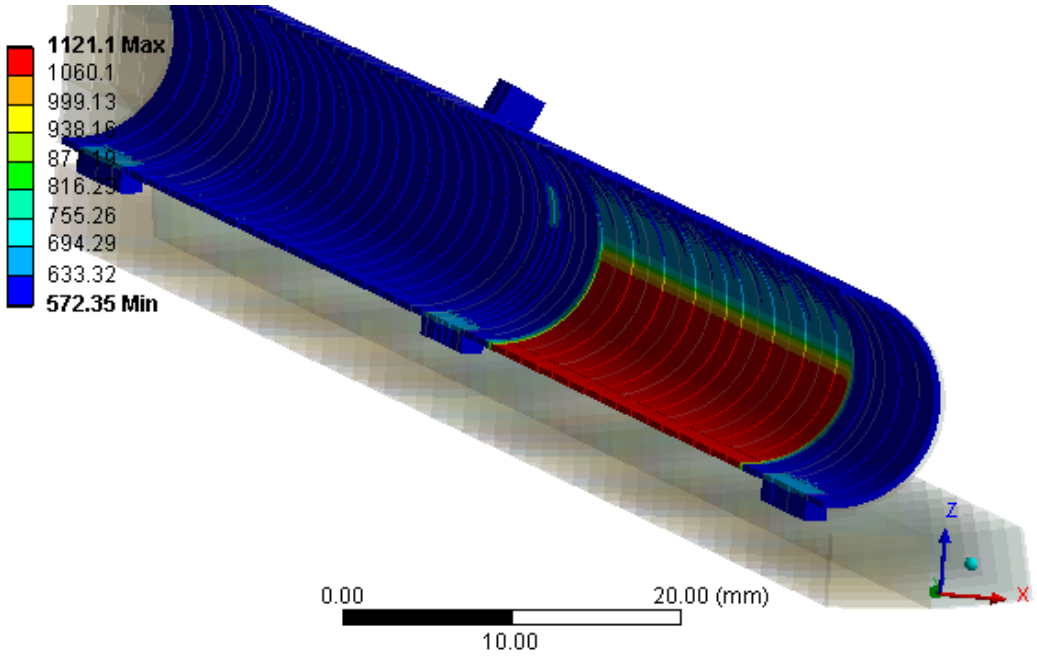

Figure 8-6: 150 mm drypatch on the bottom sheath surface facing the pressure tube.

The Cracked-fuel Stack Model has been demonstrated as a conservative model for predicting fuel element deformations under both mechanical and thermal loads. On the other hand, the Individual Fuel Pellet Model was shown to exhibit a stiffer fuel element response, which may be more representative of an actual fuel element inside a reactor. Utilizing both models in this analysis will provide some bounding estimate for the possibility of FE-PT contact as a function of fuel element stiffness.

8.3 Results of Drypatch Analysis

The fuel element deformation profile was extracted from the bottom sheath surface along the longitudinal plane of symmetry for each load step. The series of deformation profiles for the Cracked-fuel Stack Model with the Young's modulus reduced by a factor of 100 in the cracked-fuel region are displayed in Figure 8-7 and the series for the Individual Fuel Pellet Model are displayed in Figure 8-8.

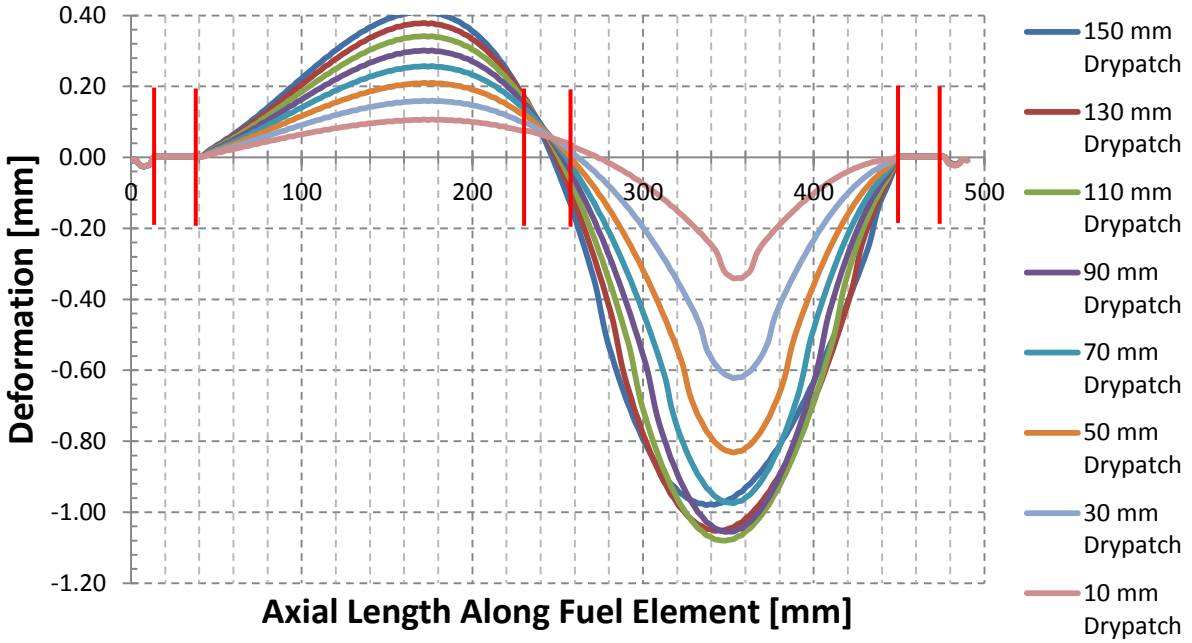

Figure 8-7: Fuel element deformation profile for various drypatch lengths for the Cracked-fuel Stack Model. Bearing pad locations are indicated by red lines.

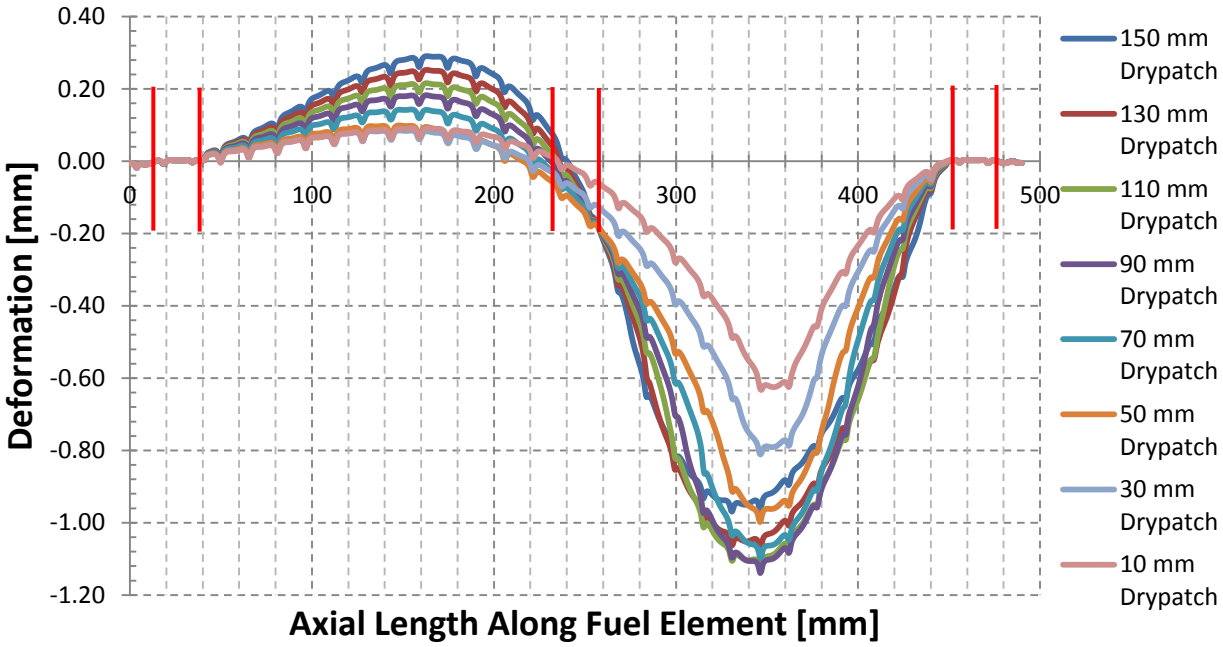

Figure 8-8: Fuel element deformation profile for various drypatch lengths for the Individual Fuel Pellet Model. Bearing pad locations are indicated by red lines.

One of the more obvious differences between the two figures is the small bumps along the deformation profile of Figure 8-8. These bumps correspond to the pellet ridges caused by the phenomenon known as pellet hourglassing. This creates a bamboo style profile along the outer sheath surface. Despite this small difference, the general deformation profiles between the two models are very similar. A comparison of the maximum deflections recorded for each drypatch length between models is tabulated in Table 8-2.

Table 8-2: Results for the maximum vertical deflection obtained for the various drypatch lengths.

	Maximum Vertical Deflection [mm]							
Drypatch Length [mm]	**150**	**130**	**110**	**90**	**70**	**50**	**30**	**10**
Individual Fuel Pellet Model	-0.969	-1.072	-1.131	-1.139	-1.098	-0.998	-0.811	-0.633
Cracked-fuel stack Model	-0.980	-1.053	-1.080	-1.055	-0.974	-0.832	-0.622	-0.341
Difference	0.011	-0.019	-0.051	-0.084	-0.123	-0.166	-0.189	-0.292

The largest deflection for the Individual Fuel Pellet Model is 1.139 mm and occurs with a drypatch length of 90 mm, whereas the Cracked-fuel Stack Model is 1.080 mm and occurs at 110 mm drypatch length. An illustration of the Individual Fuel Pellet Model's 3-dimensional deformation profile is given in Figure 8-9.

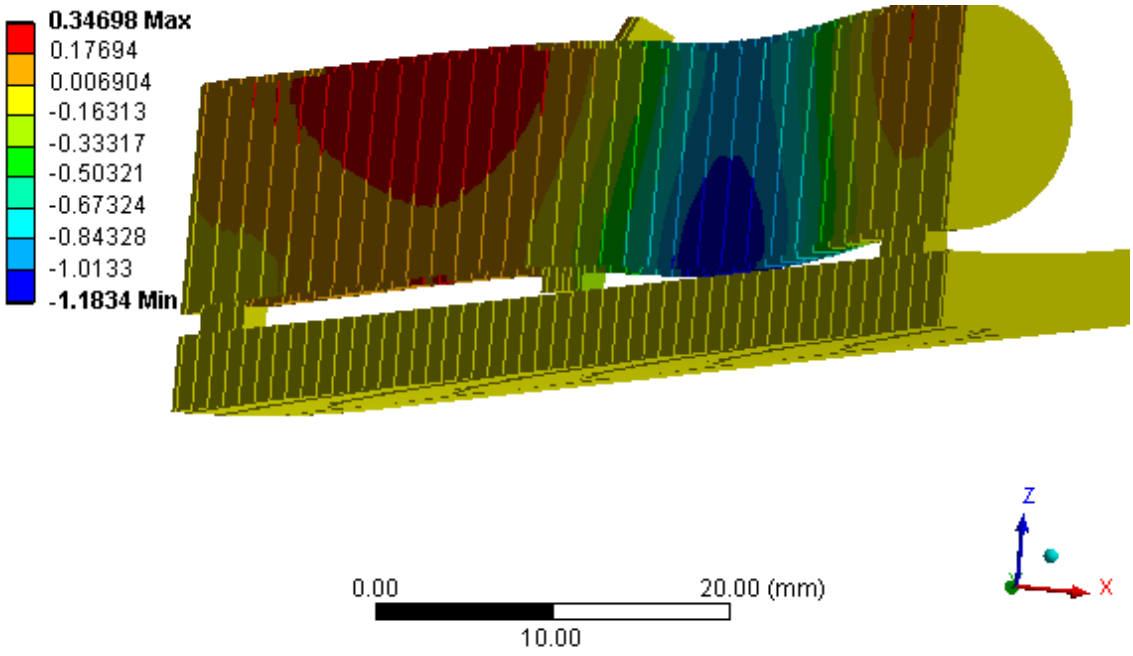

Figure 8-9: 3-dimensional deformation profile of the Individual Fuel Pellet Model for a drypatch length of 90mm.

The distance between the sheath and pressure tube is given by the height of the bearing pad, which is specified at 1.2 mm in this analysis. The difference between the model predictions is roughly 25% of this gap distance for small drypatch lengths but decreases to less than 10% for drypatch lengths greater than 70 mm. This indicates a fairly consistent estimate for the fuel element deflection between both models. A closer look between the two models for the 110 mm and 150 mm drypatch is illustrated in Figure 8-10.

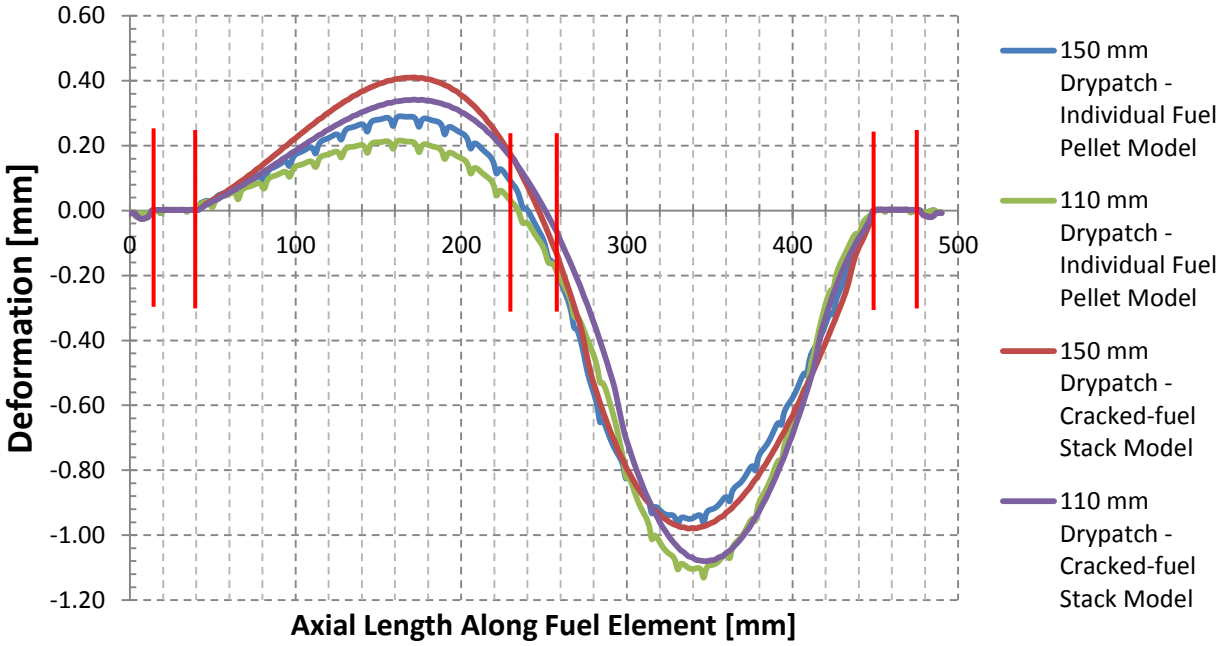

Figure 8-10: Fuel element deformation profile comparison between both fuel models for a drypatch length of 150 mm and 110mm. Bearing pad locations are indicated by red lines.

A direct comparison between the deformation profiles shows a very similar profile at both the maximum deflection and along the rest of the element. This is an intriguing result as two different fuel models, with very different flexural rigidities, behaved very similarly when constrained against the pressure tube. There were no noticeable profile effects which could be

confidently attributed to the difference in the physical representation of fuel-to-sheath contact. This is quite surprising as the results from Phase 1 clearly pointed out behavioural differences when the fuel element was not constrained against the pressure tube. Aside from asymmetric drypatch loading, the only constant which has changed is the support provided by the center bearing pad to reduce the free span length. These deflection profiles suggest the interaction of the bearing pads with the pressure tube, and the associated end plate constraints, help to limit the magnitude of deformation in between planes of bearing pads. The middle bearing pad appears to provide the majority of the resistance to sheath bowing rather than the pellet stack itself. This suggests the shape and temperature gradient of the drypatch are more influential than the stiffness of the fuel element for determining if contact with the pressure tube occurs for this type of configuration. The analysis only investigated one shape of drypatch, but additional studies with different shapes and locations may prove to find a scenario where the fuel element's stiffness and fuel-to-sheath contact configuration has a greater influence on the deflection profile.

One assumption made in the analysis is that the weight of the fuel bundle is heavy enough to maintain a flat connection between the outer bearing pads and pressure tube. The No Separation contact connection kept the two components together but allowed the fuel element to slide. The amount of fuel element deflection close to the outer bearing pad locations suggest separation of the bearing pad from the pressure tube may occur if these restraints were not enforced. This would produce a small increase in the free span length (distance between two bearing pad contact spots), which would influence the overall deformation profile. Investigating different

contact connections at the bearing pads was not pursued further but may influence the possibility of FE-PT contact.

In addition, an interesting trend observed in the results shows a relaxation in fuel element deformation once the peak magnitude has occurred. The continual increase in drypatch length consequently leads to a reduction in bowing after a certain point. This behaviour suggests that for this type of drypatch, there is an optimal length which serves to be the most challenging for FE-PT contact. The likelihood of a drypatch this size being maintained under reactor conditions before wrap around or rewetting occurs is not considered. Nevertheless, this occurred with a 90 mm drypatch in the Individual Fuel Pellet Model and 110 mm in the Cracked-fuel Stack Model.

Furthermore, contact was not observed for either model under any drypatch length simulation. The different fuel stack representations between the Individual Fuel Pellet Model and Cracked-fuel Stack Model proved to have minimal impact on the maximum deformation. It is difficult to conclude whether contact would occur under similar reactor conditions without accounting for more minor deflection contributors like flux depression and plasticity. However, the purpose of this deformation model is to demonstrate the ability to capture FE-PT contact if sufficient driving forces were to occur. Instead of investigating the individual model constraints, which may have limited deformation, another simulation was run where the sheath-to-coolant heat transfer coefficient in the drypatch area was reduced to zero.

Two different methods may be used to simulate an increase in fuel sheath temperature. The above drypatch analysis raised the bulk coolant temperature in the drypatch location to increase the surface temperature to the desired value. The second method involves reducing the sheath-to-coolant heat transfer coefficient, which decreases the boundary heat flux causing a rise in sheath temperature. This second method is used in the following drypatch analysis to demonstrate FE-PT contact. The most severe temperature gradient across a drypatch will occur if heat flow to the coolant is fully prevented. This is known as an insulated boundary condition and may be simulated by prescribing a surface heat flux of zero at the boundary. Forming a drypatch with an insulated boundary condition will produce an upper bound for the maximum sheath temperature. The same drypatch growth procedure described in the previous analysis is simulated using the insulated boundary condition in place of the convective condition. The insulated boundary induces a maximum sheath temperature of about 3200 K and is able to successfully demonstrate contact between the fuel element and pressure tube. The deflection profile of the Individual Fuel Pellet Model for different drypatch lengths is given in Figure 8-11.

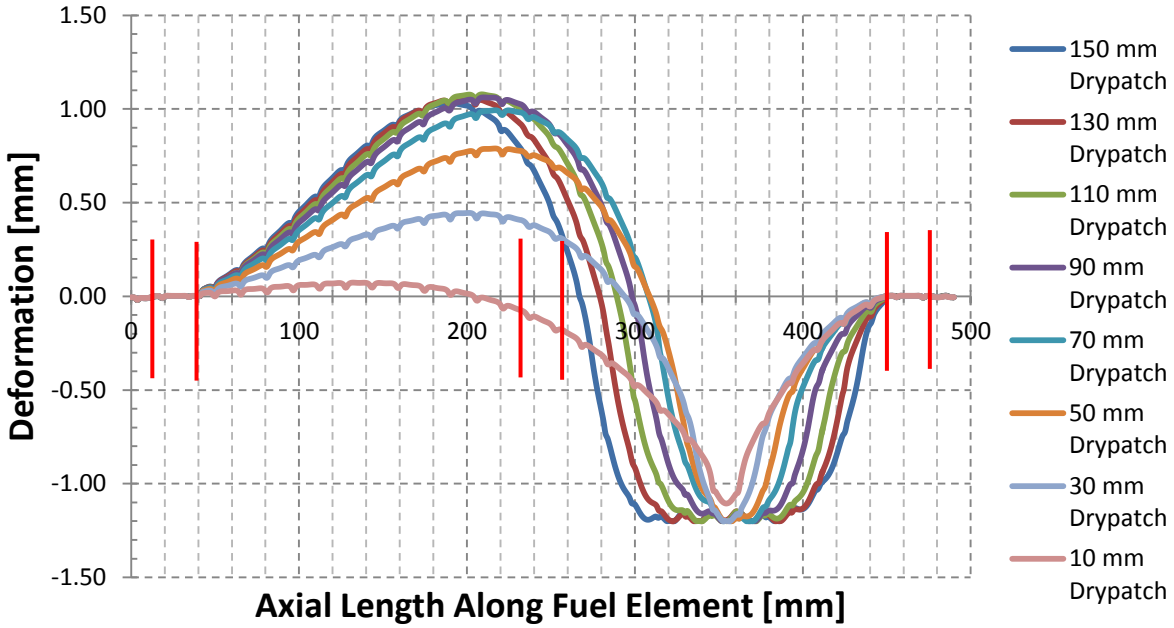

Figure 8-11: Individual Fuel Pellet Model deflection profile for insulated drypatch conditions. Bearing pad locations are indicated by red lines.

Once contact between the fuel element and rigid pressure tube occurs, any further bending is obstructed by the pressure tube and the deflection saturates at a steady value of -1.2 mm. This deflection corresponds to the step height of the outer bearing pad resting on the pressure tube. The profiles show a large increase in positive deflection on the opposing fuel element side once contact occurs. The movement is so large that the center bearing pad lifts away from the pressure tube rather than towards it. It is noted that this deflection profile occurs for a temperature gradient which is very unrealistic and any movement of this magnitude would involve local interaction with neighboring fuel elements. Also, subchannel thermalhydraulics would likely alter the local flow conditions in the contact area before a large contact area could develop. Still, the insulated boundary analysis served the purpose of demonstrating the contact capability of the model. An illustration of the gap distance between the pressure tube and the sheath is shown in

Figure 8-12. The ability to measure this gap distance in the analysis provides a unique feature in solid-element contact modelling which cannot be captured in beam analysis. The gap distance parameter could be used to adjust local flow conditions to account for laminarization of the heat transfer coefficient between the coolant and pressure tube as the bodies come into contact. This contact demonstration illustrates the ability of the ANSYS model to capture FE-PT contact if a large enough driving force is present.

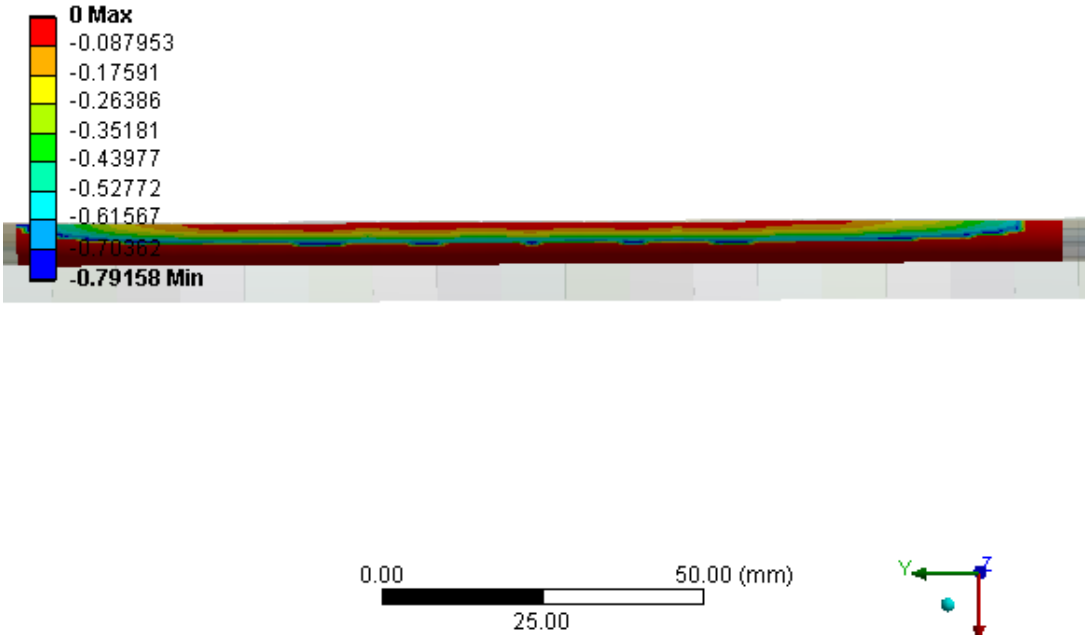

Figure 8-12: Contact gap distance between the fuel element and pressure tube for a 150 mm drypatch with an insulated boundary condition.

8.4 Multi-drypatch BOW Code Benchmark

As a method of further analyzing the above fuel element models under post-dryout conditions, the Individual Fuel Pellet Model and Cracked-fuel Stack Model are benchmarked against a drypatch simulation performed with the single element version of the BOW code. The pressure tube is removed for the models so that the full length fuel elements may be investigated by themselves. The benchmark evaluates the fuel element's deformation profile under the multi-drypatch conditions illustrated in Figure 8-13.

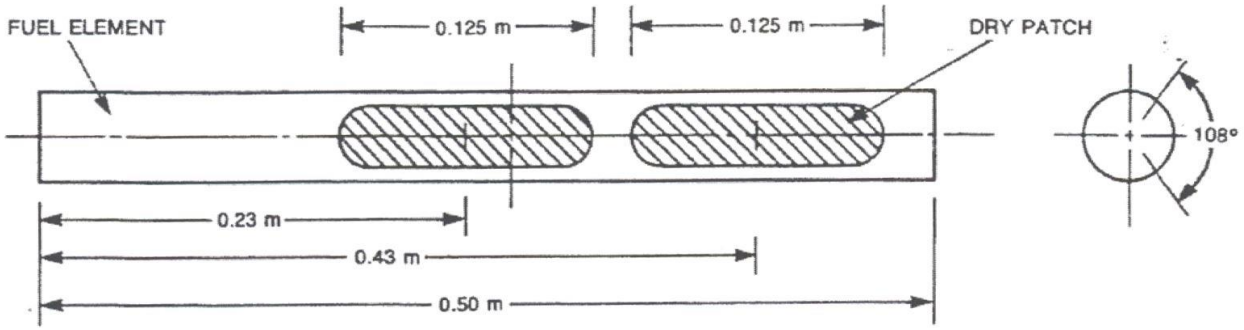

Figure 8-13: Schematic of location and circumferential arc width of drypatches for bowing simulation [35].

Two artificial drypatches are arranged on an outer fuel element facing downwards in the direction of gravity. The drypatches are treated with an elliptical shape with center of the patch being 300 K higher than the surrounding wet sheath at 573 K. This is similar to an original BOW code simulation used to demonstrate its bowing capability [17] but with slightly different values to compare against known conditions referenced by Fan et al. in [35]. The drypatches are included as prescribed temperature boundary conditions, which are shaped with a sinusoidal function varying from 873 K in the middle to 573 K outside as a thermal load step after NOC conditions are established. An illustration of the thermal loading conditions for a single drypatch

implemented in the model is given in Figure 8-14. The BOW code simulation used a 500 mm fuel element, which was slightly longer than the ANSYS model. To compensate for the difference in free span length, the axial locations of the drypatchs were normalized to the BOW code simulation. This positioned the two drypatches at 227.7 mm and 425.7 mm, respectively.

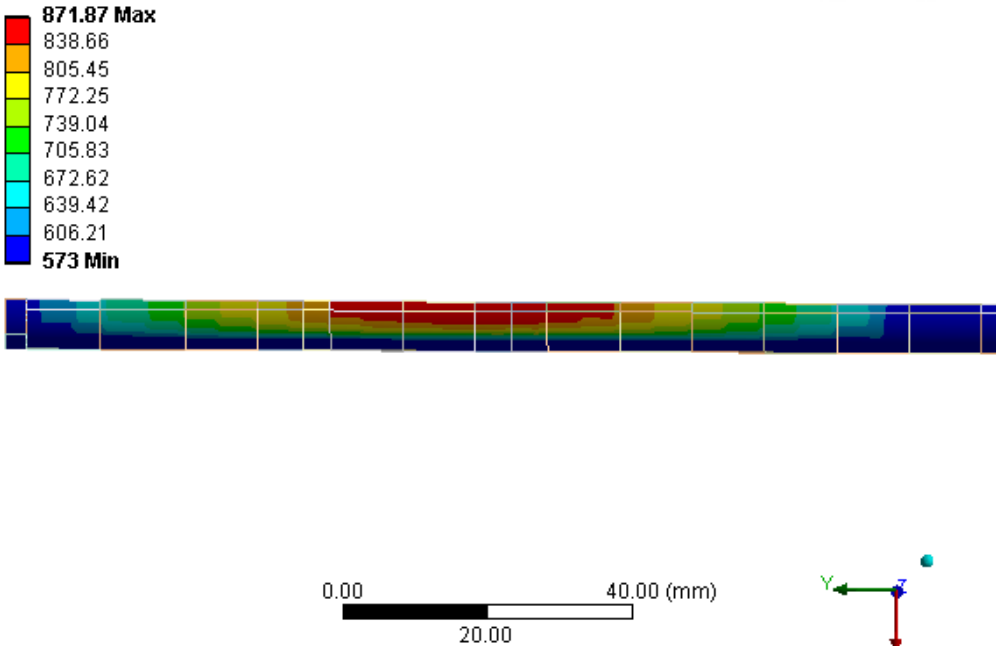

Figure 8-14: Drypatch size using a sinusoidal function to shape the gradient from a center temperature of 873 K to 573 K on the outside.

8.5 Results from Multi-drypatch BOW Code Benchmark

The BOW code simulation predicted a 1.85 mm maximum deflection compared to a prediction of 1.509 mm for Individual Fuel Pellet Model and 4.2 mm for the Cracked-fuel Stack Model with the Young's modulus reduced by a factor of 1000. The simulation results are given by the deformation profiles displayed in Figure 8-15 and the BOW Code results in Figure 8-16.

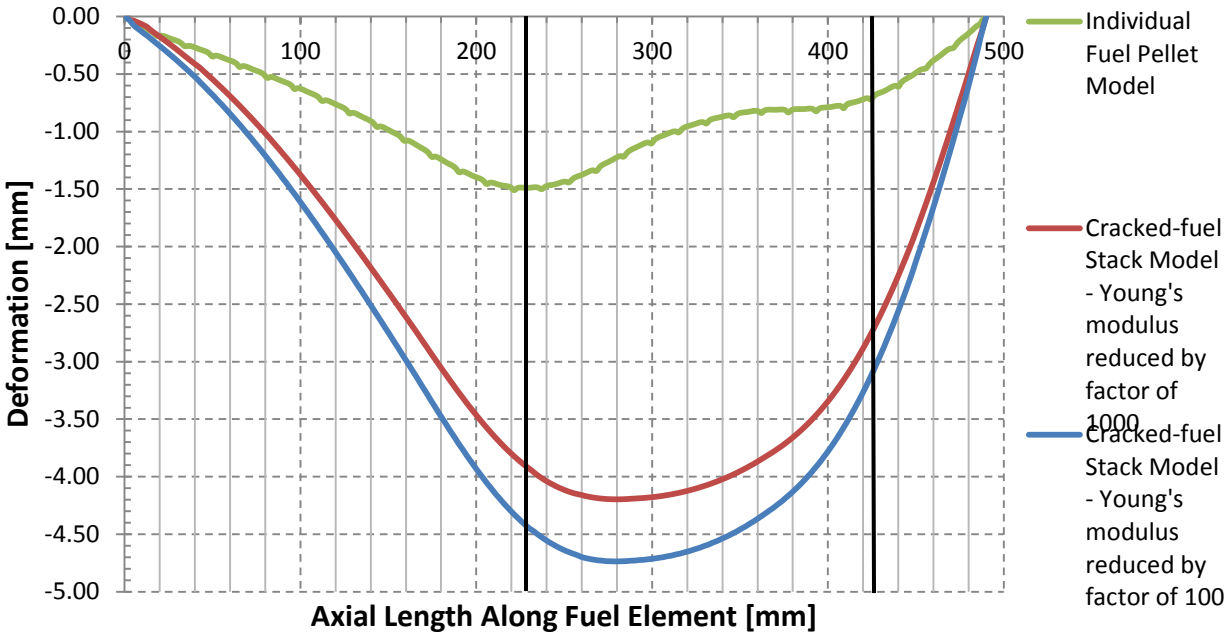

Figure 8-15: Predicted fuel element bowing with the Individual Fuel Pellet Model and Cracked-fuel Stack Model for the simulation of two drypatches. The centers of the drypatches are indicated by the bold vertical black lines.

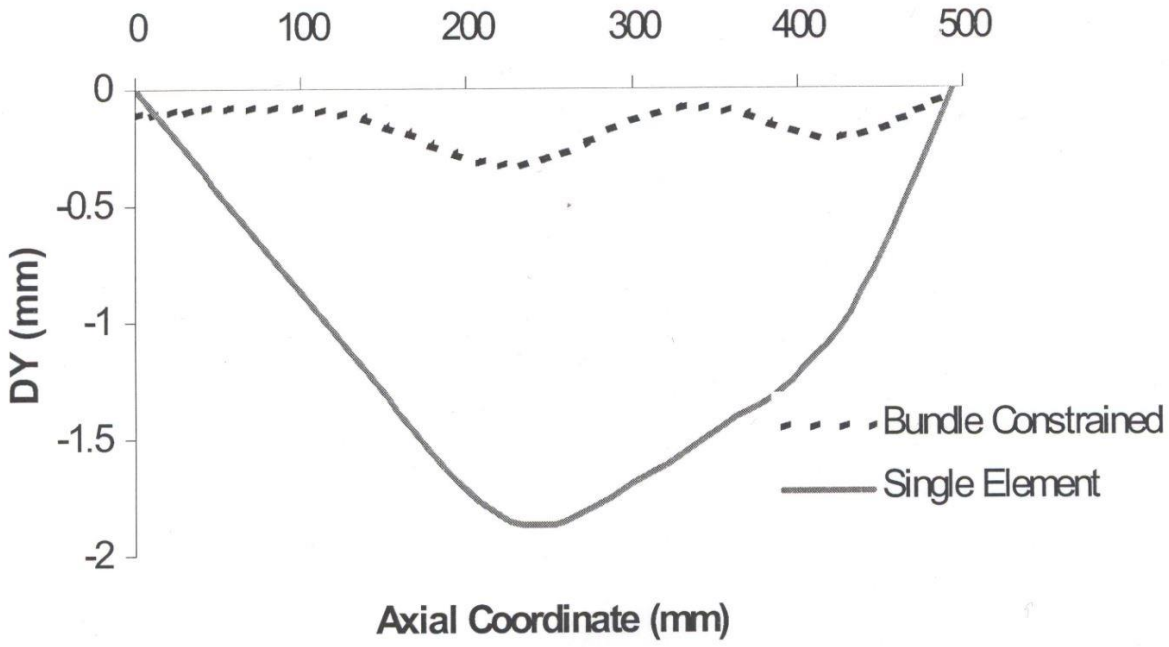

Figure 8-16: Bowing of an Outer Element induced by postulated elliptical drypatches using the BOW Code [35]. The 'bundle constrained' and 'single element' refer to the version of BOW Code.

The vertical black lines in Figure 8-15 indicate the center position for both drypatches. The model results indicate an obvious difference between the predictive abilities of both ANSYS models under multi-drypatch loading. The Individual Fuel Pellet Model predicts a substantially smaller deformation profile than the Cracked-fuel Stack Model. This behaviour was expected based on the results of the thermal gradient analysis, which showed a similar ordering of deflection between the two models. The Individual Fuel Pellet Model also has a more defined shape that follows the position of the drypatches based on the alignment with the deflection bumps in the profile. On the other hand, the Cracked-fuel Stack Model is less sensitive to the precise position of the drypatches and deforms in a smooth manner similar to having a single offset drypatch. This behaviour suggests that pellet-to-pellet contact is an important feature which influences the deformation profile when asymmetric thermal loading in present.

Furthermore, comparing the maximum deflection results shows an under prediction for the Individual Fuel Pellet Model and an over prediction for the Cracked-fuel Stack Model. The under predicted value is likely a combination of a different thermal expansion coefficient used by the BOW code as well as a lower fuel stack bending contribution to the sheath. This contribution is related to the stiffness of the fuel element and that is why the Cracked-fuel Stack Model has such a large over prediction. The very low stiffness results in a conservative estimate for maximum deflection. Unfortunately the gripping factor in the BOW simulation is unknown to calculate its flexural rigidity, but it is almost certain to fall between the Individual Fuel Pellet Model and Cracked-fuel Stack Model. Next, comparing the deformation profiles between the Cracked-fuel Stack Model and the single element profile of the BOW Code benchmark indicates a very similar asymmetric displacement across the total length. This is no surprise as the models are derived from the same BOW code formulation. If the stiffness of the Cracked-fuel Stack Model could be enhanced, better agreement of the results would likely ensue. Conversely, the Individual Fuel Pellet Model showed similarities to the bundle constrained deflection profile in Figure 8-16. The bundle version model is an updated version of the BOW Code (BOW 3.0) and accounts for more realistic bundle constraint effects [36]. Both profiles contain a higher degree of local deflection which seems to limit the total amount of bow. The conclusion of this analysis is that the Cracked-fuel Stack Model, like the single element BOW Code, is conservative for predicting maximum deflection under asymmetric thermal loading but the Individual Fuel Pellet Model may capture the true axial deformation profile more accurately, which is important when contact with neighboring components is possible.

8.6 Summary of Post-dryout Fuel Element Deformation

The second phase of this work involved analyzing FE-PT contact behaviour by investigating the effect of dryout on a fuel element that is resting on the pressure tube. A simulated drypatch was used to induce the necessary thermal gradients to drive the deformation. The convective heat transfer boundary conditions for the drypatch analysis created a maximum sheath temperature of approximately 1120 K due to the specified 1073 K bulk coolant temperature. This particular temperature range is important as time dependent processes like creep are not expected to be significant when the duration of dryout is short. Beyond 1073 K, the sheath begins to experience an alpha-beta phase transition, which causes a reduction in sheath ductility. The drypatch analysis avoided temperatures beyond this range because high temperature creep becomes an important factor, which would challenge the drypatch as the largest driving force for deformation. The location and size of the drypatch were chosen to represent severe conditions, which could possibly lead to FE-PT contact. The Individual Fuel Pellet Model represented a fuel element whose stiffness was characterized within the expected typical range, while the Cracked-fuel Stack Model was characteristic of a fuel element with extremely low stiffness. The results of the drypatch analysis indicated the stiffness and fuel-to-sheath contact representation did not influence the deformation as much as the drypatch parameters. This suggests that the bearing pads and end plate supports assisted in limiting the extent of deformation when positioned in contact with the pressure tube. Although other factors may contribute to fuel element deformation, an extremely large temperature gradient of roughly 500°C located directly between the two bearing pads would likely dominate over the other local driving factors. This behaviour is significant as contact was not achieved with the simple end plate constraints. To ensure the

ANSYS model was capable of handling FE-PT contact, insulated thermal boundary conditions were used to demonstrate the concept when a sufficient load was applied.

In addition, a multi-drypatch benchmark was analyzed to investigate whether the fuel element models would behave differently to asymmetrical loading conditions when physical constraints like the pressure tube are not present. This was confirmed as both models demonstrated unique deformation profiles under the same drypatch loading. The Cracked-fuel Stack Model deflection behaviour was similar in profile to that obtained with the BOW code. This was expected because they are derived from the same formulation. The estimates for maximum deflection varied across all models because the stiffness of the Individual Fuel Pellet Model and Cracked-fuel Stack Model provided bounding estimates for an actual fuel element and it is suspected the BOW Code single element model would have had a flexural rigidity in between. The Individual Fuel Pellet Model's deflection profile showed better agreement with the bundle version of the BOW Code compared to the single element version. It appeared the inclusion of pellet-to-pellet contact aided the shaping of the local deflection profile and therefore may be a better representation for certain analyses where this local deflection is considered.

9 Summary and Conclusions

The work of this thesis sought to develop a fuel element deformation model with the ability to simulate thermally induced deformation caused by non-uniform heat transfer resulting from dryout. A solid element approach was investigated to capture the intricate contact behaviour between the fuel and sheath. The commercially available finite element software ANSYS (V14.5) was selected for its sophisticated 3-dimensional contact modelling capabilities. The intended application of this model is to provide insight into the associated knowledge uncertainties surrounding FE-PT contact. A description of the methodology, realised models and studies performed as part of the model verification are provided in detail within the thesis. This chapter provides an overview summarizing the results and conclusions obtained from the modelling analyses.

1) The fuel stack representation and contact connection between the pellet-sheath are important factors which define the fuel element's stiffness. A monolithic fuel stack, individual fuel pellet and a cracked-fuel stack, based on the BOW Code formulation, were tested with bonded and frictionless contact connections as potential fuel element representations in the deformation model. The flexural rigidity of these models was characterized to determine the most appropriate choice to pursue for a conservative deformation study. The Individual Fuel Pellet Model was selected for its similarities to a realistic physical geometry, while having an associated stiffness that fell within the range of other referenced values. Also, the Cracked-fuel Stack Model was selected to represent a lower bound for the stiffness of an operating fuel element. Both models

included frictionless contact which was found to be the most conservative of the evaluated connections.

- The individual pellet and cracked-fuel representations considered in this thesis provide a lower and upper bound to the flexural rigidity

2) The equivalent REF ‘gripping factor’ used in beam deformation models could not be fully characterized using the solid element models. Since the total stiffness of the fuel stack could not be determined in the Individual Fuel Pellet Model, the relative contribution provided from the fuel stack to resist sheath bending could not be calculated. At high power, the flexural rigidity was expected to saturate corresponding to a gripping factor of 1. However, the effect of power analysis revealed that the flexural rigidity continued to increase and would have to be greater than 1. This discrepancy was attributed to the inability to capture pellet cracking, which would reduce the fuel stack’s ability to resist sheath bending. On the other hand, the Cracked-fuel Stack Model was found to have a consistent REF value of approximately 0.1 across all powers. This value was unrealistic at high power but could not be adjusted due to the frictionless contact connection.

   - The Individual Fuel Pellet Model has an equivalent REF greater than 1whereas the Cracked-fuel Stack Model had a value of 0.1

3) The transverse deflection behaviour of the Individual Fuel Pellet Model and Cracked-fuel Stack Model were characterized for linear thermal gradients and compared with first-principle formulations. The results of the thermal gradient analysis demonstrated the fuel stack has an important role in contributing to the total deflection. The Individual Fuel Pellet Model was observed to deflect slightly more than that of an

empty sheath under similar temperature gradients. This implied the individual fuel pellet representation was able to transfer a small portion of its curvature to the sheath to increase deflection. In contrast, the Cracked-fuel Stack Model predicted the largest deflection out of all the models indicating the fuel stack contributed a larger portion of its curvature to the sheath. To verify the predicted deflection of the Individual Fuel Pellet Model, the results were compared against an analytical beam model proposed by Veeder and Schankula [13], and Suk et al. [33]. The ANSYS model predicted larger deflections for each gradient but observed a similar linear dependence to that of the gradient magnitude. It is hypothesized that the observed curvature transfer between the fuel stack and sheath is not fully captured in the 1-dimensional analytical model.

- Thermally induced deflection of a simply-supported fuel element is highly dependent on the fuel stack representation. The Cracked-fuel Stack Model predicted larger deflections than the Individual Fuel Pellet Model.

4) The distinct stiffness characteristics of the Individual Fuel Pellet Model and Cracked-fuel Stack Model had insignificant effects on the fuel element's deflection profile when an asymmetric thermal load was applied to the sheath, while in contact with the pressure tube. The drypatch analysis evaluated the deformation profile of both fuel element models when subjected to axially varying drypatches. The bearing pads were observed to play an important role in limiting the extent of thermally driven deformation. The models exhibited very similar deflection profiles despite showing different responses in the thermal gradient analysis when no restraints were present. This behaviour was an important result that emphasised the significance of brazed appendages for reducing the free span length.

- The center bearing pad appears to provide the majority of the resistance to sheath bowing rather than the pellet stack itself

5) For an induced drypatch thermal gradient of roughly 500°C, no FE-PT contact occurred under the evaluated conditions. The analyzed drypatches specified a maximum sheath temperature of about 800°C, which is 200°C higher than that specified in the current trip parameter acceptance criteria of G-144. There has been an on-going initiative by the CANDU industry to better quantify possible FE-PT contact behaviour for sheath temperatures greater than 600°C. The developed models in this thesis may be used to gain better insight into the uncertainties associated with FE-PT contact for non-uniform thermal conditions. The drypatch analysis employed severe temperature conditions, which could arise and dominate the deflection driving process under the transient reactor conditions for which G-144 is responsible. Since contact was not observed under the current analysis conditions, insulated convective heat transfer conditions were applied to the sheath to generate a sufficiently high thermal load to make sure contact occurred. This study was conducted to prove the solid element contact model was capable of capturing the contact phenomena if the proper initiating conditions are present.
   - The developed solid element model is capable of simulating FE-PT contact
6) A drypatch simulation benchmark was performed to compare the Individual Fuel Pellet Model and Cracked-fuel Stack Model against the single element BOW Code prediction. Two artificial drypatches were placed asymmetrically on the fuel sheath to induce thermally driven deformation. Since the Cracked-fuel Stack Model was designed on the BOW Code formulation, similar predictions were expected. The

results indicated a similar deformation profile but the maximum deflections were over predicted. The apparent offset in values was attributed to a combination of different thermal expansion coefficients and characteristic flexural rigidities. The Individual Fuel Pellet Model displayed a different deformation profile altogether with a more distinct sensitivity to local hot spots. The pellet-to-pellet contact was suspected of influencing this behaviour and is a significant result. The maximum deflection was under predicted, which led to the conclusion that the flexural rigidity of the fuel element benchmark was somewhere between the Individual Fuel Pellet Model and Cracked-fuel Stack Model. This assumption was based on the predicted flexural rigidity range calculated during the analytical comparison to the Cracked-fuel Stack Model in the flexural rigidity analysis.

- Pellet-to-pellet contact plays a significant role in predicting fuel element deformation under simple-supports with two drypatches.

In conclusion, this thesis work investigates the use of ANSYS for developing a 3-dimensional fuel element deformation model utilizing a solid-element approach to capture the sophisticated fuel-to-sheath contact interaction in CANDU fuel. The realized geometry utilizes a single full length outer fuel element resting in contact with a section of pressure tube. The ability to simulate post-dryout heat transfer conditions encountered during possible AOO events makes this a useful tool for further research investigations involving safety analysis acceptance criteria and to support fuel fitness-for-service. The solid element approach offers numerous advantages over the current suite of 3-dimensional beam deformation models like the ability to assess FE-PT contact with solid bodies.

10 Recommendations

The work of this thesis has demonstrated the capability of ANSYS' 3D solid element modelling for investigating FE-PT contact interactions under post-dryout heat transfer conditions. A list of recommendations are presented to suggest further studies, which incorporate the current tool, to gain additional insight into fuel deformation behaviour and FE-PT contact interactions.

1) Increase the amount of nuclear specific phenomena which contribute to the fuel element's stiffness to better predict the flexural rigidity. The approach for this thesis was to characterize a fuel element under a constant set of parameters which would yield a representative stiffness for nominal reactor conditions. This led to two different fuel element representations to provide a bounding set; a low stiffness (Cracked-fuel Stack Model) and high stiffness (Individual Fuel Pellet Model). Integrating the current fuel element models with a fuel performance code, such as ELESTRES-IST, would allow input variables such as fission gas pressure and fuel-to-sheath contact conductance to be specified for any conditions under the power-burnup envelope. In reality, the contact conductance is dynamic in nature and depends on strong feedback between the thermal and mechanical models. For a one-way coupled analysis, information related to the mechanical interaction between the fuel and sheath cannot be returned to the thermal model. This limits the functionality of the current model in comparison to a fully-coupled approach. In this thesis, a single value for the thermal conductance was selected to represent a steady-state value for solid contact, and avoid convergence issues associated with direct coupling. This was a sufficient assumption to demonstrate the capability of modelling FE-PT contact since this was the primary objective. However, it is worth

noting that this value would have changed locally in the FE-PT contact analysis, and would have altered the temperature distribution in the fuel element, which was responsible for driving the deformation. This is important for determining whether FE-PT contact could occur in actuality under the specified drypatch characteristics. Also, radial flux depression across the fuel element was not included in the thermal model. A uniform internal heat generation rate was applied throughout the solid-body pellets which resulted in a higher fuel centerline temperature prediction. Accounting for flux depressed internal heat generation will provide a better estimate for the fuel element temperature profile, which will influence the deformation behaviour due to the temperature dependent material models. Furthermore, adding more advanced features like sheath plasticity and fuel pellet cracking would help to improve accuracy for predicting fuel element flexural rigidity. Williams [20] has shown that a bilinear plasticity model may be successfully implemented in ANSYS as a look-up table in the Zircaloy material model. The absence of plasticity in the analysis will impact the overall deformation result if the yield stress of the material is exceeded in any simulation. High stress points can occur at the pellet ridges and lead to local sheath strain. Over the length of the fuel element, the cumulative effect of these strains can be important. Cracking may be implemented through the 'progressive damage' feature in ANSYS, where an instant material stiffness reduction occurs once stresses reach the damage limit. Basic testing of this feature with the Individual Fuel Pellet Model showed promising results, however, the initial spatial constraints on pellets caused the material damage feature to occur sooner than expected and led to contact convergence difficultly because of unrealistic stresses. Including these added features in the current model would allow better characterization of the fuel

element and offer an improved estimate for the REF value. In addition, implementing friction contact may help to characterize the CTF equivalent value. Quantifying these empirical values under different operating conditions is highly sought after for the purposes of developing a look-up style table to be used in deformation modelling with composite beam models.

2) Enhance the model capability by integrating an external subchannel thermalhydraulic code, such as ASSERT-PV [37], to assess upstream coolant and heat transfer conditions on the location and extent of dryout. The current thermal model accounts for sheath-to-coolant heat exchange through a convective boundary condition. In the drypatch analysis, the convective heat transfer coefficient is assumed constant along the axial length leading up to the dryout location. This is an assumed simplification as deteriorating flow conditions throughout the subchannel will alter the convective heat transfer coefficient. Consequently, complex temperature distributions would develop and contribute to the overall fuel element deformation behaviour. These conditions are critical for determining the size and location of dryout. Ideally, a computational fluid dynamic analysis would be coupled to the thermomechanical model to capture the important feedback between the mechanical deformation and thermalhydraulic flow. This magnitude of coupling can be computationally intensive and very difficult to obtain convergence. An alternate approach would be to utilize an external code to calculate the heat transfer coefficients for various fuel channel conditions, and map those values to the ANSYS model. A fully coupled method could be established where the simulated deformation results are transferred back to the subchannel code, by adjusting the geometry input file, to reflect changes in subchannel areas. Difficultly may arise when transferring these parameters as the

dimensionality of subchannel codes are generally less than 3-dimensions. Nevertheless, if a validated subchannel code is available, appropriate convective heat transfer coefficients may be applied to the current fuel element model to assess how changes in CHF and drypatch locations impact fuel element deformation and interaction with the pressure tube.

3) Investigate the effect of hydraulic drag on fuel element bow. During reactor operation, coolant flowing through the fuel channel forces the fuel string against a latch at the downstream end of the channel. The hydraulic drag force is supported by the outer fuel elements in contact with the latch. Thermally induced deflections become a moment arm for any axial bearing load. Axial loads are generated in the reactor from hydraulic drag of the coolant or by the refueling ram. This so called pressure-delta effect (P-δ) causes an additional deflection of the element so that the total curvature is increased. This effect may become important for large drypatch deflections.
4) Extend the physical geometry to include additional fuel elements. The current fuel element and pressure tube model may be the largest solid element contact model created for CANDU fuel using individual pellet parts. Contact interaction was successfully established between 31 fuel pellets interacting with each other and the sheath as well as FE-PT contact. The application of spatial contact constraints on the fuel pellets over serval load steps provided a smooth convergent approach to bringing the fuel element up to operating conditions. Solid-element modelling requires an enormous amount of computing power due to the overall numerical size of the problem. Accounting for multiple nuclear phenomena in the model can add further complexity, which requires more computing power and increases the overall solving difficulty. Modelling the

Individual Fuel Pellet Model required over a weeks' worth of solving time with common computer resources on an academic license. Expanding the number of fuel elements in the model would require high performance computing to achieve results under a reasonable time frame. ANSYS provides high performance computing licenses to allow solving with multiple core processors on shared computer clusters. If access to these resources is available, there is a good chance expanding the fuel element model with more fuel elements will be successful using the same approach to convergence. Adding more components would allow FE-FE contact interactions to be investigated and remove idealized boundary constraints that are currently applied to the solid element end cap in place of physical end plates.

References

[1] A. Bychkov, "The Growth of Nuclear Power in the Pacific and the IAEA's Support for its Development," in *19th Pacific Basin Nuclear Conference*, Vancouver, 2014.

[2] International Atomic Energy Agency, "Nuclear Power Reactors in the World 2014 Edition," IAEA, Vienna, May 2014.

[3] "Key Canadian Electricity Statistics," Canadian Electricity Association, 10 06 2014. [Online]. Available: http://www.electricity.ca/resources/industry-data.php. [Accessed 12 September 2014].

[4] "Ontario's Long-Term Energy Plan," Ministry of Energy, Toronto, Ontario, 2013.

[5] A. I. Miller, J. Luxat, E. G. Price, R. B. Duffey and P. J. Fehrenbach, in *Nuclear Engineering Handbook*, Boca Raton, FL, Taylor and Franscis Group, LLC, 2009, p. 144.

[6] "CANDU 6 Technical Summary," CANDU 6 Program Team, AECL, May 2005. [Online]. Available: https://canteach.candu.org/Content%20Library/CANDU6_TechnicalSummary-s.pdf.

[7] E. Kohn and M. J. Notley, "Fuel Element Sheath Strains at High Power and Burnups: Rationalising the Reference Bundle Overpower Envelope," in *6th International CNS CANDU Fuel Conference*, Niagara Falls, 1999.

[8] CNSC, "Trip Parameter Acceptance Criteria for the Safety Analysis of CANDU Nuclear Power Plants," Canadian Nuclear Safety Comission, Ottawa, May 2006.

[9] E. Kohn, R. H. Hu, G. I. Hadaller and R. A. Fortman, "Understanding CANDU Fuel Bowing in Dryout: An Industry Approach," in *Proceedings of the 5th International Conference on CANDU Fuel*, Toronto, 1997.

[10] N. E. Todreas and M. S. Kazaimi, Nuclear Systems 1 Thermal Hydraulic Fundamentals, New York: Hemisphere Publishing Corporation, 1990.

[11] J. R. Thome, "Engineering Data Book III, Chapter 10 Boiling Heat Transfer Inside Plain Tubes," Wolverine Tube, Inc., Lausanne, Switzerland, 2007.

[12] Z. Cheng, Y. F. Rao and G. M. Waddington, "Assessment of ASSERT-PV for prediction of post-dryout heat transfer in CANDU bundles," *Nuclear Engineering and Design*, vol. 278, pp. 239-248, 2014.

[13] J. Veeder and M. H. Schankula, "Bowing of Pelletized Fuel Elements: Theory and In-Reactor Experiments," *Nuclear Engineering and Design*, vol. 29, pp. 167-179, 1974.

[14] "N290.1 Requirments for Shutdown Systems of Nuclear Power Plants," Canadian Standards Association, Ottawa, 2013.

[15] H. H. Wong, E. Alp, W. R. Clendening, M. Tayal and L. R. Jones, "ELESTRES: A Finite Element Model for Normal Operating Condition," *Journal of Nuclear Technology*, vol. 57, pp. 203-212, May 1982.

[16] H. E. Sills, "ELOCA Fuel Element Behaviour during High-Temperature Transients," Atomic Energy of Canada Technical Report, AECL-6357, 1979.

[17] M. Tayal, "Modelling the Bending/Bowing of Composite Beams such as Nuclear Fuel: The BOW Code," *Nuclear Engineering and Design*, vol. 116, pp. 149-159, 1989.

[18] J. S. Bell and B. J. Lewis, "CANDU fuel bundle deformation modelling with COMSOL multiphysics," *Nuclear Engineering and Design,* vol. 250, pp. 134-141, 2012.

[19] L. C. Walters and A. F. Williams, "Fuel Bundle Deformation Model," in *8th International Conference on CANDU Fuel*, Honey Harbour, ON, 2003.

[20] A. F. Williams and S. Yatabe, "Current Status of 3D Modelling of CANDU Fuel Using Finite Elements: Progress, Capabilities and Limitations," in *PHWR Safety 2014 / CANSAS-2014 Workshop*, Ottawa, Ontario, June 2014.

[21] M. R. McCluskey, "A Three Dimensional Finite Element Analysis of a CANDU Fuel Element," MASc Thesis, Royal Military College of Canada, Kingston, Ontario, 2012.

[22] K. A. Gamble, "Modeling Three-Dimensional Deformation Mechanisms in CANDU Reactor Fuel Elements," MASc Thesis, Royal Military College of Canada, Kingston, Ontario, May 2014.

[23] S. D. Yu, M. Tayal and P. N. Singh, "Improvements, Verifications and Validations of the Bow Code," in *CNS 4th International Conference on CANDU Fuel, Volume 2*, Pembroke, Canada, October 1995 .

[24] ANSYS Inc., "ANSYS Mechanical APDL Structural Analysis Guide," Release 14.5, Canonsburg, PA, October 2012.

[25] ANSYS Inc., "ANSYS Mechanical APDL Thermal Analysis Guide," Release 14.5, Canonsburg, PA, October 2012.

[26] ANSYS Inc., "ANSYS Mechanical APDL Theory Reference Manual," Release 14.5, Canonsburg, PA, October 2012.

[27] E. Madenci and I. Guven, The Finite Element Method and Applications in Engineering Using ANSYS, New York: Springer Science + Business Media, LLC, 2006.

[28] ANSYS Inc., "ANSYS Mechanical User Guide," Release 14.5, Canonsburg, PA, October 2012.

[29] ANSYS Inc., "ANSYS Mechanical APDL Verification Manual," Release 14.5, Canonsburg, PA, October 2012.

[30] A. M. Ross and R. L. Stoute, "Heat Transfer Coefficient Between UO2 and Zircaloy-2," Atomic Energy of Canada Technical Report, AECL-1552, 1962.

[31] ANSYS Inc., "ANSYS Mechanical APDL Contact Technology Guide," Release 14.5, Canonsburg, PA, October 2012.

[32] Idaho National Engineering and Environmental Laboratory, "SCDAP/RELAP5/MOD3.2 Code Manual Volume IV: MATPRO--A Library of Material Properties for Light-Water-Reactor Accident Analysis," Idaho Falls, ID, Oct, 1997.

[33] H. C. Suk, K. S. Sim, J. H. Park and G. S. Park, "Thermally-induced Bowing of CANDU Fuel Elements," in *Canadian Nuclear Society's 4th International Conference on CANDU Fuel*, Pembroke, Ontario, October 1995.

[34] L. Jiang, K. MacKay and R. Gibb, "Numerical Model for Thermal and Mechnical Behaviour of a CANDU 37-Element Bundle," in *11th International Conference on CANDU Fuel*, Niagara Falls, October 2010.

[35] H. Z. Fan, H. Liu, A. Ranger and S. G. Xu, "Assessment of Fuel Element Patchy Dryout and Bowing in Fuel Bundle," in *10th CNS International Conference on CANDU Fuel*, Ottawa, ON, October, 2008.

[36] S. G. Xu, Z. Xu, S. D. Yu, M. Tayal, L. Lai and B. Wong, "BOW Code Development, Modelling of In-Reactor Bundle Deformation," in *Canadian Nuclear Society's 9th International Conference on CANDU Fuel*, Belleville, Ontario, September 18-21, 2005.

[37] M. B. Carver, C. J. Kiteley, R. Q.-N. Zhou and S. V. Junop, "VALIDATION OF THE ASSERT SUBCHANNEL CODE - PREDICTION OF CRITICAL HEAT-FLUX IN STANDARD AND NONSTANDARD CANDU BUNDLE GEOMETRIES," *Nuclear Technology*, vol. 112, no. 3, pp. 299-314, 1995.

Appendices

Appendix A – Analytical Flexural Rigidity Calculations

The following calculation is performed to obtain the analytical flexural rigidity of the monolithic pellet stack and empty sheath displayed in Table 7-4.

```
> restart;
> # Calculate the monolithic pellet stack's analytical flexural
rigidity
> E[p]:=189705*MPa; #Young's Modulus of Pellet at 573 K
```

$$E_p := 189705\ MPa$$

```
> a[p]:=6.09*mm; #Pellet Radius
```

$$a_p := 6.09\ mm$$

```
>
> II[p]:=Pi/4*a[p]^4; # Second moment of inertia
```

$$II_p := 343.8817905\ \pi\ mm^4$$

```
> EI[p]=evalf(II[p]*E[p]/mm^2/MPa*N); #Flexural rigidity of
monolithic pellet stack
```

$$EI_p = 2.049452370\ 10^8\ mm^2\ N$$

```
> # Calculate the empty sheath's analytical flexural rigidity
> E[s]:=77456*MPa; #Young's Modulus of Sheath at 573K
```

$$E_s := 77456\ MPa$$

```
> a:=6.13*mm; #Inner Sheath Radius
```

$$a := 6.13\ mm$$

```
> b:=6.54*mm; #Outer Sheath Radius
```

$$b := 6.54\ mm$$

```
>
> II[s]:=Pi/4*(b^4-a^4); # Second moment of inertia
```

$$II_s := 104.3465882\ \pi\ mm^4$$

```
> EI[s]=evalf(II[s]*E[s]/mm^2/MPa*N); #flexural rigidity
```

$$EI_s = 2.539119797\ 10^7\ mm^2\ N$$

Appendix B – Cracked-fuel Stack Model Calculations

The following calculation evaluates the shift in neutral axis in the Cracked-fuel Stack Model. The corresponding shift is used to calculate the analytical flexural rigidity using a pellet-to-sheath gripping factor of 1 in Table 7-7.

```
> #Define variables for equations
> E[p]:=166000; #Young's Modulus of Pellet (MPa)
```

$$E_p := 166000$$

```
> E[s]:=77200; #Young's Modulus of Sheath (MPa)
```

$$E_s := 77200$$

```
> a:=6.13; #Inner Sheath Radius (mm)
```

$$a := 6.13$$

```
> b:=6.54; #Outer Sheath Radius (mm)
```

$$b := 6.54$$

```
> #Transcendental equation to determine shift in neutral axis:
> E[p]*(1/3*(a^2-eta^2)^(1/2)*(2*a^2+eta^2)-
eta*a^2*arccos(eta/a))-E[s]*eta*Pi*(b^2-a^2)=0;
```

$$\frac{166000}{3}\sqrt{37.5769-\eta^2}\left(75.1538+\eta^2\right) - 6.237765400\ 10^6\ \eta \arccos\left(0.1631321370\ \eta\right) - 4.010308400\ 10^5\ \eta\ \pi = 0$$

```
> solve( { % }, eta ); #Solve for eta
```

$$\{\eta = 3.258711677\}$$

```
> eta:=3.258711677; # Distance of neutral axis from centroid
```

$$\eta := 3.258711677$$

```
> #Calculate the flexural rigidity of the fuel element:
> G[ps]:=1; #For a pellet-to-sheath gripping factor equal to 1
```

$$G_{ps} := 1$$

```
> EI:=E[s]*(Pi/4*(b^4-
a^4))+G[ps]*E[p]*(a^4/4*arccos(eta/a)+eta/12*(a^2-
eta^2)^(1/2)*(2*eta^2-5*a^2));
```

$$EI := 8.055556612\ 10^6\ \pi + 2.019894338\ 10^7$$

```
> evalf( % ); #Analytical Flexural Rigidity (N mm^2)
```

$$4.550622086\ 10^7$$

Appendix C – Thermal Bowing Calculations

The following sample calculation evaluates the analytical formulations of Veeder and Schankula, and Suk et al. as stated for a 300 K thermal difference listed in Table 7-9 of the thermal bowing analysis.

```
> restart;
> #Define variables for equations
> G[ps]:=1; #Pellet-to-sheath gripping factor
```

$$G_{ps} := 1$$

```
> h[sc]:=50000*W/m^2/K; #Sheath-to-coolant heat transfer
coefficient
```

$$h_{sc} := \frac{50000\ W}{m^2\ K}$$

```
> h[ps]:=9500*W/m^2/K; #Pellet-to-sheath heat transfer
coefficient
```

$$h_{ps} := \frac{9500\ W}{m^2\ K}$$

```
> L:=490*mm; # Fuel element length
```

$$L := 490\ mm$$

```
> t:=0.42*mm; # Sheath thickness
```

$$t := 0.42\ mm$$

```
> kappa[p]:=3*W/m/K; #Thermal conductivity of pellet
```

$$\kappa_p := \frac{3\ W}{m\ K}$$

```
> kappa[s]:=16.75*W/m/K;#Thermal conductivity of sheath
```

$$\kappa_s := \frac{16.75\ W}{m\ K}$$

```
> alpha[p]:=1.01e-5/K;#Coefficient of thermal expansion for
pellet
```

$$\alpha_p := \frac{0.0000101}{K}$$

```
> alpha[s]:=1.26e-5/K;#Coefficient of thermal expansion for
sheath
```

$$\alpha_s := \frac{0.0000126}{K}$$

```
> beta:=(T[c_max]-573*K)/(T[c_max]+573*K); #Quantity relating to
variation of bulk coolant temperatures
```

$$\beta := \frac{T_{c\_max} - 573\ K}{T_{c\_max} + 573\ K}$$

```
> a:=6.13*mm; #Inner Sheath Radius
```

$$a := 6.13\ mm$$

```
> b:=6.54*mm; #Outer Sheath Radius
```

$$b := 6.54\ mm$$

```
> T[c]:=573*K; #Nominal bulk coolant temperature
```

$$T_c := 573\ K$$

```
> D1:=0; #Flux depression factor
```

$$D1 := 0$$

```
> q:=50000*W/m;#Linear power rating
```

$$q := \frac{50000\ W}{m}$$

```
> gamma1:=(h[sc]-h[sc])/(h[sc]+h[sc]);#Quantity relating to
variation of sheath-to-coolant heat transfer coefficients
```

$$\gamma 1 := 0$$

```
> K[1]:=1+kappa[p]/a/(m/1000/mm)/h[ps]+kappa[p]*(b-
a)/a/kappa[s]; #Quantity related to Suk et al formulation
```

$$K_1 := 1.063494667$$

```
> K[2]:=kappa[p]+a*(m/1000/mm)*h[sc]*(1-gamma1^2)*K[1];#Quantity
related to Suk et al formulation
```

$$K_2 := \frac{328.9611154\ W}{m\ K}$$

```
> K[3]:=alpha[p]-alpha[s];#Quantity related to Suk et al
formulation
```

$$K_3 := -\frac{0.0000025}{K}$$

```
> K[4]:=K[3]*(1/h[ps]+1/h[sc]+(b-
a)*(m/1000/mm)/kappa[s])+(alpha[s]/h[ps]);#Quantity related to
Suk et al formulation
```

$$K_4 := \frac{9.519638645\ 10^{-10}\ m^2}{W}$$

```
> omega:=evalf(q/2/Pi/b*1000*mm/m); #Surface heat flux on fuel
sheath
```

$$\omega := \frac{1.216780910\ 10^{6}\ W}{m^2}$$

```
> alias(`&Delta;T[vs]`=VS,`&Delta;T[Suk]`=Suk); #Define Veeder
and Schankula, and Suk et al. Model
```

$$\Delta T[vs],\ \Delta T[Suk]$$

```
> T[c_max]:=873*K; #For a 300 K temperature gradient
```

$$T_{c\_max} := 873\ K$$

```
>
VS:=2*beta*T[c]/(1+h[ps]/h[sc]*(kappa[p]/(kappa[p]+a*(m/1000/mm)
*h[ps]))); #Temperature gradient equivalent for non-uniform
coolant in V&S Model
```

$$\Delta T[vs] := 235.5665876\ K$$

```
> delta[VS]=-alpha[s]*L^2*VS/16/b; #Deflection for non-uniform
coolant in V&S Model
```

$$\delta_{235.5665876\ K} = -6.810494788\ mm$$

```
> Suk:=2*(a*(m/1000/mm)*K[1]*(h[sc]*(1-gamma1^2)*beta*T[c]-
gamma1*omega)-2*b*omega*D1)/K[2]; #Temperature gradient
equivalent for non-uniform coolant in Suk et al Model
```

$$\Delta T[Suk] := 235.5910616\ K$$

```
> delta[Suk]=-alpha[s]*L^2*Suk/16/b;#Deflection for non-uniform
coolant in Suk et al Model
```

$$\delta_{235.5910616\ K} = -6.811202362\ mm$$

```
> Suk:=2*G[ps]*b/a/alpha[s]*(beta*T[c]*(K[3]-
K[4]*h[sc]*kappa[p]*(1-
gamma1^2)/K[2])+K[4]*omega*(kappa[p]*gamma1-
2*h[sc]*(1*gamma1^2)*b*D)/K[2]); #Temperature gradient
equivalent for pellet/sheath interaction in Suk et al Model
```

$$\Delta T[Suk] := -59.06849036\ K$$

```
> delta[Suk]=-alpha[s]*L^2*Suk/16/b;#Deflection for
pellet/sheath interaction in Suk et al Model
```

$$\delta_{-59.06849036\ K} = 1.707736440\ mm$$

```
>
```

Appendix D – Gap Conductance

In Section 6.1.2 Thermal Contact, it was mentioned that a gap conductance model named after the work of Ross and Stoute [30] is useful for calculating the dynamic gap behaviour between the fuel and sheath. For the purposes of demonstrating FE-PT contact, a constant value for the thermal contact conductance, TCC, of 9500 W m^{-2} K^{-1} was used to simplify the analysis with minor impacts on the deformation, as this was primarily driven by external mechanisms. However, it is useful to estimate the ranges of the thermal contact conductance expected for the simulations if the Ross and Stoute model had been implemented. Since the linear power rating was set at 50 kW m^{-1}, it is expected that the Solid-to-Solid component of the gap conductance model would dominate the heat transfer process due to the high interaction between the fuel and sheath. Analyzing this component of the Ross and Stoute model, the thermal contact conductance was calculated for average sheath temperatures of 631 K and 900 K. Two different areas in the fuel element were evaluated to offer insight into the influence of the interfacial pressure, between the fuel and sheath, on the heat transfer value. These locations corresponded to the center and end region of a pellet in the Individual Fuel Pellet Model. The end of the pellet is subjected to hourglassing which causes a higher contact pressure compared to the center region. Average interfacial pressure values for the center and end region were taken as 48 MPa and 150 MPa, respectively. Four new centerline temperatures were simulated in ANSYS with the thermal contact conductance calculated below. They ranged from 2629 K for a TCC of 9137 W m^{-2} K^{-1} and 2400 K for a TCC of 52698 W m^{-2} K^{-1}

```
> restart;
> #Define the modified Ross and Stoute model for solid-to-solid
conductance
> h[s]:=k[hm]*sqrt(P)/a[0]/sqrt(R[surface])/H;#Solid-to-solid
component
```

$$h_s := \frac{k_{hm}\sqrt{P}}{a_0\sqrt{R_{surface}}\,H}$$

```
> #Define the required variables
> k[hm]:=2*k[UO2]*k[Zr]/(k[UO2]+k[Zr]); #The harmonic mean of
the fuel and sheath's conductivities
```

$$k_{hm} := \frac{2\,k_{UO2}\,k_{Zr}}{k_{UO2}+k_{Zr}}$$

```
> R[surface]:=sqrt((R[f]^2+R[s]^2)/2);#Root-mean squared surface
roughness of fuel and sheath
```

$$R_{surface} := \frac{1}{2}\sqrt{2\,R_f^2+2\,R_s^2}$$

```
> H:=(exp(26.034-0.026394*T[s]*(1/K)+4.3504e-5*T[s]^2*(1/K^2)-
2.5621e-8*T[s]^3*(1/K^3)))/1e6*MPa;#Meyers hardness of the
sheath as a function of the average sheath temperature (MATPRO)
```

$$H := \frac{0.000001}{e^{26.034-\frac{0.026394\,T_s}{K}+\frac{0.000043504\,T_s^2}{K^2}-\frac{2.5621\,10^{-8}\,T_s^3}{K^3}}}\,MPa$$

```
> a[0]:=8.6e-3*m^0.5*MPa^(-0.5);# Constant
```

$$a_0 := \frac{0.0086\,m^{0.5}}{MPa^{0.5}}$$

```
> R[f]:=1e-6*m;# Assumed surface roughness of the fuel
```

$$R_f := 0.000001\,m$$

```
> R[s]:=1e-6*m;# Assumed surface roughness of the sheath
```

$$R_s := 0.000001\,m$$

```
> #For an average sheath temperature of 631K
> T[s]:=631*K;# Sheath temperature
```

$$T_s := 631\,K$$

```
> k[UO2]:=4.55*W/m/K; #Thermal conductivity of the fuel
```

$$k_{UO2} := \frac{4.55\,W}{m\,K}$$

```
> k[Zr]:=16.85*W/m/K; #Thermal conductivity of the sheath
```

$$k_{Zr} := \frac{16.85\,W}{m\,K}$$

```
> #For an interfacial pressure of 48 MPa, the solid-to-solid
conductance is...
```

```
> P:=48*MPa:evalf(h[s]);
```

$$\frac{9137.307041\ W}{m^{1.5}\ K\ \left(m^2\right)^{1/4}}$$

```
> #Centerline temperature via Individual Fuel Pellet Model in
Ansys is..
> T[centerline]:=2629*K;
```

$$T_{centerline} := 2629\ K$$

```
> #For an interfacial pressure of 150 MPa, the solid-to-solid
conductance is...
> P:=150*MPa:evalf(h[s]);
```

$$\frac{16152.62942\ W}{m^{1.5}\ K\ \left(m^2\right)^{1/4}}$$

```
> #Centerline temperature via Individual Fuel Pellet Model in
Ansys is..
> T[centerline]:=2518*K;
```

$$T_{centerline} := 2518\ K$$

```
> #For an average sheath temperature of 900K
> T[s]:=900*K;# Sheath temperature
```

$$T_s := 900\ K$$

```
> k[UO2]:=3.27*W/m/K; #Thermal conductivity of the fuel
```

$$k_{UO2} := \frac{3.27\ W}{m\ K}$$

```
> k[Zr]:=20.17*W/m/K; #Thermal conductivity of the sheath
```

$$k_{Zr} := \frac{20.17\ W}{m\ K}$$

```
> #For an interfacial pressure of 48 MPa, the solid-to-solid
conductance is...
> P:=48*MPa:evalf(h[s]);
```

$$\frac{29810.55995\ W}{m^{1.5}\ K\ \left(m^2\right)^{1/4}}$$

```
> #Centerline temperature via Individual Fuel Pellet Model in
Ansys is..
> T[centerline]:=2423*K;
```

$$T_{centerline} := 2423\ K$$

```
> #For an interfacial pressure of 150 MPa, the solid-to-solid
conductance is...
> P:=150*MPa:evalf(h[s]);
```

$$\frac{52698.12271\ W}{m^{1.5}\ K\ \left(m^2\right)^{1/4}}$$

```
> #Centerline temperature via Individual Fuel Pellet Model in
Ansys is..
> T[centerline]:=2400*K;
```

$$T_{centerline} := 2400\ K$$